

INFORMATION TO USERS

This manuscript has been reproduced from the microfilm master. UMI films the text directly from the original or copy submitted. Thus, some thesis and dissertation copies are in typewriter face, while others may be from any type of computer printer.

The quality of this reproduction is dependent upon the quality of the copy submitted. Broken or indistinct print, colored or poor quality illustrations and photographs, print bleedthrough, substandard margins, and improper alignment can adversely affect reproduction.

In the unlikely event that the author did not send UMI a complete manuscript and there are missing pages, these will be noted. Also, if unauthorized copyright material had to be removed, a note will indicate the deletion.

Oversize materials (e.g., maps, drawings, charts) are reproduced by sectioning the original, beginning at the upper left-hand corner and continuing from left to right in equal sections with small overlaps. Each original is also photographed in one exposure and is included in reduced form at the back of the book.

Photographs included in the original manuscript have been reproduced xerographically in this copy. Higher quality 6" x 9" black and white photographic prints are available for any photographs or illustrations appearing in this copy for an additional charge. Contact UMI directly to order.

U·M·I

University Microfilms International
A Bell & Howell Information Company
300 North Zeeb Road, Ann Arbor, MI 48106-1346 USA
313/761-4700 800/521-0600

Order Number 1348975

**The effects of representing the spatial variability of aquifer
characteristics on numerical ground water flow and contaminant
transport modeling**

Robinson, James Calvert, M.S.

Rice University, 1992

U·M·I

**300 N. Zeeb Rd.
Ann Arbor, MI 48106**

RICE UNIVERSITY

**THE EFFECTS OF REPRESENTING THE SPATIAL VARIABILITY
OF AQUIFER CHARACTERISTICS ON NUMERICAL GROUND
WATER FLOW AND CONTAMINANT TRANSPORT MODELING**

BY

JAMES CALVERT ROBINSON

A THESIS SUBMITTED
IN PARTIAL FULFILLMENT OF THE
REQUIREMENTS FOR THE DEGREE

MASTER OF SCIENCE

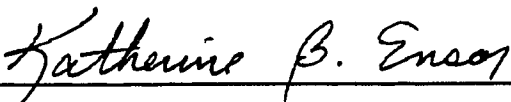
Approved, Thesis Committee



Philip B. Bedient, Chairman, Professor of
Environmental Science and Engineering



Mark R. Wiesner, Assistant Professor of
Environmental Science and Engineering



Katherine B. Ensor, Assistant Professor of
Statistics

HOUSTON, TEXAS

MAY 1992

ABSTRACT

THE EFFECTS OF REPRESENTING THE SPATIAL VARIABILITY OF AQUIFER CHARACTERISTICS ON NUMERICAL GROUND WATER FLOW AND CONTAMINANT TRANSPORT MODELING

BY

JAMES CALVERT ROBINSON

The objective of the research presented here is to determine how the representation of the spatial variability of aquifer properties affects ground water flow and contaminant transport modeling at the United Creosoting Company site in Conroe, Texas. Simulations are performed using spatial distributions of aquifer properties generated by each of three methods: constant value estimation, polynomial trend surface estimation, and kriging point estimation. The significance of using a representation of an aquifer property is dependent on the modeling purpose. In natural gradient ground water flow simulations the representation of hydraulic conductivity and bottom elevation significantly affected model calibration. The representation of aquifer properties generally did not affect model calibration of natural gradient contaminant transport modeling, but do affect the shape and size of the simulated plume. The representation of aquifer properties was very useful for identifying feasible ground water recovery options.

ACKNOWLEDGMENTS

I would like to recognize the following individuals who inspired and influenced my first 23 years: my father, George Calvert Robinson; my mother, Gwen Caudill Robinson; "Granny Polly"; my sister Margaret Robinson Chionis, and her family, Jim, John, and Michael; my brother, George Caudill Robinson, and his family, Susan, Nicole, and Oscar (tentatively); and my brother, Thomas Neil Robinson. Additional recognition goes out to certain friends who read beyond my cover: Michelle Emmer (let's ride those Harleys), George Roane (keep away from my blocks), Lori Charboneau (red dirt), Chris Johnnie (Gandhi music), Melissa Hooper (I am still barefoot), Laura Bourdier (the barn), Pam Smith (I need a man), Shana Neck (lime), Tim Biglane (it's a creeper), Debbie Labanyon Schaeffer (margaritaville), Greg Sepeda (double or nothing), Bruce Babin (Kowabunga dude!), Dr. Alawady (I am smiling now), Shankararaman Chellam (don't fear the reaper), Cyndy Allard (quarterback), and Traci Rayburn (fall on me).

*Ticking away the moments that make up a dull day
You fritter and waste the hours in an offhand way.
Kicking around on a piece of ground in your home town
Waiting for someone or something to show you the way.*

*Tired of lying in the sunshine, staying home to watch the rain.
You are young and life is long and there is time to kill today.
And then one day you find ten years have got behind you.
No one told you when to run, you missed the starting gun.*

*So you run and you run to catch up with the sun but it's sinking,
Racing around to come up behind you again.
The sun is the same in a relative way but you're older,
Shorter of breath and one day closer to death.*

*Every year is getting shorter, never seem to find the time.
Plans that either come to naught or half a page of scribbled lines.
Hanging on in quiet desperation is the English way.
The time is gone, the song is over,
Thought I'd something more to say.*

Time, by Pink Floyd

TABLE OF CONTENTS

Abstract	ii
Acknowledgments.....	iii
Table of Contents	iv
List of Figures	vii
List of Tables.....	x
1 Introduction	1
2 Previous Research	9
2.1 Variability of Aquifer Properties	9
2.2 Characterization of Aquifer Property Variability	11
2.3 Generation of Representations of Aquifer Properties.....	15
2.3.1 Constant Representation	15
2.3.2 Polynomial Representation.....	17
2.3.3 Kriging Representation.....	22
2.3.4 Tests of Goodness of Fit.....	30
2.4 Effects of Spatial Variability on Modeling.....	32
3 Aquifer Properties	35
3.1 Field Site	35
3.2 Site Hydrogeology	40
3.3 Representations of Aquifer Properties.....	44

3.3.1	Hydraulic Conductivity Representations.....	45
3.3.2	Bottom Elevation Representations	54
4	Modeling	63
4.1	Modeling Purpose.....	63
4.2	Model Selection	66
4.3	Model Design.....	72
4.3.1	Grid Design.....	73
4.3.1	Time Step Selection.....	75
4.3.3	Aquifer Properties.....	76
4.3.4	Hydraulic Loading.....	77
4.3.5	Contaminant Loading	82
4.3.6	Boundary Conditions.....	84
4.3.7	Initial Conditions	84
4.4	Model Calibration.....	86
4.5	Model Prediction	88
5	Discussion	90
5.1	Natural Gradient	90
5.1.1	Ground Water Flow	91
5.1.2	Contaminant Transport.....	97
5.2	Recovery and Injection.....	102
5.2.1	Ground Water Flow.....	103
5.2.2	Contaminant Transport.....	105

6	Conclusions	107
6.1	Representations of Aquifer Properties.....	107
6.2	Modeling.....	109
	References	112
Appendix A	Figures of GWSE for natural gradient flow (NG-GF) modeling.....	116
Appendix B	Figures of chloride concentration distribution for natural gradient transport (NG-CT) modeling	124
Appendix C	Figures of GWSE for recovery and injection system flow (RI-GF) modeling	132
Appendix D	Figures of chloride concentration distribution for recovery and injection system transport (RI-CT) modeling	140

LIST OF FIGURES

Figure 2.1	Autocorrelation function $r_Y(h)$ verses lag separation.....	13
Figure 3.1	Site plan (Weston, 1985)	37
Figure 3.2	Monitoring well locations (Weston, 1985).....	42
Figure 3.3	Polynomial representation verses estimation error for hydraulic conductivity	47
Figure 3.4	Observed values verses polynomial representation for hydraulic conductivity	48
Figure 3.5	Polynomial hydraulic conductivity representation	49
Figure 3.6	Kriging representation verses estimation error for hydraulic conductivity	51
Figure 3.7	Observed values verses kriging representation for hydraulic conductivity	52
Figure 3.8	Kriging hydraulic conductivity representation	53
Figure 3.9	Polynomial representation verses estimation error for bottom elevation	56
Figure 3.10	Observed values verses polynomial representation for bottom elevation	57
Figure 3.11	Polynomial bottom elevation representation	58
Figure 3.12	Kriging representation verses estimation error for bottom elevation.....	60
Figure 3.13	Observed values verses kriging representation for bottom elevation.....	61
Figure 3.14	Kriging bottom elevation representation	62
Figure 4.1	Waste pond loading locations.....	79

Figure 4.2	Recovery and injection system well locations.....	81
Figure 4.3	Initial naphthalene concentrations for recovery and injection system modeling.....	87
Figure A.1	GWSEs for sim. NG-GF-KB-C.....	117
Figure A.2	GWSEs for sim. NG-GF-KB-P	118
Figure A.3	GWSEs for sim. NG-GF-KB-K.....	119
Figure A.4	GWSEs for sim. NG-GF-K-P	120
Figure A.5	GWSEs for sim. NG-GF-K-K	121
Figure A.6	GWSEs for sim. NG-GF-B-P	122
Figure A.7	GWSEs for sim. NG-GF-B-K	123
Figure B.1	Chloride conc. distribution for sim. NG-CT-KB-C.....	125
Figure B.2	Chloride conc. distribution for sim. NG-CT-KB-P	126
Figure B.3	Chloride conc. distribution for sim. NG-CT-KB-K.....	127
Figure B.4	Chloride conc. distribution for sim. NG-CT-K-P.....	128
Figure B.5	Chloride conc. distribution for sim. NG-CT-K-K	129
Figure B.6	Chloride conc. distribution for sim. NG-CT-B-P.....	130
Figure B.7	Chloride conc. distribution for sim. NG-CT-B-K	131
Figure C.1	GWSEs for sim. RI-GF-KB-C.....	133
Figure C.2	GWSEs for sim. RI-GF-KB-P	134
Figure C.3	GWSEs for sim. RI-GF-KB-K	135
Figure C.4	GWSEs for sim. RI-GF-K-P.....	136
Figure C.5	GWSEs for sim. RI-GF-K-K	137

Figure C.6	GWSEs for sim. RI-GF-B-P	138
Figure C.7	GWSEs for sim. RI-GF-B-K	139
Figure D.1	Naphthalene conc. distribution for sim. RI-CT-KB-C	141
Figure D.2	Naphthalene conc. distribution for sim. RI-CT-KB-P	142
Figure D.3	Naphthalene conc. distribution for sim. RI-CT-KB-K	143
Figure D.4	Naphthalene conc. distribution for sim. RI-CT-K-P	144
Figure D.5	Naphthalene conc. distribution for sim. RI-CT-K-K	145
Figure D.6	Naphthalene conc. distribution for sim. RI-CT-B-P	146
Figure D.7	Naphthalene conc. distribution for sim. RI-CT-B-K	147

LIST OF TABLES

Table 3.1	Monitoring well locations.....	43
Table 3.2	Univariate statistics of the observed aquifer properties.....	44
Table 3.3	Comparison of hydraulic conductivity representations	46
Table 3.4	Comparison of bottom elevation representations	55
Table 4.1	Simulation list and identification.....	65
Table 4.2	Effect of grid cell side dimension on the number of cells	74
Table 4.3	Time periods for natural gradient modeling (Borden, 1986a)	75
Table 4.4	Hydraulic loading for natural gradient modeling (Borden, 1986a)	78
Table 4.5	Recovery well locations.....	80
Table 4.6	Injection well locations.....	82
Table 4.7	Chloride loading for natural gradient transport (NG-CT) modeling (Borden, 1986a)	83
Table 4.8	Naphthalene loading for generation of initial naphthalene concentrations for recovery and injection system transport (RI-CT) modeling (Borden, 1986a)	85
Table 5.1.a	Comparison of GWSEs for natural gradient flow (NG-GF) modeling, sims. KB-C, KB-P, and KB-K.....	92
Table 5.1.b	Comparison of GWSEs for natural gradient flow (NG-GF) modeling, sims. K-P and K-K	93
Table 5.1.c	Comparison of GWSEs for natural gradient flow (NG-GF) modeling, sims. B-P and B-K	94
Table 5.2	Summary of GWSE comparison for natural gradient flow (NG-GF) modeling	96

Table 5.3	Comparison of chloride concentrations for natural gradient transport (NG-CT) modeling	97
Table 5.4.a	Comparison of natural log chloride concentrations for natural gradient transport (NG-CT) modeling, sims. KB-C, KB-P, and KB-K.....	99
Table 5.4.b	Comparison of natural log chloride concentrations for natural gradient transport (NG-CT) modeling, sims. K-P and K-K	100
Table 5.4.c	Comparison of natural log chloride concentrations for natural gradient transport (NG-CT) modeling, sims. B-P and B-K	101
Table 5.5	Summary of chloride concentration comparison for natural gradient transport (NG-CT) modeling	102
Table 5.6	Comparison of relative drawdown for recovery and injection system flow (RI-GF) modeling	104
Table 5.7	Summary of relative drawdown comparison for recovery and injection system flow (RI-GF) modeling.....	105
Table 5.8	Comparison of recovery efficiency for recovery and injection system transport (RI-CT) modeling	106

INTRODUCTION

Ground water modeling is used extensively to study ground water flow and contaminant transport. In recent years, studies using ground water models have become common in risk assessment, regulatory permitting, and corrective action design. Model predictions are sensitive to several parameters. The choice of representing the spatial variability of aquifer properties in models affects model prediction.

An abandoned creosoting site in Conroe, Texas provides a typical example of a ground water contamination problem. The site was in operation by United Creosoting Company (UCC) from 1946 to 1972 as a wood preserving facility. The wood preserving process generated a great deal of wastewater that was disposed of in two unlined ponds on the property. Ground water contamination is present in the shallow unconfined aquifer underlying the site. The majority of the contamination appears to originate from the two waste disposal ponds. A plume of contaminated ground water is currently migrating in the subsurface of the site. The major organic contaminants in the plume are the polycyclic aromatics found in creosote and pentachlorophenol. The UCC site has been characterized by the National Center for Ground Water Research (NCGWR) at Rice University and the R.S. Kerr Environmental Research Laboratory (RSKERL) of the U.S. Environmental Protection Agency (EPA). Because of the extensive data

compiled at the UCC site, it serves as an ideal situation for studying flow and transport modeling.

The research presented here is primarily concerned with computer-based ground water models. A computer-based ground water model is a mathematical description of flow and transport in a ground water system, coded in a programming language, with the specific aspects of the ground water system it simulates as boundary conditions, initial conditions, and physical aquifer properties (van der Heijde et al., 1988). Ground water modeling is not a new field of study. However, the modeling of ground water systems is more common now than ever before because of trends in regulatory policies and the availability of computational ability.

Modeling is performed in an attempt to simulate what happened, is happening, or will happen. Applications of ground water models include understanding ground water flow systems, predicting contaminant migrations, and making decisions on cleaning contaminated aquifers (Committee on Ground Water Modeling Assessment, 1990). Specifically, transport modeling describes the movement and accumulation of fluid phases and fluid carried substances, such as solute contaminants, in the subsurface (Custodio et al., 1988). When designing a solution to a contamination related threat to public health or environmental protection, an essential part of the decision making process is the ability to predict the consequences of im-

plementing the proposed corrective action (Bear, 1987). The main role of ground water modeling in the regulatory process is long-term prediction of the migration of waste.

Simulation of a ground water system refers to the construction and operation of a model whose behavior assumes the appearance of the actual aquifer behavior (Mercer et al., 1986). The term modeling generally implies mathematical modeling. Mathematical models are solved in one of two approaches. Analytical solutions may be applied to an idealized problem by making simplifying assumptions. When the problem cannot be accurately represented with the simplifications necessary for an analytical solution, then a numerical solution is called for. Numerical solutions can solve the most complex systems, but require the use of a computer.

The research presented here studies methods to represent the spatial variability of aquifer properties. Representations of aquifer properties, such as hydraulic conductivity and bottom elevation, are generated by three methods. Simulations of flow and transport are performed using the various representations of an aquifer property. Information concerning the effect of using each representation is inferred from the comparison of simulation results with observations made at the site. It is hoped that the conclusions based on the simulation of the UCC site will be applicable to a large category of problems in similar environments.

Congress calls for the EPA, other regulatory entities, and the regulated community to achieve certain interrelated goals for the protection of ground water quality (Keely, 1989). Three of these goals are mentioned here. The first goal, as compiled by Keely, is assessment of the probable impact of existing pollution on ground water at points of withdrawal of discharge and is stated in the Safe Drinking Water Act of 1974 & 1986 (SDWA). Another ground water protection goal is the establishment of criteria for location, design, and operation of waste disposal activities to prevent contamination of ground water, or movement of contaminants to points of withdrawal or discharge. This goal is declared in the Resource Conservation and Recovery Act of 1976 (RCRA), and the Hazardous and Solid Waste Amendments of 1984 (HSWA). The third ground water protection goal is the development of remediation technologies that are effective in protecting and restoring ground water quality without being unnecessarily complex or costly and without unduly restricting other land use activities. The third goal is identified in the Comprehensive Environmental Response, Compensation, and Liability Act of 1980 (CERCLA, or commonly called Superfund), and the Superfund Amendments and Reauthorization Act of 1986 (SARA).

Ground water modeling is instrumental in achieving each of these three mentioned goals. Specifically, the first goal is related to risk assessment applications of ground water modeling. The second goal is closely re-

lated to the permitting applications of ground water modeling, and the last goal represents the application of ground water modeling to the design of corrective actions. Since ground water modeling is playing such an ever-increasingly important role, ways of improving the accuracy of model predictions in simulating flow and transport are needed.

The numerical modeling of flow and transport is a subjective task. One common decision is whether to carefully identify and represent the distribution of a spatially correlated aquifer property in a numerical flow or transport model, or to estimate a constant value to represent the aquifer property in the model. The detailed characterization of the distribution of a spatially correlated aquifer property is generally a very difficult and expensive task. If a sense of the type and magnitude of the effects of conducting a detailed investigation on ground water modeling can be attained, a more informed decision can be made whether or not to conduct the detailed investigation and represent the spatial variability of aquifer properties. The problem of representing the spatial variability of aquifer properties has become common since numerical flow and transport models have become readily accessible. However, the problem does not exist when considering most analytical flow and transport models because the analytical solutions seldom allow for the representation of the spatial variability of aquifer properties.

The importance of representing the spatial variability of aquifer properties is dependent on site specific conditions, and is generally not well known. Decisions that are based on predictive models may be very important from both health and financial considerations. In cases where critical decisions are based on simulation predictions, every practical way of improving the accuracy of the simulation should be studied. The research presented here studies only one of many ways of attempting to improve the accuracy of simulations.

The objective of the research presented here is to determine how the representation of the spatial variability of aquifer properties affects ground water flow and contaminant transport modeling at the UCC site. To meet the objective, the methods of representing aquifer properties are studied. Various simulations are performed using representations of aquifer properties. The simulations performed as part of the research presented here have been chosen to provide insight into the effects of using the representations in common modeling situations. Conclusions drawn on the effects of using the representations of aquifer properties may be applicable to other sites.

Ground water modeling can generally be divided into two distinct functions, ground water flow modeling and contaminant transport modeling. Ground water flow modeling is concerned with fluid movement in the porous media. Contaminant transport modeling is concerned with the

movement of contaminants carried along by fluid movement in a porous medium. Transport modeling requires information concerning the flow conditions, and is therefore often applied in conjunction with a flow model.

Two modeling scenarios are selected for study. The modeling scenarios are natural gradient flow and transport and recovery and injection system flow and transport. Natural gradient model generally concerns the long-term migration of contaminants in an aquifer. Recovery and injection system modeling involves the induced effects of a system designed to remediate contaminated ground water.

All aquifer properties are subject to spatial variability. Two aquifer properties that are relatively easy to document and have been shown to have significant effects on flow and transport are hydraulic conductivity and bottom elevation. The hydraulic conductivity of an aquifer medium is a function of several soil and fluid properties. Local and regional variations in hydraulic conductivity can result from the non-uniform deposition of soils and from chemical or physical fouling of the aquifer media. The hydraulic conductivity representation is used by models, along with the saturated thickness, to determine the transmissivity of the aquifer. Local and regional variations in the bottom elevation of an aquifer can result from non-uniform deposition, faulting or slipping, and differential settling of aquifer media. The bottom elevation representation is used by flow models, along with the

hydraulic conductivity information, to determine the transmissivity of the aquifer. Transport models have an additional use for the bottom elevation representation. The bottom elevation, and therefore saturated thickness, is used to calculate the volume of saturated media, and therefore affects the determination of mass present in the system.

Much research has been reported on generating estimates of a spatial aquifer property at unsampled locations. The three methods selected to generate representations of aquifer properties are constant value estimation, polynomial trend surface fitting, and kriging estimation.

The modeling presented here is limited in that it is unique to one particular ground water aquifer, and therefore cannot be used to make predictions directly applicable to other sites. However, general conclusions drawn from the research presented here may offer assistance in making preliminary conceptual decisions when characterizing and modeling other sites possessing similar aquifer properties.

PREVIOUS RESEARCH

Previous research leading to and related to the research presented here has studied the spatial variability of aquifer properties. Also studied are the spatial variability and the generation of representations of aquifer properties. Previous research that studies the effects of representing the spatial variability of aquifer properties on flow and transport modeling is similar to the research presented here, but usually differs in that previous research has generally been done with fabricated or constructed aquifer properties and modeling parameters.

2.1 Variability of Aquifer Properties

Generally, ground water aquifers have been observed to exhibit a high degree of spatial variability. The aquifer properties that are important in hydrogeology, such as hydraulic conductivity and bottom elevation, are all functions of space and are very often highly variable (de Marsily, 1986). However, spatial variability of such aquifer properties is not purely random. de Marsily (1986) describes the variability of aquifer properties by suggesting that if measurements are made at two different locations, the closer the measurements are made to each other, the closer the measured values will be to each other in magnitude. There is a spatial correlation in the distribution of the magnitudes and the expected difference in magnitude is a function of

separation distance. Spatially correlated quantities are called regionalized variables (de Marsily, 1986).

If the hydraulic conductivity of an aquifer is independent of position within a geologic formation, the formation is homogeneous. Whereas, if the hydraulic conductivity of an aquifer is dependent of position within a geologic formation, the formation is heterogeneous. Three types of heterogeneous configurations are layered heterogeneity, discontinuous heterogeneity, and trending heterogeneity (Freeze et al., 1979). Layered heterogeneity is described as individual beds making up a formation each having a relatively homogeneous hydraulic conductivity, but the entire system of beds is heterogeneous. Discontinuous heterogeneity is caused by faults or large-scale contrasts in stratigraphic features. Trending heterogeneity is common in response to the sedimentation processes that create deltas, alluvial fans, and glacial outwash plains. Trending heterogeneity in large formations can attain gradients of 2-3 orders of magnitude in a few miles (Freeze et al., 1979). Previous research has studied the factors influencing the spatial variability of hydraulic conductivity, such as soil physical and chemical properties (Wagenet et al., 1984).

2.2 Characterization of Aquifer Property Variability

If the actual value of an aquifer property is assumed to have a certain single magnitude, then the values of the aquifer property may be described by a probability density function. There is evidence that the probability density function for hydraulic conductivity (K) is log-normal (Freeze et al., 1979). A log-normal distribution for K is one for which a parameter Y , defined as $Y = \ln K$, shows a normal distribution. The observations of bottom elevation are generally assumed to have a normal distribution.

Let x_1, \dots, x_n be the locations of the n points of measurement and x_i denote simultaneously the two coordinates of the point i . Also, let $Z(x_i)$ be the value measured at the point i . The problem of point estimation lies in determining the estimate of the unknown quantity $Z^*(x_o)$ for any point x_o than has not been measured.

The following summary of univariate statistics is adapted from Isaaks et al. (1989). The sample estimate of the mean is

$$\bar{Z} = \frac{1}{n} \sum_{i=1}^n Z(x_i), \quad (2.1)$$

where \bar{Z} is the mean and $Z(x_i)$ are the n individual observations at points x_1, \dots, x_n . The sample estimate of the variance S_Z^2 is

$$S_Z^2 = \frac{1}{n-1} \sum_{i=1}^n [Z(\mathbf{x}_i) - \bar{Z}]^2. \quad (2.2)$$

The distribution of values of an aquifer property assumed to have a spatial correlation may be described by their mean, variance, and correlation length scale. These three parameters do not include information of the spatial structure of the data relative to the observations, but do describe the variability of the spatial structure of the data as a function of the distance from an observation.

A population of spatially variable distributions can be described with an autocorrelation (ρ) function. The autocorrelation function describes how the correlation between any values decays with separation or lag (Domenico et al., 1990; Journel et al., 1978). A lag is simply some constant separation distance h . For example, with lag 1, values being compared are a distance h apart, and with lag 2, values being compared are a distance $2h$ apart, and so on. Although there is flexibility in defining an autocorrelation function, an exponential model used commonly is

$$\rho(h) = \exp\left(\frac{-|h|}{\lambda_p}\right) \quad (2.3)$$

where $\rho(h)$ is the autocorrelation of the population at a separation h (Domenico et al., 1990). The correlation length scale λ_p (or λ_p^x , λ_p^y , and λ_p^z)

for anisotropic media) is the separation at which ρ takes on a value of e^{-1} (approximately 0.37). An example of an exponential autocorrelation function (Equation 2.3) is presented as Figure 2.1.

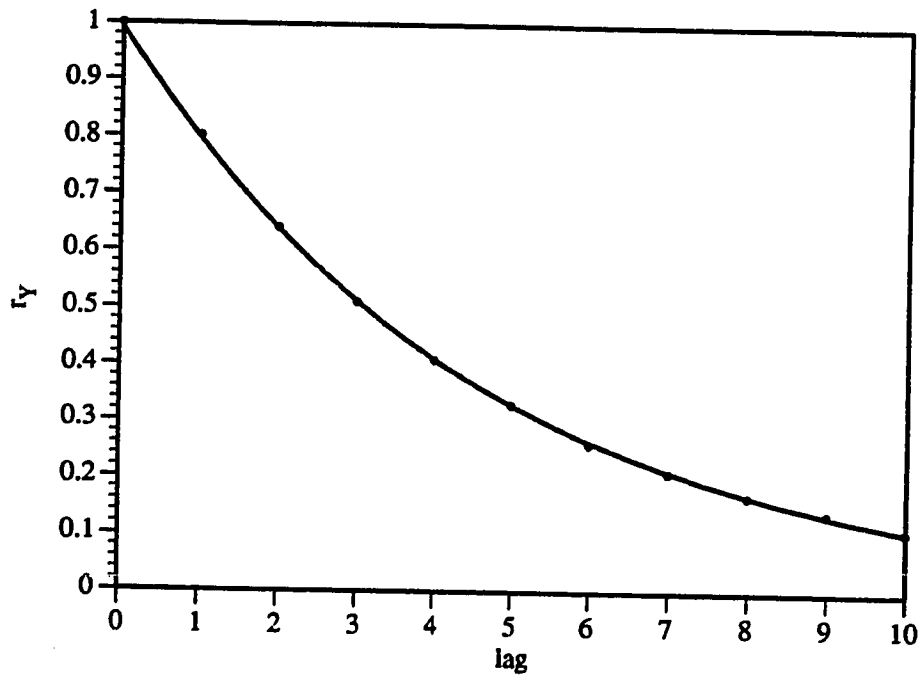


Figure 2.1 Autocorrelation function $r_Y(h)$ verses lag separation

The correlation length scale characterizing the autocorrelation function presented in Figure 2.1 is equal to approximately 4.5 lags. If the lag separation distance used in the calculation of the autocorrelation function was 25 ft, then the correlation length scale is equal to 112.5 ft.

For example, with a finite number of spatially distributed values of natural log hydraulic conductivity, the sample autocorrelation function $r_Z(h)$ can be calculated from pairs of equally spaced data. The sample autocovari-

ance (often simply called the covariance) function $C_Z(h)$ is first needed to calculate the sample autocorrelation function. The sample autocovariance function at a separation h is

$$C_Z(h) = \frac{1}{m} \sum_{i=1}^m [Z(h) - \bar{Z}] [Z(y + h) - \bar{Z}], \quad (2.4)$$

where m is the number of pairs of sample points at a given separation and $Z(h)$ and $Z(y + h)$ are a pair of sample points separated by a given range of distance. The sample autocorrelation function is formed by taking the sample autocovariance function values and dividing by the sample autocovariance function values at a separation of 0, $C_Z(0)$, which is simply the sample variance S_Z^2 . The equation of the autocorrelation function is

$$r_Z(h) = \frac{C_Z(h)}{S_Z^2}. \quad (2.5)$$

For unevenly spaced data, values are grouped into a series of class intervals with the separation distance given by the midpoint of each interval. For example, if considering spatially distributed data, and assuming a lag separation of 25 ft, then all combinations of points closer than 25 ft from each other are considered in the calculation of the autocovariance function at lag 1, all combinations of points farther than 25 ft from each and closer than 50 ft from each other are considered in the calculation of the autocovariance function at lag 2, and so on. The estimation of the correlation length scale is

made by interpolating the value of the lag separation corresponding to where the sample autocorrelation function takes on a value of e^{-1} (approximately 0.37). The correlation length scale is essentially a shape factor for the exponential model. The estimated correlation length scale is the interpolated lag separation multiplied by the separation distance.

2.3 Generation of Representations of Aquifer Properties

Three different methods are used for generating representations of aquifer properties for use in the ground water models. The first method generates a constant representation by constant value estimation. The next method generates a polynomial representation by polynomial trend surface fitting. And the last method generates a kriging representation by kriging estimation.

2.3.1 Constant Representation

Assuming that an aquifer property does not exhibit a spatial correlation, but is a constant value or a random distribution, a constant value estimation of the aquifer property may be the most appropriate means of representing the aquifer property in a model. Three methods of constant value estimation are the arithmetic mean, the harmonic mean, and the geometric mean.

In fluid flow studies, the effective hydraulic conductivity of a stratified sequence is approximated by the arithmetic mean of the hydraulic conductivity within the various strata if the flow is parallel to the strata (Isaaks et al., 1989). The arithmetic mean is the method used to calculate the value of bottom elevation used in the models for simulations requiring a constant representation of bottom elevation.

The geometric mean is an estimate of the expected value of a sample from a log-normal distribution. The use of the geometric mean in ground water modeling studies has been studied by Davis (1987). Davis found that the geometric mean gives accurate, representative hydraulic conductivity values for heterogeneous, permeable media when the distribution of heterogeneity is random or nearly so. The geometric mean is simply the exponential transform of the arithmetic mean of log transformed data and can be calculated directly by

$$Z_G = \exp \left(\frac{1}{n} \sum_{i=1}^n \ln Z(x_i) \right). \quad (2.6)$$

The geometric mean is the method used to calculate the value of hydraulic conductivity to use in the models for simulations requiring a constant representation of hydraulic conductivity.

Another method of calculating a constant representation of observed aquifer properties is the harmonic mean. In fluid flow studies, the effective hydraulic conductivity of a stratified sequence is the harmonic mean of the hydraulic conductivity within the various strata if the flow is perpendicular to the strata (Isaaks et al., 1989). The harmonic mean is simply the inverse transformation of the arithmetic mean of inversely transformed data and can be calculated directly by

$$Z_H = \frac{1}{\frac{1}{n} \sum_{i=1}^n \frac{1}{Z(\mathbf{x}_i)}}. \quad (2.7)$$

2.3.2 Polynomial Representation

On a regional scale, aquifer properties have a relatively regular structure which is amenable to deterministic representation through smooth functions (Kitanidis et al., 1983). One such smooth function is a polynomial trend surface. Polynomial trend surfaces are generalizations to more than one dimension of curve fitting by least squares (Ripley, 1981). Multidimensional generalizations of polynomial regression attempt to fit a function of the form

$$Z^*(\mathbf{x}) = \sum_{r+s \leq p} a^{rs} x_1^r x_2^s \quad (2.8)$$

to the data by least squares. The first few functions generated by Equation 2.8 are

$$a, \quad (2.9)$$

$$a + bx_1 + cx_2, \quad (2.10)$$

$$a + bx_1 + cx_2 + dx_1^2 + ex_1x_2 + fx_2^2, \text{ and} \quad (2.11)$$

$$a + bx_1 + cx_2 + dx_1^2 + ex_1x_2 + fx_2^2 + gx_1^3 + hx_1^2x_2 + ix_1x_2^2 + jx_2^3. \quad (2.12)$$

These functions cover two dimensions and are referred to as flat, linear, quadratic, and cubic respectively. The integer p is the order of the trend surface. There are

$$P = \frac{(p+1)(p+2)}{2} \quad (2.13)$$

coefficients, which are normally chosen to minimize

$$\sum_{i=1}^n [Z(\mathbf{x}_i) - Z^*(\mathbf{x}_i)]^2, \quad (2.14)$$

where $Z^*(\mathbf{x}_i)$ is the value estimated by the polynomial equation at the point \mathbf{x}_i . A zero order trend surface has only one coefficient and provides an

exact solution to only one point. Similarly, a first order trend surface has three coefficients and provides an exact solution to three points, a second order trend surface has six coefficients and provides an exact solution to six points, and a third order trend surface has ten coefficients and provides an exact solution to ten points.

Ripley (1981) describes how to rewrite eqs. 2.8 and 2.14 to make a standard least-squares or multiple regression problem. For example, the arguments $1, x_1, x_2, x_1^2, x_1x_2, x_2^2, \dots$ are labeled as $f_1(\mathbf{x}), \dots, f_P(\mathbf{x})$ and the coefficients a, b, c, d, e, f, \dots are labeled as B_1, \dots, B_P . The problem is now a multiple regression of $Z(\mathbf{x}_i)$ on $f_1(\mathbf{x}_i), \dots, f_P(\mathbf{x}_i)$. The surface may be rewritten as

$$Z(\mathbf{x}) = \mathbf{f}(\mathbf{x})^T \mathbf{B} + r(\mathbf{x}), \quad (2.15)$$

$$\mathbf{f}(\mathbf{x}) = \begin{bmatrix} f_1(\mathbf{x}) \\ \vdots \\ f_P(\mathbf{x}) \end{bmatrix}, \text{ and} \quad (2.16)$$

$$\mathbf{B} = \begin{bmatrix} B_1 \\ \vdots \\ B_P \end{bmatrix} \quad (2.17)$$

where $r(x)$ are the residuals of the polynomial trend surface and observed points. The surface may also be written as

$$\mathbf{Z}_N = \mathbf{F}\mathbf{B} + \mathbf{r}, \quad (2.18)$$

$$\mathbf{Z}_N = \begin{bmatrix} Z(\mathbf{x}_1) \\ \vdots \\ Z(\mathbf{x}_N) \end{bmatrix}. \quad (2.19)$$

$$\mathbf{F} = \begin{bmatrix} \mathbf{f}(\mathbf{x}_1)^T \\ \vdots \\ \mathbf{f}(\mathbf{x}_N)^T \end{bmatrix}, \quad (2.20)$$

$$\mathbf{r} = \begin{bmatrix} r(\mathbf{x}_1) \\ \vdots \\ r(\mathbf{x}_N) \end{bmatrix}. \quad (2.21)$$

Equations 2.15 through 2.21 find an orthogonal matrix \mathbf{Q} and an upper triangular matrix $\tilde{\mathbf{R}}$ so that

$$\mathbf{Q}\mathbf{F} = \mathbf{R} = \begin{bmatrix} \tilde{\mathbf{R}} \\ 0 \end{bmatrix} \quad \mathbf{Q}_{N \times N}, \mathbf{F}_{N \times P}, \tilde{\mathbf{R}}_{P \times P}. \quad (2.22)$$

The least-squares estimate of \mathbf{B} is found by

$$\sum_{i=1}^n [Z(\mathbf{x}_i) - \mathbf{f}(\mathbf{x}_i)^T \mathbf{B}]^2 = (\mathbf{Z}_N - \mathbf{F}\mathbf{B})^T (\mathbf{Z}_N - \mathbf{F}\mathbf{B}) \quad (2.23)$$

$$\sum_{i=1}^n [Z(\mathbf{x}_i) - \mathbf{f}(\mathbf{x}_i)^T \mathbf{B}]^2 = [\mathbf{Q}(\mathbf{Z}_N - \mathbf{F}\mathbf{B})]^T [\mathbf{Q}(\mathbf{Z}_N - \mathbf{F}\mathbf{B})] \quad (2.24)$$

$$\sum_{i=1}^n [Z(\mathbf{x}_i) - \mathbf{f}(\mathbf{x}_i)^T \mathbf{B}]^2 = (\mathbf{Q}\mathbf{Z}_N - \mathbf{R}\mathbf{B})^T (\mathbf{Q}\mathbf{Z}_N - \mathbf{R}\mathbf{B}) \quad (2.25)$$

$$\sum_{i=1}^n [Z(\mathbf{x}_i) - \mathbf{f}(\mathbf{x}_i)^T \mathbf{B}]^2 = \mathbf{Y}_2^T \mathbf{Y}_2 + (\mathbf{Y}_1 - \tilde{\mathbf{R}}\mathbf{B})^T (\mathbf{Y}_1 - \tilde{\mathbf{R}}\mathbf{B}) \quad (2.26)$$

where

$$\mathbf{Q}\mathbf{Z}_N = \begin{bmatrix} \mathbf{Y}_1 \\ \mathbf{Y}_2 \end{bmatrix}, \quad (\mathbf{Y}_1)_{P \times 1}, (\mathbf{Y}_2)_{(N-P) \times 1}. \quad (2.27)$$

The minimum sum of squares occurs when

$$\mathbf{Y}_1 = \tilde{\mathbf{R}}\mathbf{B}, \quad (2.28)$$

therefore

$$\hat{\mathbf{B}} = \tilde{\mathbf{R}}^{-1} \mathbf{Y}_1 \quad (2.29)$$

Since $\tilde{\mathbf{R}}$ is upper triangular, it is easy to solve for the coefficients B_1, \dots, B_P . The equation of the polynomial trend surface is now known and estimates at any point \mathbf{x}_o can be made by

$$Z^*(\mathbf{x}_o) = \mathbf{f}(\mathbf{x}_o)^T \hat{\mathbf{B}}. \quad (2.30)$$

To improve the accuracy of the numerical solution to the multiple regression, it is desirable to transform the x_1 and x_2 coordinates of the observations to a square with sides $[-1, +1]$ to avoid extremely large or small values in $f_i(\mathbf{x})$ (Ripley, 1981).

An undesirable feature of trend surfaces is the tendency to wave the edges to fit points in the center. The wave effect is common in polynomial regression, but is more severe in two or more dimensions where there is more boundary to be affected (Ripley, 1981).

2.3.3 Kriging Representation

There are several commonly used techniques for interpolating spatial data points. Three particular techniques studied by Satkin et al. (1991) are inverse distance squared, linear interpolation, and kriging. Satkin et al. found that kriging is a more robust and provides explicit measures of estimation accuracy. The use of geostatistical techniques such as kriging for estimating aquifer properties has been suggested for years. Different variations of kriging exist (Journel et al., 1978; Journel, 1989; de Marsily, 1986; Peck et al., 1988; Davis, 1986; Isaaks et al., 1989). Other forms of kriging are reviewed and demonstrated by Ahmed et al. (1987). The form presented here is ordinary kriging.

Ordinary kriging is a statistical interpolation method that chooses the best linear unbiased estimator (BLUE) for the variable in question. It is called linear because its estimates are weighted linear combinations of the available data. It is called unbiased because the mean estimation error $\bar{\epsilon}$ is equal to zero. It is called best because it minimizes the theoretical variance.

The variable is assumed to be a random function whose spatial correlation (structure) is defined by a variogram, which is a measure of the change in the variable with changes in distance. Higher correlation between measured points is expected for small separation distances. Kriging is different from other interpolation methods because it considers the spatial structure of the variable and provides an estimate of the interpolation error in the form of the standard deviation of the kriged values. Such error estimates are needed when assigning plausible ranges of aquifer property values prior to model calibration. Kriging also preserves the field value at measurement points, unlike some other interpolations schemes such as least-squares fitting of a polynomial.

An important concern for users of the kriging technique is the effect of the sample size on the precision of estimates obtained. Hughes et al. (1981) suggest that for sample sizes of less than approximately 50, kriging offered no clear advantage over other methods. However, kriging estimates are less variable. A smaller variance, and therefore fewer estimates that

differ greatly from the observations is desirable from the standpoint of maintaining physically reasonable estimates of aquifer properties.

The kriging process is presented in numerous places (Journel et al., 1978; Journel, 1989; de Marsily, 1986; Peck et al., 1988; Davis, 1986; Isaaks et al., 1989}. The ordinary kriging process, as presented by Peck et al. (1988) is presented here.

The estimated value $Z^*(\mathbf{x}_o)$ at a point \mathbf{x}_o is a weighted linear combination of the available known samples $Z(\mathbf{x}_i)$

$$Z^*(\mathbf{x}_o) = \sum_{i=1}^n \lambda_{\mathbf{x}_o}^i Z(\mathbf{x}_i). \quad (2.31)$$

At any point \mathbf{x}_o there are i weights λ . These weights are the unknowns of the problem and depend on both the point \mathbf{x}_o to be estimated and the measurement points \mathbf{x}_i . The set of weights changes for every position \mathbf{x}_o .

Two conditions will permit the calculations of the weighting factors λ . The first condition is that the mathematical expectation of $Z^*(\mathbf{x}_o)$ be equal to that of the true $Z(\mathbf{x}_o)$

$$E[Z(\mathbf{x}_o)] = E[Z^*(\mathbf{x}_o)] \quad (2.32)$$

or

$$E[Z^*(\mathbf{x}_o) - Z(\mathbf{x}_o)] = 0. \quad (2.33)$$

The first condition forces the estimator to be unbiased. By substituting Equation 2.31 into Equation 2.32,

$$E[Z(\mathbf{x}_o)] = E\left[\sum_{i=1}^n \lambda_{\mathbf{x}_o}^i Z(\mathbf{x}_i)\right], \quad (2.34)$$

$$E[Z(\mathbf{x}_o)] = \sum_{i=1}^n \lambda_{\mathbf{x}_o}^i E[Z(\mathbf{x}_i)], \quad (2.35)$$

and therefore

$$\sum_{i=1}^n \lambda_{\mathbf{x}_o}^i = 1. \quad (2.36)$$

We now determine the set of weights $\lambda_{\mathbf{x}_o}^i$ by imposing the second condition that the error of estimation be minimal

$$\min. E[Z^*(\mathbf{x}_o) - Z(\mathbf{x}_o)]^2 \quad (2.37)$$

and therefore

$$\min. \text{var}[Z^*(\mathbf{x}_o) - Z(\mathbf{x}_o)] \quad (2.38)$$

since $E[Z^*(\mathbf{x}_o) - Z(\mathbf{x}_o)] = 0$. The function to be minimized, Equation 2.38, can be written as

$$E \{ [Z^*(\mathbf{x}_o) - Z(\mathbf{x}_o)]^2 \} = E \left\{ \left\{ \sum_{i=1}^n \lambda_{\mathbf{x}_o}^i [Z(\mathbf{x}_i) - Z(\mathbf{x}_o)] \right\}^2 \right\} \quad (2.39)$$

$$E \{ [Z^*(\mathbf{x}_o) - Z(\mathbf{x}_o)]^2 \} = E \left\{ \sum_{i=1}^n \lambda_{\mathbf{x}_o}^i [Z(\mathbf{x}_i) - Z(\mathbf{x}_o)] \sum_{j=1}^n \lambda_{\mathbf{x}_o}^j [Z(\mathbf{x}_j) - Z(\mathbf{x}_o)] \right. \\ \left. - \sum_{i=1}^n \sum_{j=1}^n \lambda_{\mathbf{x}_o}^i \lambda_{\mathbf{x}_o}^j E \{ [Z(\mathbf{x}_i) - Z(\mathbf{x}_o)][Z(\mathbf{x}_j) - Z(\mathbf{x}_o)] \} \right\} \quad (2.40)$$

The definition of the variogram is needed

$$\gamma(\mathbf{x}_i - \mathbf{x}_j) = \frac{1}{2} E \{ [Z(\mathbf{x}_i) - Z(\mathbf{x}_j)]^2 \} \quad (2.41)$$

$$\gamma(\mathbf{x}_i - \mathbf{x}_j) = \frac{1}{2} \left\{ \{ [Z(\mathbf{x}_i) - Z(\mathbf{x}_o)] - [Z(\mathbf{x}_j) - Z(\mathbf{x}_o)] \}^2 \right\} \quad (2.42)$$

$$\gamma(\mathbf{x}_i - \mathbf{x}_j) = \frac{1}{2} E \{ [Z(\mathbf{x}_i) - Z(\mathbf{x}_o)]^2 \} + \frac{1}{2} E \{ [Z(\mathbf{x}_j) - Z(\mathbf{x}_o)]^2 \} \\ - E \{ [Z(\mathbf{x}_i) - Z(\mathbf{x}_o)][Z(\mathbf{x}_j) - Z(\mathbf{x}_o)] \} \quad (2.43)$$

$$\gamma(\mathbf{x}_i - \mathbf{x}_j) = \gamma(\mathbf{x}_i - \mathbf{x}_o) + \gamma(\mathbf{x}_j - \mathbf{x}_o) \\ - E \{ [Z(\mathbf{x}_i) - Z(\mathbf{x}_o)][Z(\mathbf{x}_j) - Z(\mathbf{x}_o)] \} \quad (2.44)$$

The variogram $\gamma(\mathbf{x}_i - \mathbf{x}_j)$ is commonly called the semi-variogram. It is related to the autocovariance function $C_Z(h)$ by subtracting the sample variance S_Z^2 , which is commonly called the sill value

$$\gamma(\mathbf{x}_i - \mathbf{x}_j) = S_Z^2 - C_Z(h). \quad (2.45)$$

From Equation 2.44 the mathematical expectation needed in Equation 2.40 can be calculated. By substitution

$$\begin{aligned} E\{[Z^*(\mathbf{x}_o) - Z(\mathbf{x}_o)]^2\} &= -\sum_{i=1}^n \sum_{j=1}^n \lambda_{\mathbf{x}_o}^i \lambda_{\mathbf{x}_o}^j \gamma(\mathbf{x}_i - \mathbf{x}_j) \\ &\quad + \sum_{i=1}^n \sum_{j=1}^n \lambda_{\mathbf{x}_o}^i \lambda_{\mathbf{x}_o}^j \gamma(\mathbf{x}_i - \mathbf{x}_o) \\ &\quad + \sum_{i=1}^n \sum_{j=1}^n \lambda_{\mathbf{x}_o}^i \lambda_{\mathbf{x}_o}^j \gamma(\mathbf{x}_j - \mathbf{x}_o) \end{aligned} \quad (2.46)$$

Equation 2.46 may be simplified to

$$\begin{aligned} E\{[Z^*(\mathbf{x}_o) - Z(\mathbf{x}_o)]^2\} &= -\sum_{i=1}^n \sum_{j=1}^n \lambda_{\mathbf{x}_o}^i \lambda_{\mathbf{x}_o}^j \gamma(\mathbf{x}_i - \mathbf{x}_j) \\ &\quad + \sum_{i=1}^n \lambda_{\mathbf{x}_o}^i \gamma(\mathbf{x}_i - \mathbf{x}_o) + \sum_{j=1}^n \lambda_{\mathbf{x}_o}^j \gamma(\mathbf{x}_j - \mathbf{x}_o) \end{aligned} \quad (2.47)$$

since

$$\sum_{i=1}^n \lambda_{\mathbf{x}_o}^i = \sum_{j=1}^n \lambda_{\mathbf{x}_o}^j = 1. \quad (2.48)$$

Equation 2.47 can further be simplified to

$$\begin{aligned} E\{[Z^*(\mathbf{x}_o) - Z(\mathbf{x}_o)]^2\} &= -\sum_{i=1}^n \sum_{j=1}^n \lambda_{\mathbf{x}_o}^i \lambda_{\mathbf{x}_o}^j \gamma(\mathbf{x}_i - \mathbf{x}_j) \\ &\quad + 2 \sum_{i=1}^n \lambda_{\mathbf{x}_o}^i \gamma(\mathbf{x}_i - \mathbf{x}_o) \end{aligned} \quad (2.49)$$

since

$$\sum_{i=1}^n \lambda_{\mathbf{x}_o}^i \gamma(\mathbf{x}_i - \mathbf{x}_o) = \sum_{j=1}^n \lambda_{\mathbf{x}_o}^j \gamma(\mathbf{x}_j - \mathbf{x}_o) \quad (2.50)$$

The minimization of Equation 2.49, subject to the linear constraint of Equation 2.34 is found by using the method of Lagrange multipliers. The expression

$$\frac{1}{2} E\{[Z^*(\mathbf{x}_o) - Z(\mathbf{x}_o)]^2\} - \mu \left[\sum_{i=1}^n \lambda_{\mathbf{x}_o}^i - 1 \right] \quad (2.51)$$

is minimized where μ is a new unknown, called a Lagrange multiplier, which is added to the n previous unknowns $\lambda_{\mathbf{x}_o}^i$. By substituting Equation 2.49 into Equation 2.51 and equating to zero the partial derivatives with respect to $\lambda_{\mathbf{x}_o}^i$ and μ , a linear system is formed

$$\left. \begin{aligned} \sum_{j=1}^n \lambda_{\mathbf{x}_o}^i \gamma(\mathbf{x}_i - \mathbf{x}_j) + \mu &= \gamma(\mathbf{x}_i - \mathbf{x}_o) \\ \sum_{i=1}^n \lambda_{\mathbf{x}_o}^i &= 1. \end{aligned} \right\} \quad i = 1, \dots, n \quad (2.52)$$

The complete linear system of kriging may be written in matrix form

$$\begin{bmatrix} 0 & \gamma_{12} & \dots & \gamma_{1n} & 1 \\ \gamma_{21} & 0 & \dots & \gamma_{2n} & 1 \\ \cdot & \cdot & \dots & \cdot & \cdot \\ \cdot & \cdot & \dots & \cdot & \cdot \\ \gamma_{n1} & \gamma_{n2} & \dots & 0 & 1 \\ 1 & 1 & \dots & 1 & 0 \end{bmatrix} \begin{bmatrix} \lambda_{\mathbf{x}_o}^1 \\ \lambda_{\mathbf{x}_o}^2 \\ \cdot \\ \cdot \\ \lambda_{\mathbf{x}_o}^n \\ 0 \end{bmatrix} = \begin{bmatrix} \gamma_{10} \\ \gamma_{20} \\ \cdot \\ \cdot \\ \gamma_{n0} \\ 1 \end{bmatrix} \quad (2.53)$$

with γ_{ij} denoting $\gamma(\mathbf{x}_i - \mathbf{x}_j)$. The diagonal is zero since

$$\gamma_{ii} = \gamma(\mathbf{x}_i - \mathbf{x}_i) \quad (2.54)$$

$$\gamma_{ii} = \gamma(0) \quad (2.55)$$

$$\gamma_{ii} = 0. \quad (2.56)$$

The matrix on the left of Equation 2.53 only needs to be inverted once for all points \mathbf{x}_o .

2.3.4 Tests of Goodness of Fit

Given a set of estimates at several locations, it is natural to compare their distribution to the distribution of the true values at the same locations. We would like the distribution of the estimated values to be similar to the distribution of true values. It is expected that the estimate $Z^*(\mathbf{x}_i)$ will differ somewhat from the true value $Z(\mathbf{x}_i)$ by an amount called the estimation error, $r(\mathbf{x}_i)$, also referred to as the residual (Isaaks et al., 1989)

$$r(\mathbf{x}_i) = Z^*(\mathbf{x}_i) - Z(\mathbf{x}_i). \quad (2.57)$$

A measure of the estimated value's match to the observed values is the mean estimation error, \bar{r}

$$\bar{r} = \frac{1}{n} \sum_{i=1}^n r(\mathbf{x}_i). \quad (2.58)$$

A positive or negative mean of the residuals reflects a general tendency toward overestimation or underestimation, respectively. The mean of the estimation error distribution is often referred to as the bias (Isaaks et al., 1989).

Even though the mean estimation error may be zero, the estimates may scatter wildly about the correct values. The scatter can be expressed as the estimation error variance, \bar{S}_r^2

$$S_r^2 = \frac{1}{n-1} \sum_{i=1}^n [r(\mathbf{x}_i) - \bar{r}]^2. \quad (2.59)$$

The estimation error variance is the same sort of variance that Equation 2.2 represents, except that Equation 2.59 is the variance of the estimation errors, and Equation 2.2 is the variance of either the estimated values or the observed values. The square root of the estimation error variance is called the standard error of the estimate.

A summary statistic that incorporates both the bias and the spread of the estimation error distribution is the mean squared error,

$$MSE = \frac{1}{n} \sum_{i=1}^n r(\mathbf{x}_i)^2. \quad (2.60)$$

The *MSE* can be related to the other statistics of the estimation error distribution,

$$MSE = S_r^2 + \bar{r}^2. \quad (2.61)$$

The *MSE* is often reported as the root mean squared error, *RMSE*

$$RMSE = \sqrt{MSE}. \quad (2.62)$$

Use of the *RMSE* as a measure of correlation between simulated results and observations is common (Haselow et al., 1991; Weston, 1985).

2.4 Effects of Spatial Variability on Modeling

The representation of an aquifer property affects flow and transport modeling results. The degree to which the modeling results are affected is a function of the relative change in the aquifer property observed and the scale at which the change is observed. For example, the spatial variability of an aquifer having a saturated thickness decreasing from 30 ft to 10 ft over 500 ft has a greater effect on the flow and transport than would the spatial variability of an aquifer having a saturated thickness decreasing from 200 ft to 180 ft over the same distance. The relative change in saturated thickness is the parameter of concern.

Anderson (1987) states that the importance of geologic heterogeneity in controlling flow is widely recognized, but development of ways for defining heterogeneity in the field and for incorporating geologic information into flow and transport models is a new area of research (Anderson, 1987). Anderson performed numerical experiments involving flow through a two-dimensional graded bed system viewed at three different scales of heterogeneity and flow through a system viewed under different interpretations of the heterogeneity pattern and under two different flow regimes. One conclusion drawn from these experiments suggests that for flow modeling, the scale at which heterogeneity is simulated should match the measurement scale used to obtain the field heads that serve as the calibration standard.

Another conclusion directly related to the research presented here is that the sensitivity of a model to representations of heterogeneity depends on the boundary conditions. Perhaps the most profound conclusion is that proper treatment of large scale heterogeneity patterns and trends in the hydraulic conductivity distribution is critical to obtaining an accurate representation of the flow field and accurate flow estimates. The experiments by Anderson (1987) primarily differ from the research presented here in that Anderson's research was calibrated to a flow system constructed in the laboratory and the research presented here is calibrated to field observations at an actual site. Another difference is that Anderson's research used a vertical hydraulic conductivity distribution constructed for the experiments and the research presented here uses representations of hydraulic conductivity generated from sparse observations.

Laboratory experiments on dispersion of miscible fluids in a porous medium have been performed by Haselow et al. (1991). Haselow et al. packed two-dimensional models with both homogeneous and idealized heterogeneous hydraulic conductivity distributions. The results of these experiments indicate that the inclusion of hydraulic conductivity differing from the surrounding medium could result in both Gaussian and non-Gaussian tracer distributions depending upon the location of the inclusion, and sys-

tems with heterogeneous permeability distributions sometimes resulted in dispersion similar to that for homogeneous media.

AQUIFER PROPERTIES

A field site is selected to serve as a practical modeling application and provide realistic data. The previously documented observed aquifer properties were compiled and reviewed for integrity. Representations of the spatial variability of aquifer properties are generated from the spatial distribution of observations. The representations are generated specifically for the purpose of incorporating into ground water flow and contaminant transport models.

3.1 Field Site

The research presented here models the ground water flow and contaminant transport at the UCC site in Conroe, Texas. The city of Conroe lies about 100 miles from the Gulf of Mexico in Montgomery County. The UCC site is an abandoned wood treatment facility that has been studied by the NCGWR and the RSKERL since 1982. The United Creosoting Company operated a wood preservation facility in from 1946 to 1972. In the summer of 1972, the facility was closed and the major equipment removed. The wood treatment facilities were decommissioned and demolished prior to 1975. While in operation, the UCC used a pressurized treatment process in which pentachlorophenol (PCP) and creosote were added into lumber such as telephone poles and railroad ties. Two large ponds were used to treat or

dispose of waste materials (Weston, 1985). A site plan showing the property boundary and waste pond locations is presented as Figure 3.1.

Between 1972 and 1977 the land was subdivided and sold for use by the Conroe Construction Company and for development of the Tanglewood East residential subdivision. An inspection of the site by the Texas Department of Water Resources (TDWR) (presently called the Texas Water Commission) in July 1977 revealed that the Tanglewood East residential subdivision was being constructed on the western portion of the former UCC property. The inspection also revealed that the former waste ponds had been drained and were being back-filled in 1975 (Weston, 1985).

During the summer of 1980, citizens complained of creosote odors from soils obtained at the site and used on various road projects around Montgomery County. On the basis of these complaints, a site investigation was conducted in 1981. Three ground water monitoring wells were installed and soil and ground water samples taken. Soils from the former waste ponds were found to be contaminated with PCP. Further studies at the site indicated extensive soil contamination within the former waste pond area and the existence of a plume of contaminated ground water originating from the region of the former waste ponds. The site was placed on the CERCLA National Priorities List (NPL) on September 1, 1983. A site investigation was begun by TDWR in 1984 (Weston, 1985).

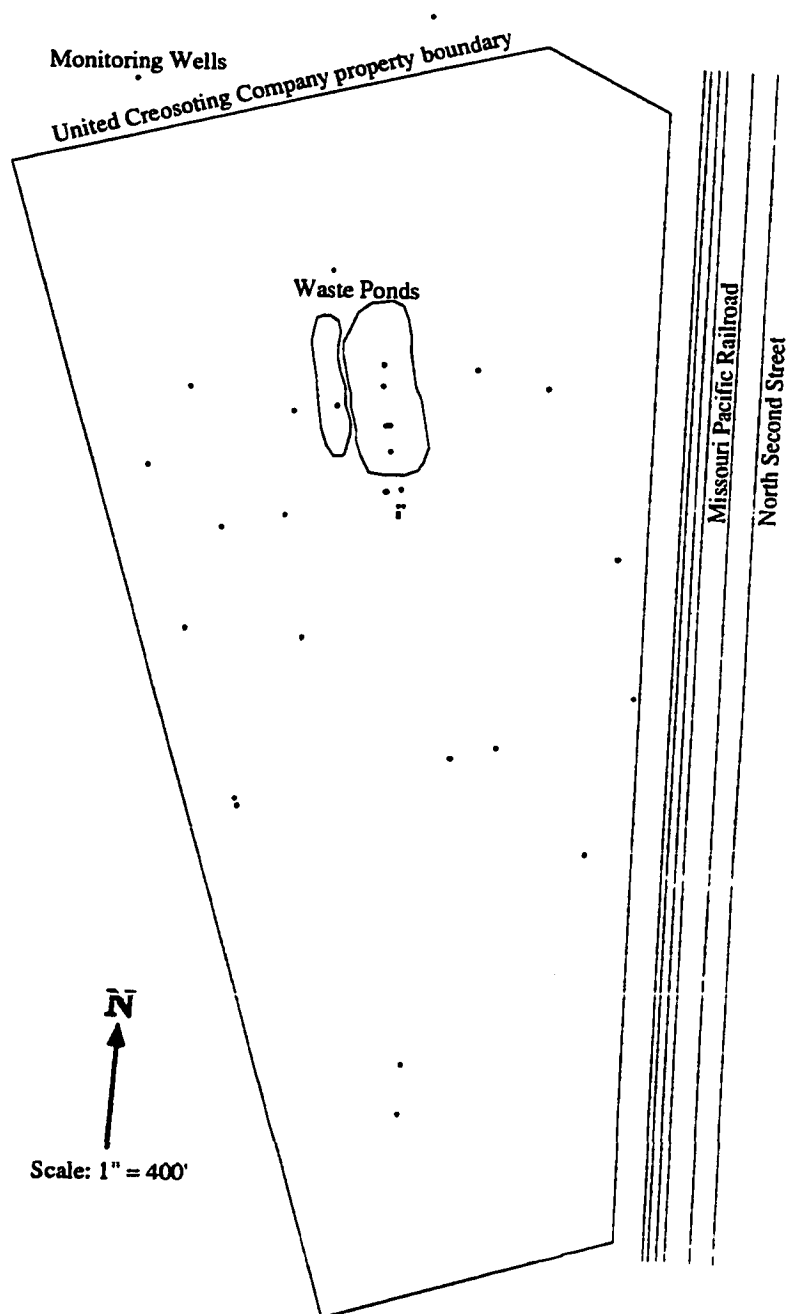


Figure 3.1 Site plan (Weston, 1985)

The chemicals used in wood preservation at the UCC site were PCP and creosote. Creosote was produced at the UCC site in a coal tar distillation unit. Destructive distillation of coal tar yields creosote and other distillate fractions which contain polynuclear aromatic organic compounds of varying molecular weights. Naphthalene is one of the polynuclear aromatic organic compounds produced. Also produced is a dark brown to black amorphous residue known as pitch. The coal tar pitch is an unusable process by-product which was probably disposed of in the larger of two waste ponds (Weston, 1985).

Past research at the site has been aimed at characterizing the major physical, chemical and biological processes affecting the transport and fate of organic contaminants in ground water (Borden, 1986a). An initial site characterization was performed by NCGWR and included sampling soils and water quality at 35 boreholes and 14 monitoring wells (Bedient, 1984). Results from six sampling events over two years showed wells around the site possessed naphthalene concentrations above 800 $\mu\text{g/l}$. Conservative constituents, traced by chloride concentrations up to 75 mg/l, were shown to have migrated approximately 300 ft downgradient of the site. Organic contaminants had been adsorbed and microbially degraded in their migration from the waste source as evidenced by their attenuated concentrations. Detailed field pump tests had been performed to evaluate hydraulic conduc-

tivity at several of the shallow wells. The U.S. Geological Survey solute transport model (Konikow et al., 1978) had been used to predict chloride plume patterns and evaluate parameters which govern transport processes at the site (Bedient, 1984).

The NCGWR at Rice University continued studies at the UCC site aimed at developing mathematical models for simulating the degradation processes affecting the transport and biodegradation of dissolved hydrocarbons (Borden et al., 1986). Hydrocarbon transport and degradation at the site is simulated where oxygen-limited biodegradation is known to occur. The studies by the NGWMC hydrologically and microbiologically characterized the site. Bedient et al. (1984) described the site geology, hydrology, and the major contaminants present. Lee et al. (1984b) and Wilson et al. (1985) have characterized the subsurface microbiology using sterilized sampling techniques and provided estimates of the rates of microbial degradation. Organic hydrocarbons were also determined to be present at substantial concentrations and have been shown to be nonlimiting for biotransformation (Bedient et al., 1984; Lee et al., 1984a). A three well injection-production test was performed at the UCC site to estimate the effective in situ retardation factors for adsorption and to evaluate the significance of biotransformation in the transport of contaminants (Borden et al., 1987). The results sug-

gested that biotransformation is the major process limiting the transport of naphthalene and similar compounds at the UCC site.

3.2 Site Hydrogeology

The site is underlain by unconsolidated sediments (sand, gravel, and clay) in alluvial fan deposits. The shallow water bearing zone at the UCC site consists of a shallow unconfined zone which is sometimes horizontally subdivided by silty clays so as to create several localized semi-confined zones found at lower elevations. The silty clay unit which separates the shallow water bearing zone into unconfined and semi-confined strata is discontinuous across the site. The dip of the shallow water bearing zone is consistent with regional trends, but below the site it varies in thickness and elevation over short distances. The complex interbedding of sand, silt, and clay, responsible for the rapid changes in thickness and elevation, are the product of deposition within a fluvial-deltaic system controlled by swift temporal and lateral variations (Weston, 1985).

A network of 34 monitoring wells is present at the site. Approximately half of the wells were installed by the NCGWR, a few were installed by the TDWR, and the others were installed by Weston. The wells (and associated well borings) provide information concerning the soil strata, ground water surface elevation (GWSE), soil and ground water quality, and

aquifer flow properties. Observations of hydraulic conductivity and bottom elevation were collected at several of the monitoring wells by Weston in 1985.

A coordinate system aligned with the eastern site property boundary is established at the site and used for documenting the location of each monitoring well and is referred to as the site coordinate system. The primary directions of the site coordinate system are site North and site East. A modified coordinate system is established to facilitate the model grid construction and is referred to as the grid coordinate system. The orientation of the grid coordinate system is described later. The primary directions of the grid coordinate system are grid north and grid east. A plan view of the existing monitoring well locations is shown in Figure 3.2. The scale of Figure 3.2 (approx. 1" = 300') is slightly larger than the scale of Figure 3.1 (approx. 1" = 400'). The coordinates of the existing monitoring wells are presented in Table 3.1.

Observed values of hydraulic conductivity are obtained by analyzing aquifer hydraulic test data for several of the monitoring wells. The aquifer tests were performed during the initial site investigation (Weston, 1985). The results of the analysis of the aquifer tests are presented later in the comparison of the representations of hydraulic conductivity to observations of

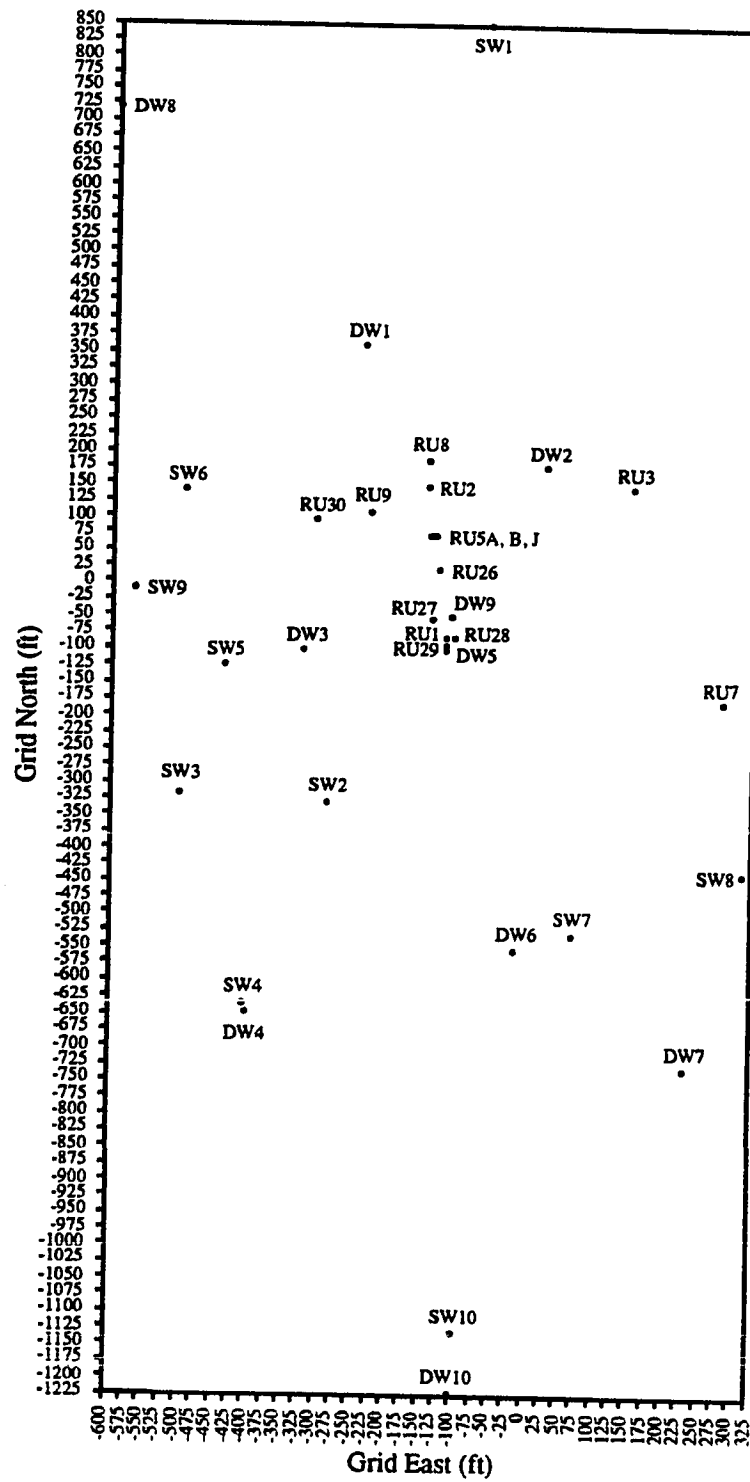


Figure 3.2 Monitoring well locations (Weston, 1985)

Well ID	Site North (ft)	Site East (ft)	Grid North (ft)	Grid East (ft)	Row	Col.
SW1	846.70	38.90	845.39	-61.04	1	22
SW2	-294.80	-319.40	-330.35	-282.48	48	13
SW3	-260.00	-530.00	-320.58	-495.71	47	5
SW4	-584.70	-476.30	-636.70	-404.16	60	8
SW5	-76.00	-446.20	-127.99	-434.15	40	7
SW6	193.10	-474.30	135.93	-493.73	29	5
SW7	-536.57	7.86	-531.91	70.97	56	27
SW8	-471.32	263.16	-437.07	316.81	52	37
SW9	54.49	-562.74	-12.13	-565.24	35	2
SW10	-1114.66	-225.62	-1133.47	-92.84	80	21
RU1	-80.00	-125.00	-94.16	-114.71	38	20
RU2	160.00	-125.00	144.17	-142.96	29	19
RU3	125.00	170.00	144.14	154.10	29	31
RU5A	87.00	-120.00	72.27	-129.41	32	19
RU5B	87.00	-125.00	71.68	-134.37	32	19
RU5J	87.00	-130.00	71.09	-139.34	32	19
RU7	-210.00	260.00	-177.94	282.91	42	36
RU8	200.00	-120.00	184.48	-142.71	27	19
RU9	130.00	-210.00	104.38	-223.84	30	16
RU26	33.00	-125.00	18.06	-128.02	34	19
RU27	-40.00	-140.00	-56.20	-134.32	37	19
RU28	-70.00	-125.00	-84.23	-115.89	38	20
RU29	-90.00	-125.00	-104.09	-113.54	39	20
RU30	130.00	-290.00	94.96	-303.29	31	12
DW1	384.90	-193.00	359.51	-236.97	20	15
DW2	173.10	50.00	177.78	29.28	27	26
DW3	-65.80	-331.20	-104.33	-321.15	39	12
DW4	-600.00	-473.10	-651.52	-399.18	61	9
DW5	-68.96	-110.00	-81.43	-101.12	38	20
DW6	-550.00	-75.00	-555.00	-9.74	57	24
DW7	-756.30	145.00	-733.97	233.02	64	34
DW8	779.57	-507.85	714.37	-596.08	6	1
DW9	-40.00	-110.00	-52.67	-104.53	37	20
DW10	-1204.24	-239.96	-1224.11	-96.54	83	21
Site	Coordinate system established at the site (Weston, 1985)					
Grid	Coordinate system aligned with the general direction of ground water flow					

Table 3.1 Monitoring well locations

hydraulic conductivity. The univariate statistics for observed natural log hydraulic conductivity are presented in Table 3.2. Observed values of bottom elevation are obtained from interpreting the drilling logs of several of

	ln(K)		BE	
Number	11	dim.	25	dim.
Mean	0.4	ln(ft/day)	198.94	ft MSL
Variance	2.1	ln(ft/day) ²	47.41	ft ²
Minimum	-2.7	ln(ft/day)	176.84	ft MSL
25th percentile	-0.5	ln(ft/day)	196.69	ft MSL
Median	0.6	ln(ft/day)	200.28	ft MSL
50th percentile	1.0	ln(ft/day)	212.19	ft MSL
Maximum	3.0	ln(ft/day)	214.77	ft MSL
ln(K)	Natural log hydraulic conductivity			
BE	Bottom elevation			

Table 3.2 Univariate statistics of the observed aquifer properties

the monitoring wells. The monitoring well drilling logs are documented in the initial site investigation (Weston, 1985). The results of the analysis of the drilling logs are presented later in the comparison of the representations of bottom elevation to observations of bottom elevation. The univariate statistics for the observed values of bottom elevation are presented in Table 3.2.

3.3 Representations of Aquifer Properties

Representations of aquifer properties are generated at each cell of a model grid. The representations of aquifer properties generated are for hydraulic conductivity and bottom elevation.

3.3.1 Hydraulic Conductivity Representations

Each cell of a model requires a reasonable representative value of hydraulic conductivity. A constant representation, polynomial representation, and kriging representation of values of natural log hydraulic conductivity are generated.

The constant value estimate of hydraulic conductivity for the aquifer is 1.49 ft/day. The geometric mean of the 11 aquifer tests results is used to derive the constant value estimate. The geometric mean of the 11 aquifer tests results is 0.4 ln(ft/day). The notation “ln(ft/day)” indicates that the measurement units of the log transformed hydraulic conductivity are ft/day. A comparison of observed natural log hydraulic conductivity to the constant representation is presented in Table 3.3.

The polynomial representation of hydraulic conductivity for the aquifer is generated using a second order polynomial function. A computer code called TrendSurface (RockWare, 1990) is used to perform the calculations to fit a second order polynomial function to the observed hydraulic conductivity data. A second order polynomial function is used because it is the highest order polynomial function that maintained stability in regions where control points are scarce. The *RMSE* of the polynomial representation is lower than the *RMSE* of the constant representation. A comparison of the

Well ID	Obs. ln(K) ln(ft/day)	C ln(K) ln(ft/day)	P ln(K) ln(ft/day)	K ln(K) ln(ft/day)	C _r ln(ft/day)	P _r ln(ft/day)	K _r ln(ft/day)
SW1	3.0	0.4	3.2	2.7	2.6	-0.2	0.3
SW2	-2.7	0.4	-0.5	-1.7	-3.1	-2.2	-1.0
SW3	0.6	0.4	0.6	0.4	0.2	0.0	0.2
SW4	1.0	0.4	0.2	0.7	0.6	0.8	0.3
SW5	0.9	0.4	0.4	0.6	0.5	0.5	0.3
SW7	-0.6	0.4	-1.0	-0.6	-1.0	0.4	0.0
SW8	-0.5	0.4	-0.4	-0.5	-0.9	-0.1	0.0
SW9	1.4	0.4	1.5	1.3	1.0	-0.1	0.1
SW10	0.3	0.4	0.3	0.4	-0.1	0.0	-0.1
RU2	1.1	0.4	-0.1	0.9	0.7	1.2	0.2
RU3	-0.2	0.4	0.0	0.0	-0.6	-0.2	-0.2
<i>RMSE</i>					1.4	0.8	0.4
Obs.	Observed natural log hydraulic conductivity (Weston, 1985)						
C	Constant representation of natural log hydraulic conductivity						
P	Polynomial representation of natural log hydraulic conductivity						
K	Kriging representation of natural log hydraulic conductivity						
ln(K)	Natural log hydraulic conductivity						
_r	Estimation error						
<i>RMSE</i>	Root mean squared error						

Table 3.3 Comparison of hydraulic conductivity representations

observed values of hydraulic conductivity to the polynomial representation at a location corresponding to the location of each observation is presented in Table 3.3. The greatest estimation error occurs at monitoring well SW2, where the minimum observed value is recorded. The polynomial trend surface was not able to conform to the extreme observed value at SW2, which is located in the interior of the domain and in the center of several other control points. A scatter plot of the polynomial representation of hydraulic conductivity verses the estimation error of each estimated value is presented as Figure 3.3. The point with greatest estimation error can be observed in

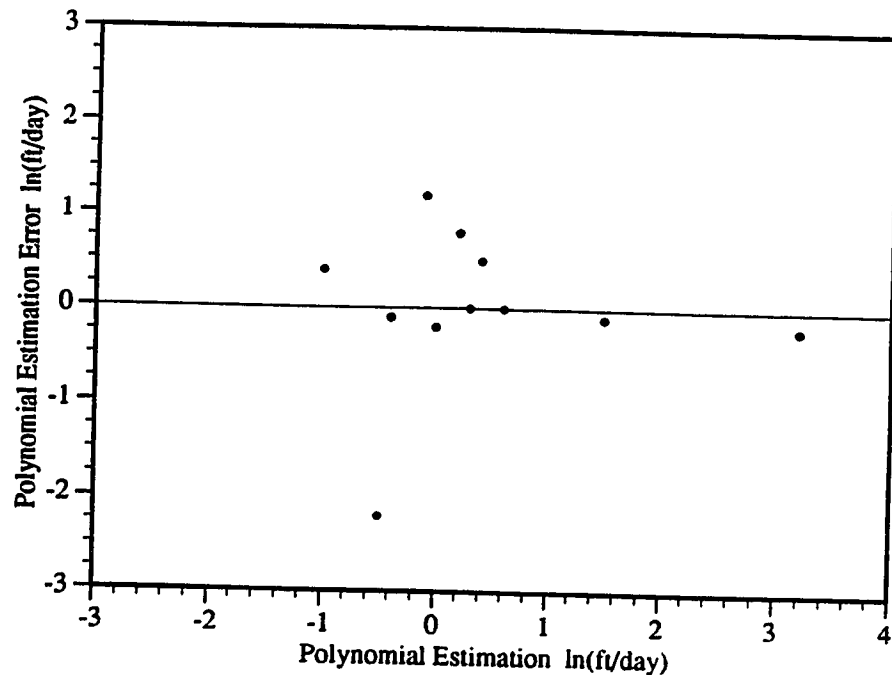


Figure 3.3 Polynomial representation verses estimation error for hydraulic conductivity

the scatter plot of the observed values of hydraulic conductivity verses the polynomial representation, presented as Figure 3.4. A contour plot of the resulting polynomial hydraulic conductivity representation is presented as Figure 3.5.

The contour plot of the polynomial hydraulic conductivity representation shows an apparent “bowl” shape. The minimum estimated values of hydraulic conductivity, analogous to the “bottom” of the “bowl,” appear in the region of monitoring well SW7 (see figs. 3.2 and 3.5). The estimated values of hydraulic conductivity approach unreasonably high values in the four corners of the region of estimated values. In the region of greatest

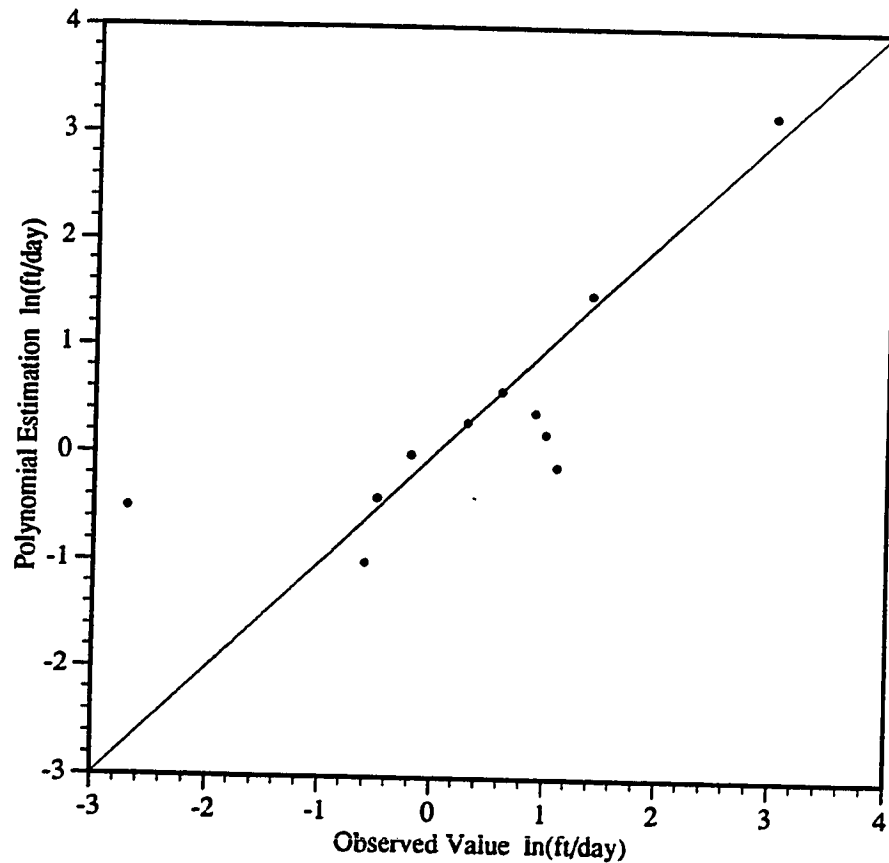


Figure 3.4 Observed values versus polynomial representation for hydraulic conductivity

concern, near the waste ponds (see Figure 3.1), the estimated values of hydraulic conductivity generally slope from greater values to smaller values, moving from northwest to southeast (see Figure 3.5).

The kriging representation of hydraulic conductivity for the aquifer is generated using ordinary block kriging. A computer code called KRIGE, which is part of the geostatistical environmental assessment software package Geo-EAS (Englund et al., 1991), is used to perform the calculations of

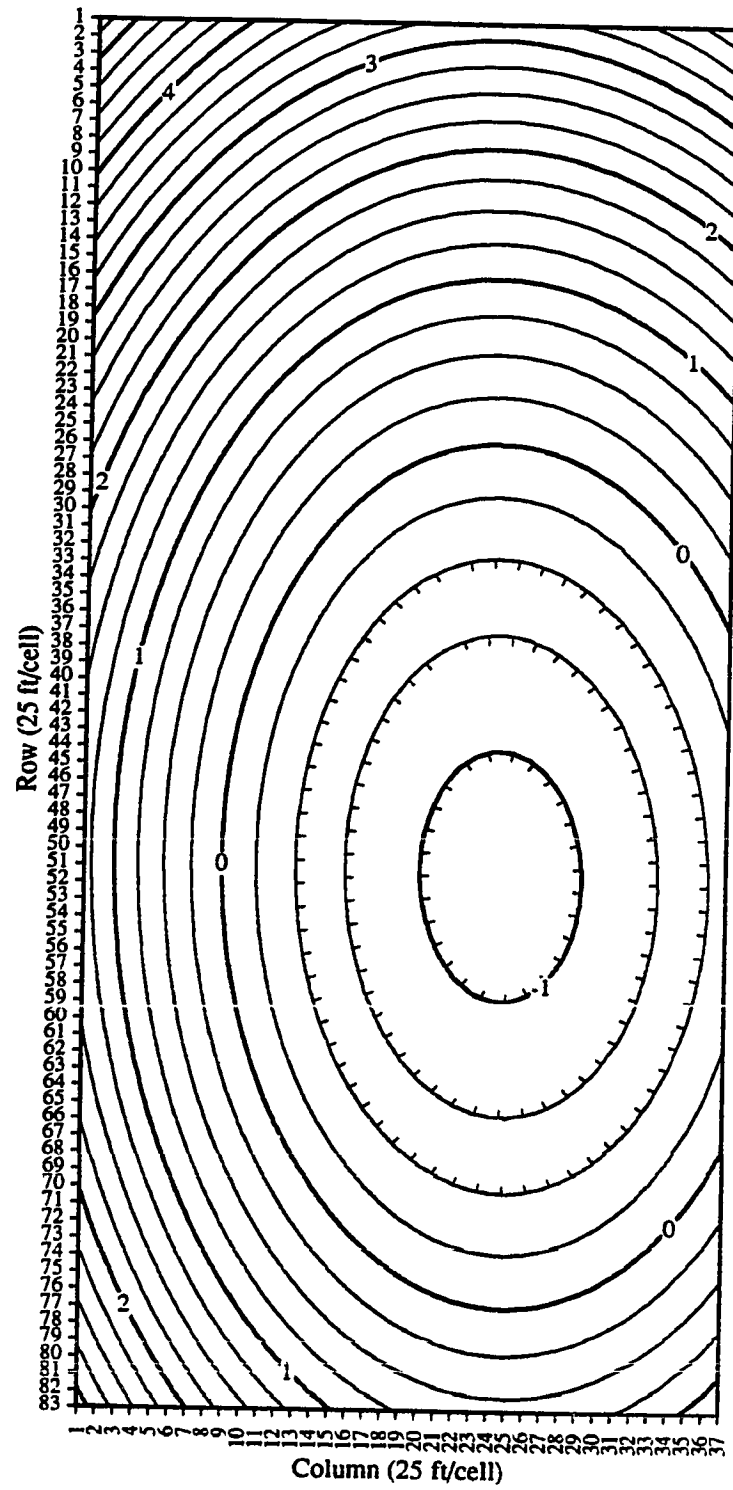


Figure 3.5

Polynomial hydraulic conductivity representation

estimated values of hydraulic conductivity at each cell. A lag separation of 50 ft is used in the modeling of the variogram. An exponential model is commonly used to model the variogram for aquifer properties (Englund, 1991). The *RMSE* of the kriging representation of hydraulic conductivity is lower than the *RMSEs* of both the constant representation and the polynomial representation. A comparison of the observed values of hydraulic conductivity to the kriging representation at a location corresponding to the location of each observation is presented in Table 3.3. The kriging representation of hydraulic conductivity provides the best match to the observations. A scatter plot of the kriging representation of hydraulic conductivity verses the estimation error of each estimated value is presented as Figure 3.6. A scatter plot of the observed values of hydraulic conductivity verses the kriging representation is presented as Figure 3.7. A contour plot of the resulting kriging hydraulic conductivity representation is presented as Figure 3.8.

The contour plot of the kriging hydraulic conductivity representation shows much of the same distinguishing features as the contour plot of the polynomial representation of hydraulic conductivity. The minimum estimated values of hydraulic conductivity appear in the region of monitoring well SW2 (see figs. 3.2, 3.5, and 3.8). The minimum kriging estimated values appear closer the minimum observed value, monitoring well SW2, than

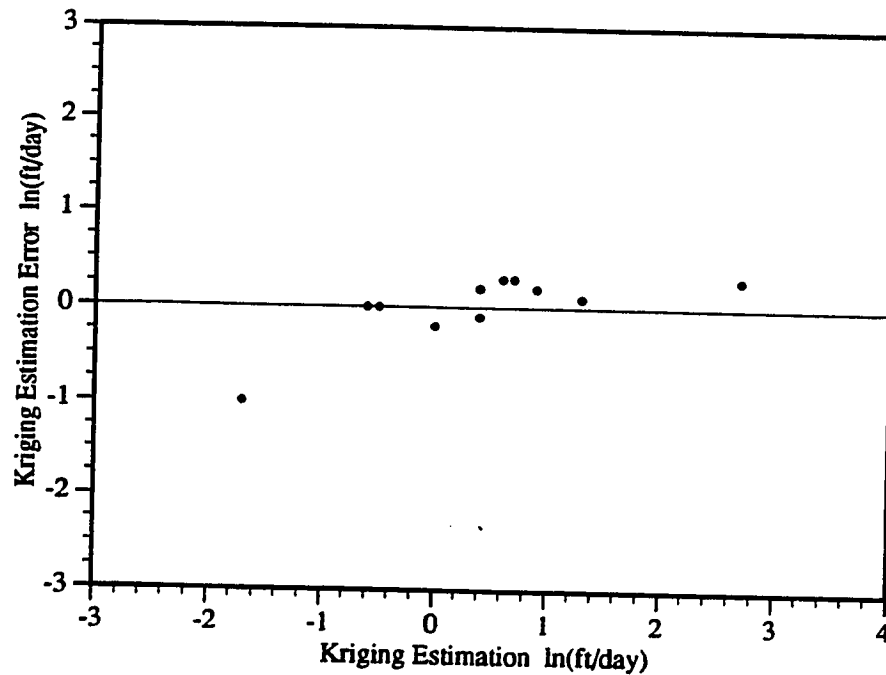


Figure 3.6 Kriging representation verses estimation error for hydraulic conductivity

the minimum polynomial estimated values. The estimated values of hydraulic conductivity maintain reasonable values over the entire region of estimated values. In the region of greatest concern, near the waste ponds (see Figure 3.1), the kriging estimated values of hydraulic conductivity are of approximately the same magnitude as the polynomial estimated values and generally slope from greater values to smaller values, moving from northwest to southeast (see figs. 3.5, 3.8), just as the polynomial estimated values. Both the kriging and the polynomial estimated values of hydraulic conductivity are approximately the same magnitude as the constant value estimation in the region of the waste ponds.

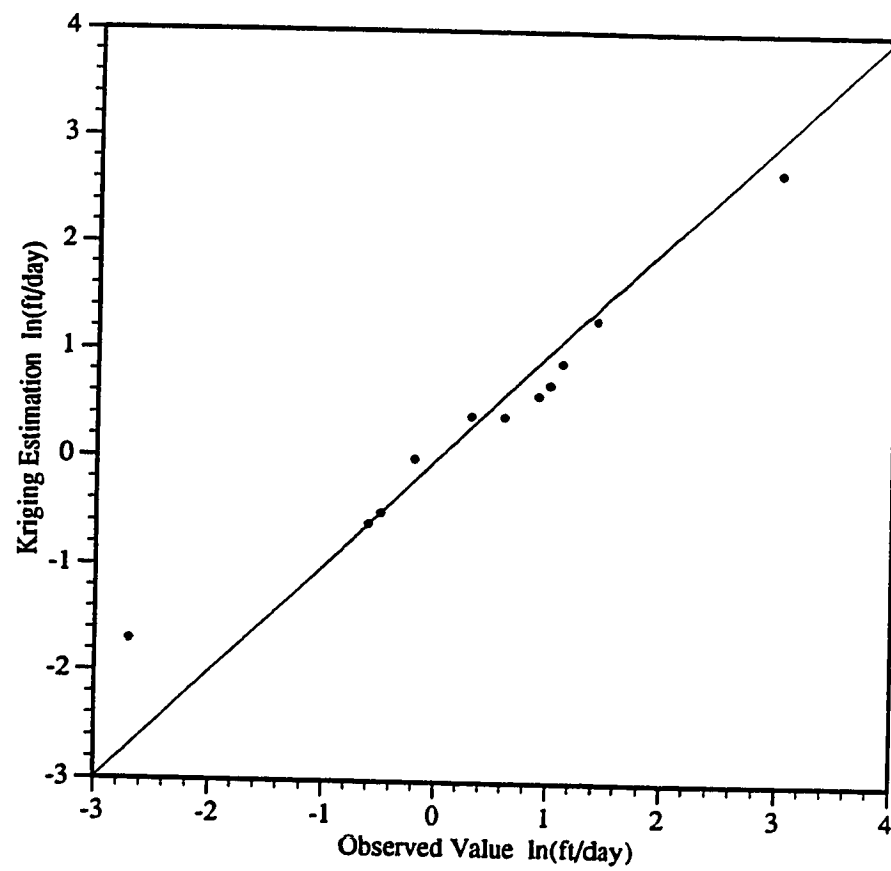


Figure 3.7 Observed values versus kriging representation for hydraulic conductivity

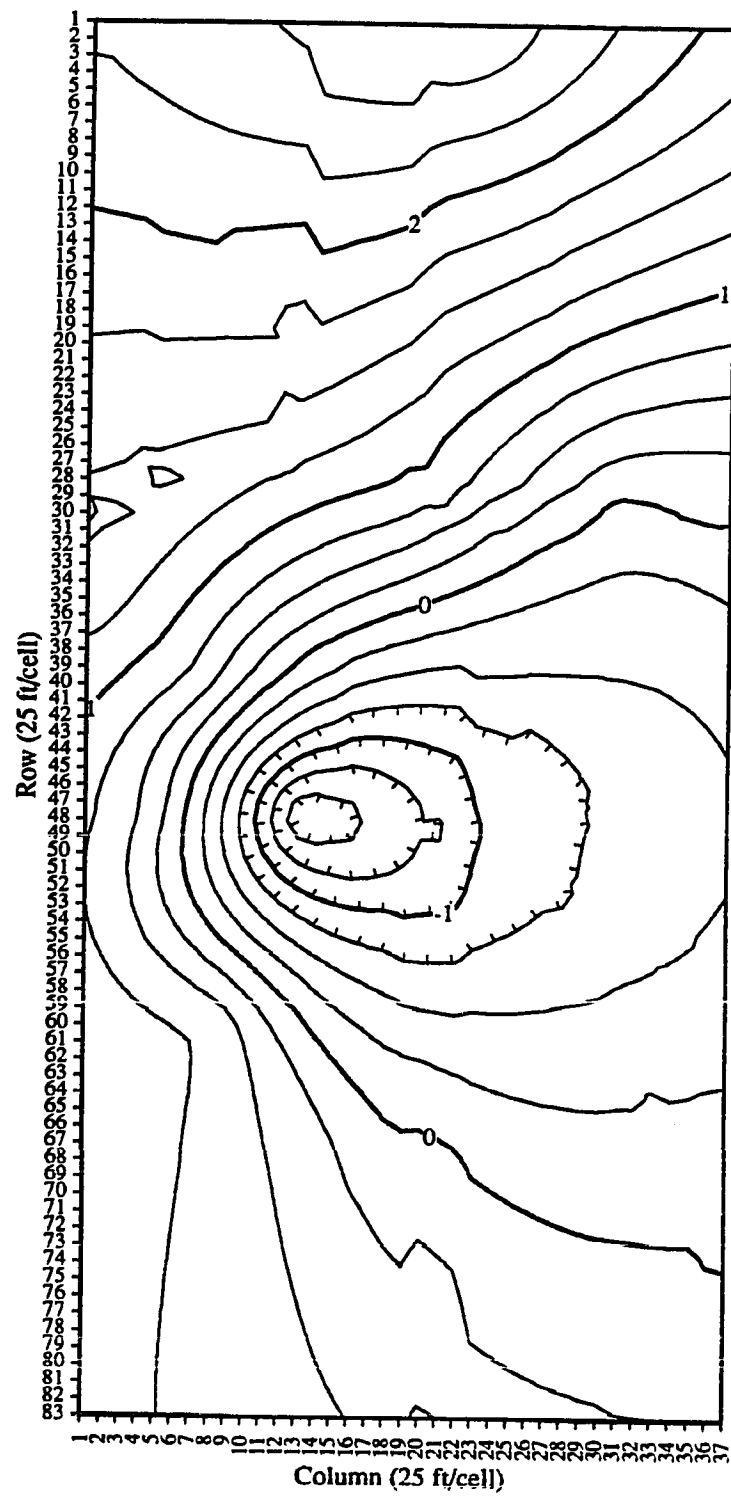


Figure 3.8 Kriging hydraulic conductivity representation

3.3.2 Bottom Elevation Representations

Each cell of the numerical flow and transport models requires either a representative value of bottom elevation or saturated thickness, which is directly computed from bottom elevation. A single value estimation, polynomial representation, and kriging representation of values of bottom elevation for the aquifer are generated for use with the models. The values of bottom elevation must be physically reasonable.

The constant value estimate of bottom elevation for the aquifer is 198.94 ft MSL. The notation "ft MSL" indicates that the measurement unit of the bottom elevation is vertical ft referenced to mean sea level. The arithmetic mean of values of bottom elevation interpreted from 25 soil boring drilling logs is used to calculate the constant value estimate. A comparison of the observed values of bottom elevation to the constant representation is presented in Table 3.4.

The polynomial representation of bottom elevation for the aquifer is generated using a third order polynomial function. The calculations to fit the polynomial function to the observed bottom elevation data are performed using the same computer code called TrendSurface (RockWare, 1990) that is used to fit a polynomial function to the observed hydraulic conductivity data. A third order polynomial function is used because it is the highest order

Well ID	Obs. BE (ft MSL)	C BE (ft MSL)	P BE (ft MSL)	K BE (ft MSL)	C <i>r</i> (ft)	P <i>r</i> (ft)	K <i>r</i> (ft)
SW1	203.94	198.94	204.58	203.99	5.00	-0.64	-0.05
SW2	194.88	198.94	197.70	196.02	-4.06	-2.82	-1.14
SW3	197.76	198.94	197.94	197.95	-1.18	-0.18	-0.19
SW4	196.88	198.94	196.89	196.41	-2.06	-0.01	0.47
SW5	203.56	198.94	198.43	202.03	4.62	5.13	1.53
SW6	195.92	198.94	199.08	197.22	-3.02	-3.16	-1.30
SW7	202.16	198.94	197.55	200.47	3.22	4.61	1.69
SW8	203.12	198.94	204.70	202.69	4.18	-1.58	0.43
SW9	195.43	198.94	197.12	196.48	-3.51	-1.69	-1.05
SW10	176.84	198.94	181.37	179.33	-22.10	-4.53	-2.49
RU1	196.70	198.94	201.87	198.86	-2.24	-5.17	-2.16
RU2	205.40	198.94	203.89	205.13	6.46	1.51	0.27
RU3	203.87	198.94	202.59	203.90	4.93	1.28	-0.03
RU5J	205.08	198.94	203.21	204.21	6.14	1.87	0.87
RU27	200.60	198.94	201.94	200.22	1.66	-1.34	0.38
DW1	205.78	198.94	205.43	205.31	6.84	0.35	0.47
DW2	205.14	198.94	203.82	205.01	6.20	1.32	0.13
DW3	204.85	198.94	199.78	203.11	5.91	5.07	1.74
DW4	196.69	198.94	196.21	195.89	-2.25	0.48	0.80
DW5	199.49	198.94	201.87	198.86	0.55	-2.38	0.63
DW6	196.86	198.94	195.93	197.39	-2.08	0.93	-0.53
DW7	198.16	198.94	197.88	197.70	-0.78	0.28	0.46
DW8	201.84	198.94	201.72	201.79	2.90	0.12	0.05
DW9	200.28	198.94	202.14	199.93	1.34	-1.86	0.35
DW10	182.22	198.94	179.08	181.34	-16.72	3.14	0.88
RMSE					6.75	2.65	1.04
Obs.	Observed bottom elevation (Weston, 1985)						
C	Constant representation of bottom elevation						
P	Polynomial representation of bottom elevation						
K	Kriging representation of bottom elevation						
BE	Bottom elevation						
<i>r</i>	Estimation error						
RMSE	Root mean squared error						

Table 3.4 Comparison of bottom elevation representations

polynomial function that maintained stability in regions where control points are scarce. The *RMSE* of the polynomial representation is lower than the *RMSE* of the constant representation. A comparison of the observed values

of bottom elevation to the polynomial representation at a location corresponding to the location of each observation is presented in Table 3.4. A scatter plot of the polynomial representation of bottom elevation verses the estimation error of each estimated value is presented as Figure 3.9.

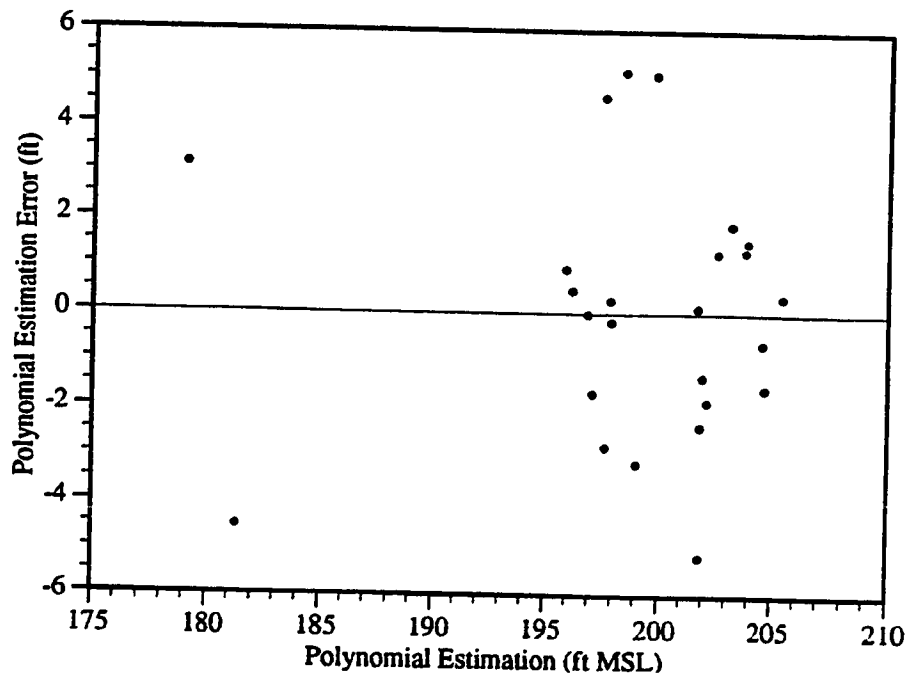


Figure 3.9 Polynomial representation verses estimation error for bottom elevation

A scatter plot of the observed values of bottom elevation verses the polynomial representation is presented as Figure 3.10. A contour plot of the resulting polynomial bottom elevation representation is presented as Figure 3.11. The contour plot of the polynomial bottom elevation representation shows a shape with two “saddles.” The minimum estimated values of bottom elevation appear in the region of monitoring wells SW10 and DW10; and the

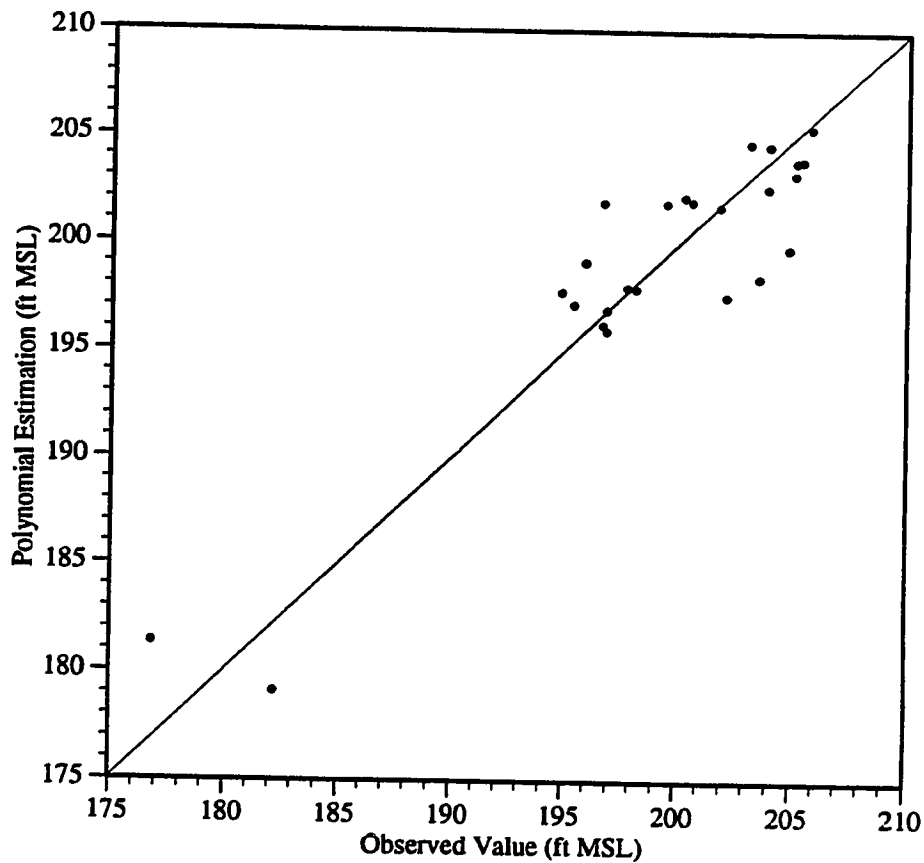


Figure 3.10 Observed values verses polynomial representation for bottom elevation

maximum estimated values appear in the region of monitoring well SW1 (see figs. 3.2 and 3.11). The estimated values of bottom elevation approach unreasonably high values in the southwest corner of the region of estimated values; and approach unreasonably low values in the northeast corner. In the region of greatest concern, near the waste ponds (see Figure 3.1), the estimated values of bottom elevation generally slope from greater values to smaller values, moving from northeast to southwest (see Figure 3.11).

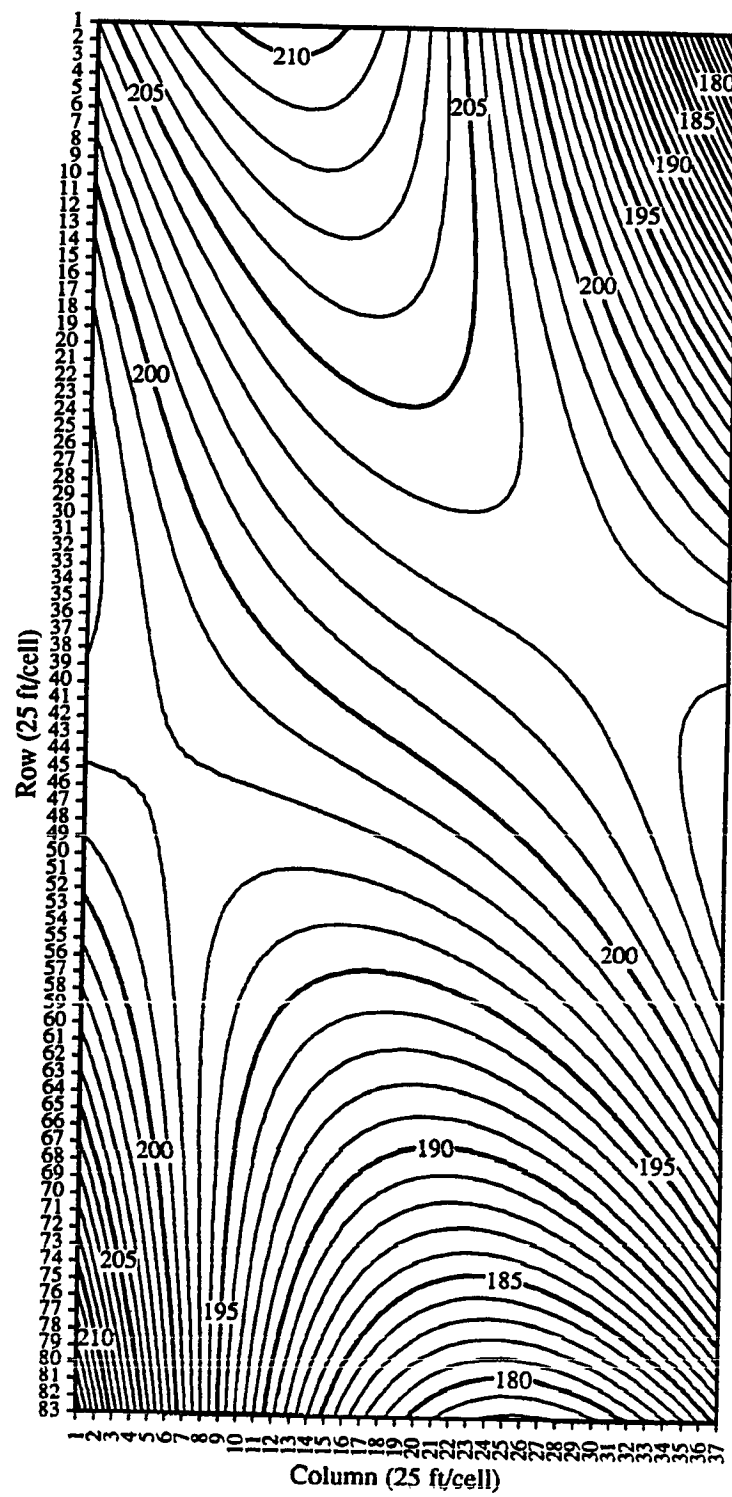


Figure 3.11 Polynomial bottom elevation representation

The kriging representation of bottom elevation for the aquifer is generated using ordinary block kriging. The calculations of estimated values of bottom elevation at each cell are performed using the same computer code called KRIGE (Englund et al., 1991) that is used to generate estimated values of hydraulic conductivity at each cell. The same lag separation of 50 ft is used in the modeling of the variogram. An exponential model is again used to model the variogram. The *RMSE* of the kriging representation of bottom elevation is lower than the *RMSEs* of both the constant representation and the polynomial representation. A comparison of the observed values of bottom elevation to the kriging representation at a location corresponding to the location of each observation is presented in Table 3.4. The kriging representation of bottom elevation provides the best match to the observations. A scatter plot of the kriging representation of bottom elevation verses the estimation error of each estimated value is presented as Figure 3.12. A scatter plot of the observed values of bottom elevation verses the kriging representation is presented as Figure 3.13. A contour plot of the resulting kriging bottom elevation representation is presented as Figure 3.14.

The contour plot of the kriging bottom elevation representation shows much of the same distinguishing features as the contour plot of the polynomial representation of bottom elevation. The minimum estimated values of hydraulic conductivity appear in the region of monitoring wells SW10 and

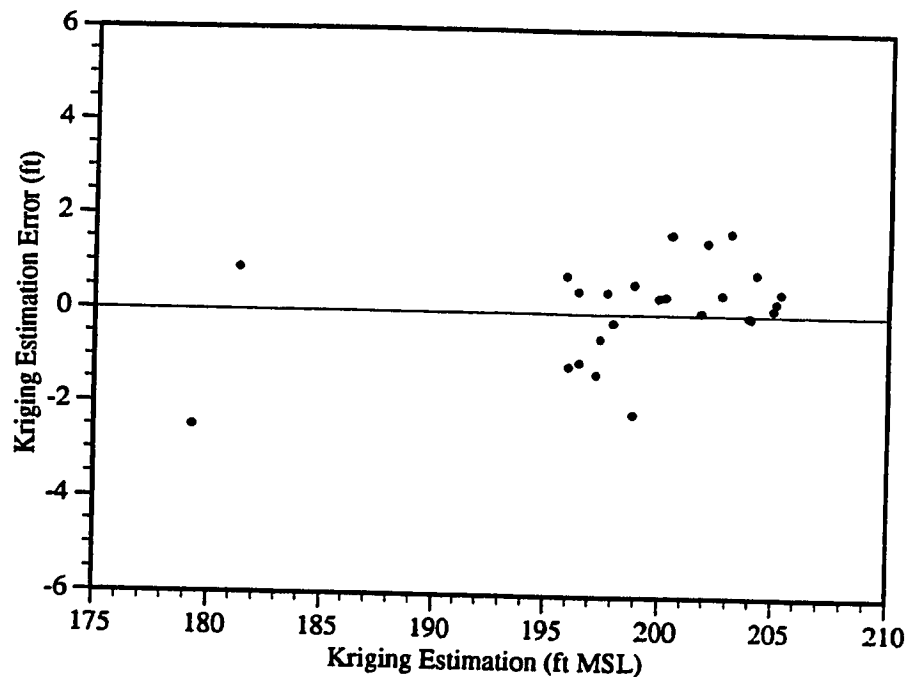


Figure 3.12 Kriging representation versus estimation error for bottom elevation

DW10 (see figs. 3.2, 3.11, and 3.14). A plateau of kriging estimated values appears in the region between monitoring wells SW1 and RU2 that is not indicated by the polynomial estimated values (see figs. 3.2, 3.11, and 3.14). The estimated values of bottom elevation maintain reasonable values over the entire region of estimated values. In the region of greatest concern, near the waste ponds (see Figure 3.1), the kriging estimated values of bottom elevation are of approximately the same magnitude as the polynomial estimated values and generally slope from greater values to smaller values, moving from northwest to southeast (see figs. 3.11, 3.14), just as the polynomial estimated values.

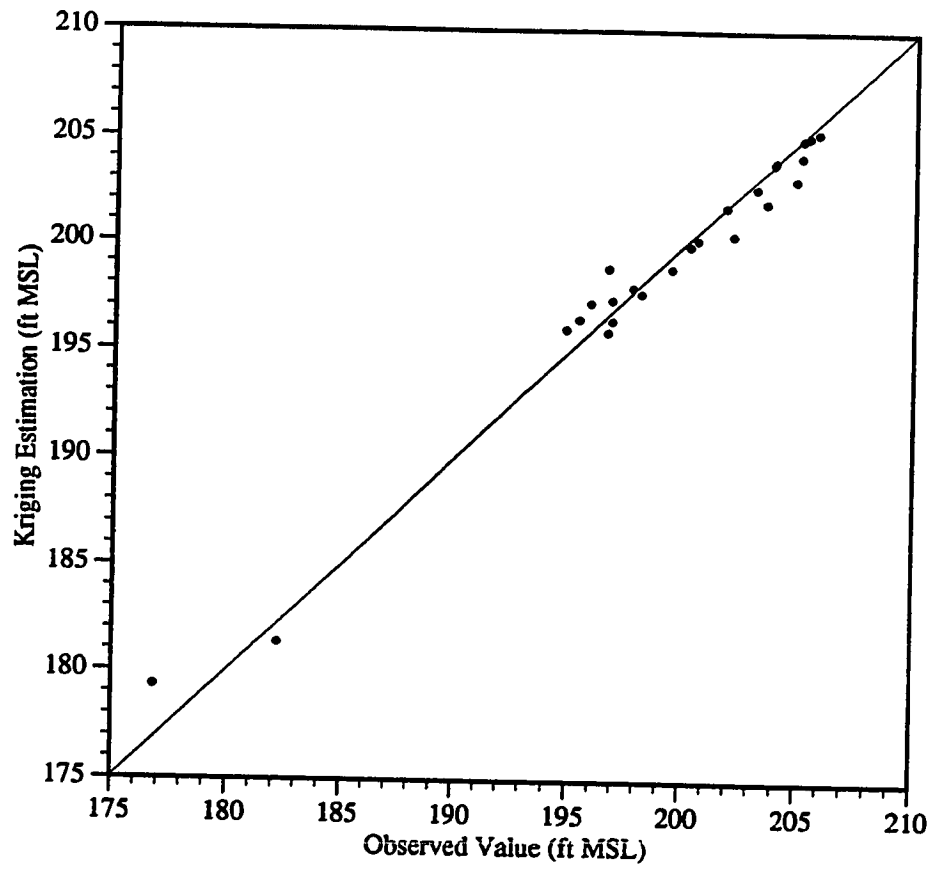


Figure 3.13 Observed values versus kriging representation for bottom elevation

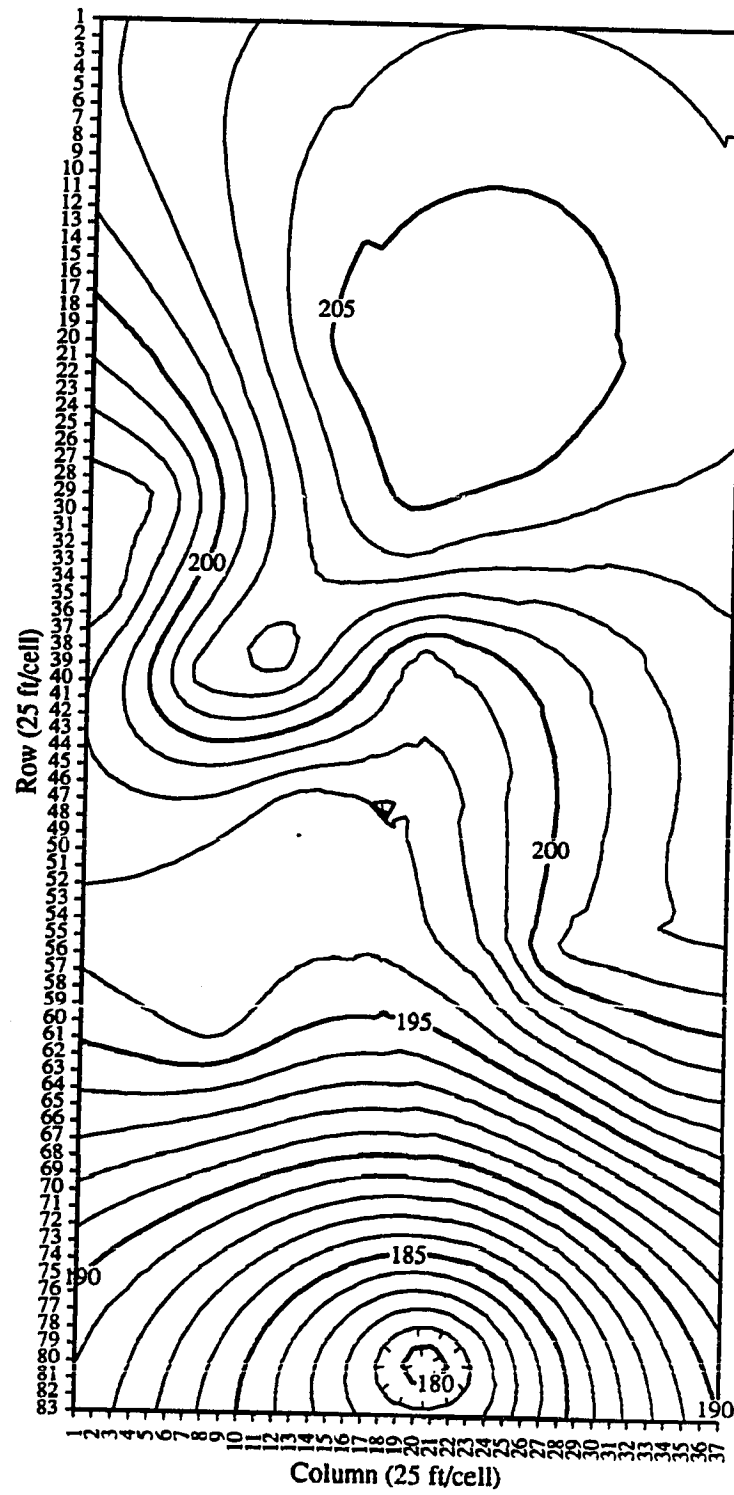


Figure 3.14 Kriging bottom elevation representation

MODELING

Modeling, as performed in the research presented here, refers to approximating a field situation. The modeling process applied to the research presented here is structured after that presented by Anderson et al. (1992). The research presented here differs from that suggested by Anderson et al. (1992) in that the calibration and prediction processes are not performed as they would be in a truly predictive modeling application. In this research, the calibration and prediction processes serve as the means by which comparisons are made of the effects of using different representations of aquifer properties in the modeling.

4.1 Modeling Purpose

The purpose of constructing the models is for system interpretation. Information is desired concerning the significance of using different representations of aquifer properties. The effects of using different representations of aquifer properties on the system are observed from the simulation results. Specific purposes of modeling include observing the effects of representing the spatial variability of aquifer properties on different types and scenarios of modeling.

Types of modeling studied are flow and transport modeling. Ground water flow modeling is concerned with fluid movement in the porous media.

Contaminant transport modeling is concerned with the movement of contaminants carried along by fluid movement in a porous medium.

Modeling scenarios studied are natural gradient and recovery and injection system modeling. Natural gradient model generally concerns the long-term migration of contaminants in an aquifer. Recovery and injection system modeling concerns the induced effects of a system designed to remediate contaminated ground water.

The simulations performed to study the effects of representing the spatial variability of aquifer properties and the corresponding identification are presented in Table 4.1. From the results of these simulations, conclusions about the effects of each representation can be made.

The research presented here does not attempt to quantify the effects of using different magnitudes of values representing aquifer properties, hydraulic loading, or contaminant loading on modeling. In order to isolate the effects of representing the spatial variability of aquifer properties, reasonable values of the other parameters are held constant for the simulations. The differences in the simulation results can be attributed to the differences in the representations of aquifer properties.

Sim. Number	Sim. ID
1	NG - GF - KB - C
2	NG - GF - KB - P
3	NG - GF - KB - K
4	NG - GF - K - P
5	NG - GF - K - K
6	NG - GF - B - P
7	NG - GF - B - K
8	NG - CT - KB - C
9	NG - CT - KB - P
10	NG - CT - KB - K
11	NG - CT - K - P
12	NG - CT - K - K
13	NG - CT - B - P
14	NG - CT - B - K
15	RI - GF - KB - C
16	RI - GF - KB - P
17	RI - GF - KB - K
18	RI - GF - K - P
19	RI - GF - K - K
20	RI - GF - B - P
21	RI - GF - B - K
22	RI - CT - KB - C
23	RI - CT - KB - P
24	RI - CT - KB - K
25	RI - CT - K - P
26	RI - CT - K - K
27	RI - CT - B - P
28	RI - CT - B - K

Sim ID: Col. 1:	NG	Natural gradient modeling
	RI	Recovery and injection system modeling
Col. 2:	GF	Ground water flow modeling
	CT	Contaminant transport modeling
Col. 3:	KB	Varying hydraulic conductivity and bottom elevation
	K	Varying hydraulic conductivity, constant bottom elevation
	B	Varying bottom elevation, constant hydraulic conductivity
Col. 4:	C	Constant representation
	P	Polynomial representation
	K	Kriging representation

Table 4.1 Simulation list and identification

4.2 Model Selection

The purpose of building a conceptual model is to simplify the field problem and organize the associated field data so that the system can be analyzed. Stratigraphic units and system boundaries are identified. Field data are assembled including information on the water balance and data needed to assign values to aquifer properties and hydraulic loading.

The first step in formulating the conceptual model is to define the boundaries of the model. The true hydrogeologic boundaries of the shallow unconfined aquifer at the UCC site are beyond the area that is to be simulated. A region of the aquifer is selected based on the region in which data are collected. The model domain is roughly the same size and shape as the UCC property boundaries (see Figure 3.1). The dimensions of the model domain are roughly 1000 ft by 2000 ft. The exact dimensions are determined by the number of cells and the cell dimensions.

Within the region covered by the model domain, the shallow unconfined aquifer is conceptually modeled as a single unconfined layer. The *GWSE* data indicate that ground water flow is in a uniform southerly direction. A conceptual model with two constant head boundary conditions on the north and south, and two no-flow boundary conditions on the east and west can represent the natural gradient ground water flow pattern.

A mathematical model simulates ground water flow or contaminant transport indirectly by means of a governing equation thought to represent the physical processes that occur in the system, together with boundary and initial conditions (McDonald et al., 1988). The differential equation for simulating the movement of ground water of constant density through a confined aquifer is usually written

$$\frac{\partial}{\partial x_i} \left(T_{ij} \frac{\partial h}{\partial x_j} \right) - W = S \frac{\partial h}{\partial t} \quad (4.1)$$

where x_i are the cartesian coordinates (L), T_{ij} are the components of the transmissivity tensor (L^2/T), h is the potentiometric head (L), W is the source or sink term (L/T), S is the storage coefficient (dim.), and t is time (T) (Bedient et al., 1985). Equation 4.1 may be rewritten as

$$\frac{\partial}{\partial x_i} \left(K_{ij} \frac{\partial h}{\partial x_j} \right) - W^* = S_s \frac{\partial h}{\partial t} \quad (4.2)$$

where K_{ij} is the hydraulic conductivity (L/T), W^* is the volumetric flux per unit volume (the source or sink term) ($1/T$), and S_s is the specific storage ($1/L$) (McDonald et al., 1988).

Provided the coordinate directions are aligned with the principal axes of hydraulic conductivity, the hydraulic conductivity tensor may be ex-

pressed by values in the direction of coordinate axes. For two-dimensional flow, Equation 4.2 may be written

$$\frac{\partial}{\partial x_1} \left(K_{11} \frac{\partial h}{\partial x_1} \right) + \frac{\partial}{\partial x_2} \left(K_{22} \frac{\partial h}{\partial x_2} \right) - W^* = S_s \frac{\partial h}{\partial t} \quad (4.3)$$

Equation 4.3 describes ground water flow under non-equilibrium conditions in a heterogeneous and anisotropic medium. If steady-state flow is assumed, as is in the case of the modeling presented here, eq 4.3 becomes

$$\frac{\partial}{\partial x_1} \left(K_{11} \frac{\partial h}{\partial x_1} \right) + \frac{\partial}{\partial x_2} \left(K_{22} \frac{\partial h}{\partial x_2} \right) - W = 0. \quad (4.4)$$

Steady state conditions are represented in the models by equating the specific storage to zero. Equation 4.4, together with specification of boundary conditions, constitutes a mathematical representation of a confined aquifer ground water flow system (McDonald et al., 1988).

Ground water flow in unconfined aquifers is represented by a differential equation usually written

$$\frac{\partial}{\partial x_i} \left(K_{ij} h \frac{\partial h}{\partial x_j} \right) - W = S_y \frac{\partial h}{\partial t} \quad (4.5)$$

where S_y is the specific yield (dim.) (Anderson et al., 1992).

Provided the coordinate directions are aligned with the principal axes of hydraulic conductivity, the two-dimensional form of Equation 4.5 may be written

$$\frac{\partial}{\partial x_1} \left(K_{11} \frac{\partial h^2}{\partial x_1} \right) + \frac{\partial}{\partial x_2} \left(K_{22} \frac{\partial h^2}{\partial x_2} \right) - 2W = 2S_y \frac{\partial h}{\partial t} \quad (4.6)$$

by realizing that

$$\frac{\partial h^2}{\partial x_1} = 2h \frac{\partial h}{\partial x_1}, \quad (4.7)$$

$$\frac{\partial h^2}{\partial x_2} = 2h \frac{\partial h}{\partial x_2}. \quad (4.8)$$

Equation 4.6 describes ground water flow under non-equilibrium conditions in a heterogeneous and anisotropic medium. If steady-state ground water flow is assumed, as is in the case of the modeling presented here, eq 4.6 becomes

$$\frac{\partial}{\partial x_1} \left(K_{11} \frac{\partial h^2}{\partial x_1} \right) + \frac{\partial}{\partial x_2} \left(K_{22} \frac{\partial h^2}{\partial x_2} \right) - 2W = 0. \quad (4.9)$$

Mathematical models can either be solved analytically or numerically. The research presented here calls for numerical mathematical models because of the representation of heterogeneity and the number of loadings applied to the system. Except for very simple systems, analytical solutions of

eqs. 4.4 and 4.9 are rarely possible, so numerical methods are employed to obtain approximate solutions (McDonald et al., 1988). One such approach is the finite-difference method, wherein the continuous systems described in eqs. 4.4 and 4.9 are replaced by a finite set of discrete points in space, and the partial derivatives are replaced by terms calculated from the differences in head values at these points. The process leads to systems of simultaneous linear algebraic difference equations. Their solution yields values of head at specific points.

The differential equation for simulating contaminant transport through porous earth is usually written

$$\frac{\partial}{\partial x_i} \left(D_{ij} \frac{\partial C}{\partial x_j} \right) - \frac{\partial}{\partial x_i} (C V_i) - \frac{C_o W}{nb} + \Sigma R_k = \frac{\partial C}{\partial t} \quad (4.10)$$

where D_{ij} is the coefficient of dispersion tensor (L^2/T), C is the concentration of solute (M/L^3), V_i is the seepage velocity (L/T), n is porosity (dim.), and R_k is the rate of addition or removal of solute (\pm) (M/L^3T) (Bedient et al., 1985). The various terms in Equation 4.10 are usually referred to as dispersive transport, advective transport, source or sink, and reaction, respectively. All of these terms sum to produce a change in species concentration.

There are difficulties in attempting to use the mass transport equation (Equation 4.10) to describe an actual site in two-dimensions. Directional

dispersivity is hard to estimate due to the presence of heterogeneities and other reactions in the porous media. Estimation of hydraulic conductivity is also related to the presence of field heterogeneities that are often unknown. The source and sink terms that drive the model and the reaction term, which may represent adsorption, ion exchange, or decay are seldom known with great confidence. Despite all of these problems, mass transport models still offer the most reliable approach to prediction of contaminant migration and management of corrective actions (Bedient et al., 1985).

The code is the computer program that contains an algorithm to solve the mathematical model numerically. The code is generic, whereas a model includes a set of boundary and initial conditions, a site specific nodal grid, site specific aquifer property values, and hydraulic loading. The codes used in the research presented here are selected because they are well documented, easy to use, can simulate a variety of flow conditions including injection and production wells, can include representations of variable hydraulic conductivity and bottom elevation (or saturated thickness), and are verified.

The flow simulations are performed using MODFLOW, the U.S. Geological Survey modular three-dimensional finite-difference ground water flow model (McDonald et al., 1988). The MODFLOW code simulates a three-dimensional system as a sequence of layers. Although only one layer

is used in the research presented here, the MODFLOW code is capable of solving the governing equation of flow for systems with many layers represented.

The transport simulations are performed using BIOPLUME II, a block-centered finite-difference code that simulates solute migration (Rifai et al., 1987). BIOPLUME II is a code based on the U.S. Geological Survey solute transport two-dimensional code commonly called MOC (Konikow et al., 1978). The model computes the changes in concentration over time due to advection, dispersion, and reactions. Although no reactions are simulated in the research presented here, the BIOPLUME II code is capable of solving the governing equation of transport for systems under the influence of oxygen-limited biodegradation. BIOPLUME II is also capable of simulating reaeration and anaerobic biodegradation as a first order decay (Rifai et al., 1987).

4.3 Model Design

The model design includes designing the grid, selecting time steps, setting boundary and initial conditions, and selecting values for aquifer properties, hydraulic loading, and contaminant loading.

4.3.1 Grid Design

In the numerical models, the continuous problem domain is replaced by a discretized domain consisting of an array of nodes and associated finite difference cells. The nodal grid forms the framework of the numerical model. A horizontal grid is generated by specifying grid dimensions in the coordinate directions. Hydraulic conductivity and bottom elevation arrays may vary in values at each location within a grid.

The orientation of the modeling grid is determined by a least-squares first order polynomial approximation of a plane to the observed *GWSE* data recorded by Weston (1985). A least-squares first order polynomial approximation is used in order to determine the best fit of a plane passing through the observations of *GWSE*. From the best plane, the gradient and direction of greatest gradient are determined. The grid is aligned in the direction of greatest gradient, or commonly referred to as the strike of the plane representing the observed *GWSE* distribution. The grid coordinate system aligned in the direction of greatest gradient is oriented 6.76° clockwise from the orientation of the site coordinate system established by Weston (1985). A rotation of axes is performed to generate the coordinates of the monitoring well locations in the grid coordinate system. The primary directions of the grid coordinate system are grid North and grid East.

The modeling domain is represented by 37 columns of cells in the east-west direction and 83 rows of cells in the north-south direction. A square cell with side dimension of 25 ft is used to calculate the number of rows and columns. Using a 25 ft cell size, the modeling domain measures 925 ft by 2075 ft. The area of the modeling domain corresponds to the area displayed in the figure showing the locations of monitoring wells (Figure 3.2). The basis of the cell dimension selection is computational expense. A cell with side dimension of 25 ft results in 3071 cells used to represent the modeling domain. The effect of grid cell side dimension on the number of cells needed to represent the aquifer is presented in Table 4.2.

Cell side dimension (ft)	Cols.	Rows	Number of Cells
100	10	21	210
75	13	28	364
50	19	42	798
25	37	83	3071
10	92	208	19136

Table 4.2 Effect of grid cell side dimension on the number of cells

The transport simulations using the BIOPLUME II code use a grid 39 columns by 85 rows. The increase in size is due to the code's requirement of a border of inactive cells around the modeling domain of active cells. Adjustments are made to the locations of aquifer properties and loadings to reflect the discrepancy in row and column numbers. All reported row and

column coordinates have been converted to the grid coordinates without the inactive border cells.

4.3.1 Time Step Selection

Time steps for the natural gradient modeling were reported by Borden (1986a). The years in which the waste ponds at the UCC facility were receiving waste comprise Period 1. The years after the UCC facility was closed and the waste ponds present at the site were not receiving waste but may have still contributed residual hydraulic and contaminant loading to the unconfined aquifer comprise Period 2. The last time period represents the years from when the land had been sold and used for other purposes until the date of the initial site investigation and comprise Period 3. A summary of the selected time periods used in the natural gradient modeling is presented in Table 4.3.

	Dates			Duration (years)
Period 1	1946	-	1972	26
Period 2	1972	-	1977	5
Period 3	1977	-	1985	8
Total duration				39

Table 4.3 Time periods for natural gradient modeling (Borden, 1986a)

The recovery and injection system modeling is carried out for a single time step with a simulation time of 5 years. The simulation time length is se-

lected to facilitate comparison of recovery and injection system transport (RI-CT) modeling. If a very large length of time is selected, the effects of the representations would be shrouded by the fact that each simulation would completely remove the initial contamination and therefore not offer a basis for comparison to one another.

4.3.3 Aquifer Properties

The hydraulic conductivity and bottom elevation (or saturated thickness) values used in the models are variable as a function of which simulation is performed. The representations of these aquifer properties have been presented as figs. 3.5, 3.8, 3.11, and 3.14.

The only other aquifer properties used in the flow modeling are the anisotropy factor and storage coefficient. The anisotropy factor is the ratio of longitudinal and transverse hydraulic conductivity. An anisotropy factor of 1.0 (dim.) is assumed and corresponds to isotropic conditions. A storage coefficient of zero (dim.) is assumed and corresponds to assumption of steady-state hydraulic conditions.

Additional aquifer properties used in the transport modeling include effective porosity, characteristic length, ratio of transverse to longitudinal dispersivity, anisotropy factor, and storage coefficient. An estimate of 0.345 (dim.) is used for effective porosity and is the mean value reported by

Weston (1985). A length of 1.0 ft is used for characteristic length (longitudinal dispersivity) and is an estimate based on reported typical values ranging from 0.3 ft to 6.6 ft for field sites with relatively short transport distances (Domenico et al., 1990). A ratio of transverse to longitudinal dispersivity of 0.1 (dim.) is assumed and is an estimate based on reported typical values ranging from 0.01 (dim.) to 0.2 (dim.) for field sites (de Marsily, 1986).

4.3.4 Hydraulic Loading

Hydraulic loading is involved in both the natural gradient and the recovery and injection system modeling. Hydraulic loading is represented by wells located at the center of cells. Wells can either have a role of recovering (pumping) or injecting water.

The hydraulic loading used in the natural gradient modeling is based on estimates of total infiltration from the ponds to the shallow unconfined aquifer made by Borden (1986a). The infiltration from the ponds to the aquifer is represented by 86 injection wells, one well at the center of each finite-difference cell falling into the area of the waste ponds. The small pond is represented with 25 cells, and the large pond by 61 cells. During period 1, infiltration from the ponds into the shallow unconfined aquifer produced

significant mounding of the *GWSEs* near the region of the waste ponds. The hydraulic loading for natural gradient modeling is summarized in Table 4.4.

	Area (ft ²)	Cells	IR Period 1 (ft/yr)	IR Period 2 (ft/yr)	IR Period 3 (ft/yr)
Small Pond	15625	25	0.531	0.053	0.006
Large Pond	38125	61	0.743	0.074	0.008
IR	Infiltration rate				

Table 4.4 Hydraulic loading for natural gradient modeling (Borden, 1986a)

The locations of the injections wells representing the large and small ponds are presented in Figure 4.1.

The hydraulic loading used in the recovery and injection system modeling is based on a proposed corrective action design presented by Borden (1986a). The corrective action design is a basic form of pump-and-treat technology. Pump-and-treat is a common means of containing or remediating contaminated ground water by extracting the water, treating it at the surface, and then (optionally) reinjecting the treated water back into the aquifer (Mercer et al., 1990). Slight modification to the recovery and injection well geometry as presented by Borden (1986a) is made to improve the recovery efficiency. A pumping and injection rate of 0.2 gpm (gallons per minute) is used in all wells for all the simulations and is estimated to be the pumping rate that produces a 20% drawdown of the aquifer at the well bore.

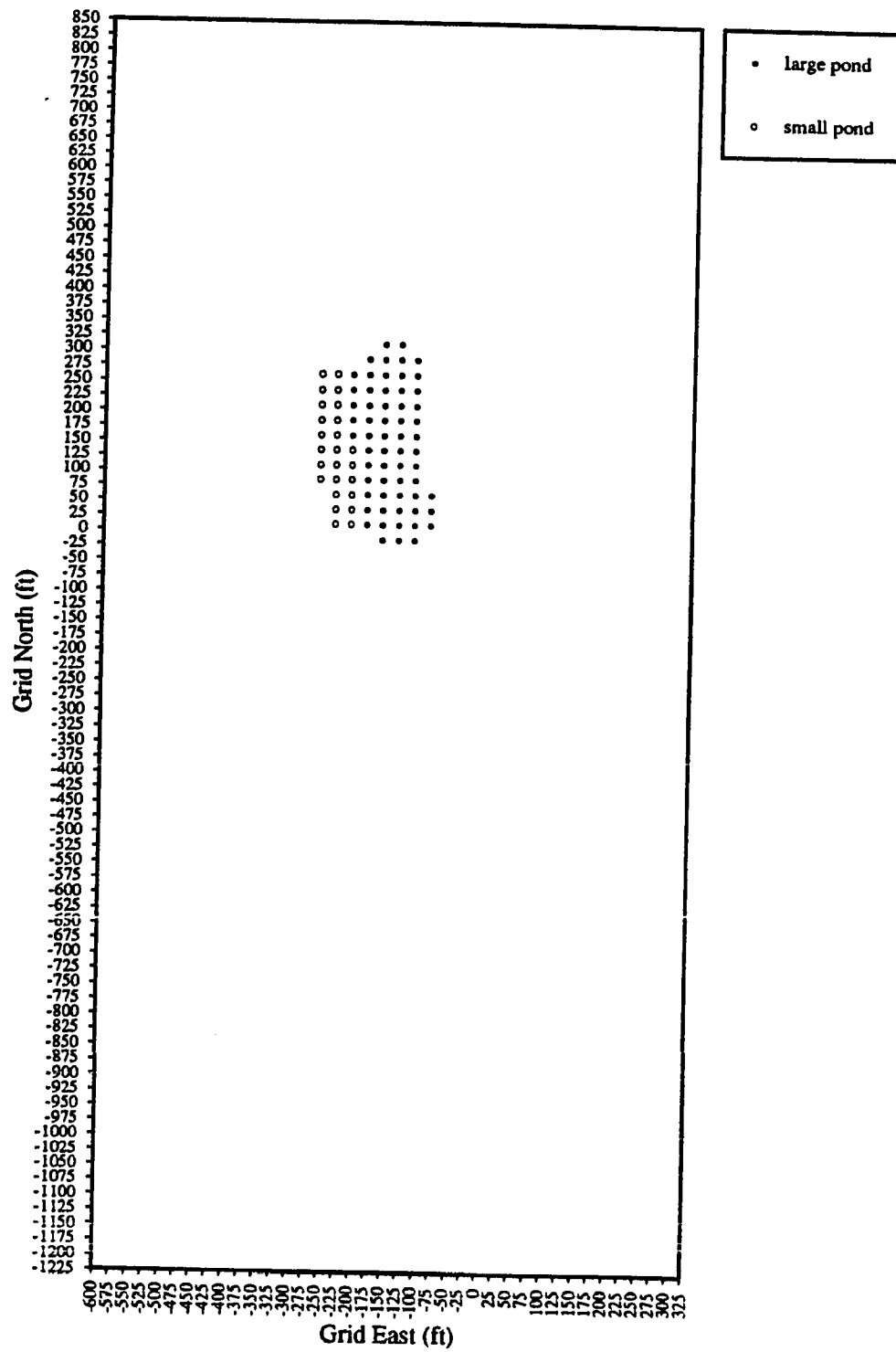


Figure 4.1 Waste pond loading locations

Analytical modeling of a single pumping well using constant representations of hydraulic conductivity and bottom elevation derived the estimated pumping rate of 0.2 gpm. The 20% drawdown criteria is a general design goal for corrective action plans. The coordinates of the recovery wells are presented in Table 4.5.

Well ID	Site North (ft)	Site East (ft)	Grid North (ft)	Grid East (ft)	Row	Col.
R1	228.87	-337.91	187.50	-362.50	27	10
R2	30.26	-361.45	-12.50	-362.50	35	10
R3	-168.35	-384.99	-212.50	-362.50	43	10
R4	-366.96	-408.54	-412.50	-362.50	51	10
R5	316.40	-226.83	287.50	-262.50	23	14
R6	117.79	-250.38	87.50	-262.50	31	14
R7	-80.82	-273.92	-112.50	-262.50	39	14
R8	-279.43	-297.46	-312.50	-262.50	47	14
R9	-478.04	-321.00	-512.50	-262.50	55	14
R10	205.32	-139.30	187.50	-162.50	27	18
R11	6.71	-162.84	-12.50	-162.50	35	18
R12	-191.89	-186.38	-212.50	-162.50	43	18
R13	-390.50	-209.93	-412.50	-162.50	51	18
R14	292.86	-28.22	287.50	-62.50	23	22
R15	94.25	-51.77	87.50	-62.50	31	22
R16	-104.36	-75.31	-112.50	-62.50	39	22
R17	-302.97	-98.85	-312.50	-62.50	47	22
R18	-501.58	-122.39	-512.50	-62.50	55	22
R19	181.78	59.31	187.50	37.50	27	26
R20	-16.83	35.77	-12.50	37.50	35	26
R21	-215.44	12.23	-212.50	37.50	43	26
R22	-414.05	-11.32	-412.50	37.50	51	26
Site	Coordinate system established at the site (Weston, 1985)					
Grid	Coordinate system aligned with the general direction of ground water flow					

Table 4.5 Recovery well locations

The locations of the recovery and injection wells are presented in Figure 4.2.

The coordinates of the injection wells are presented in Table 4.6. Analytical

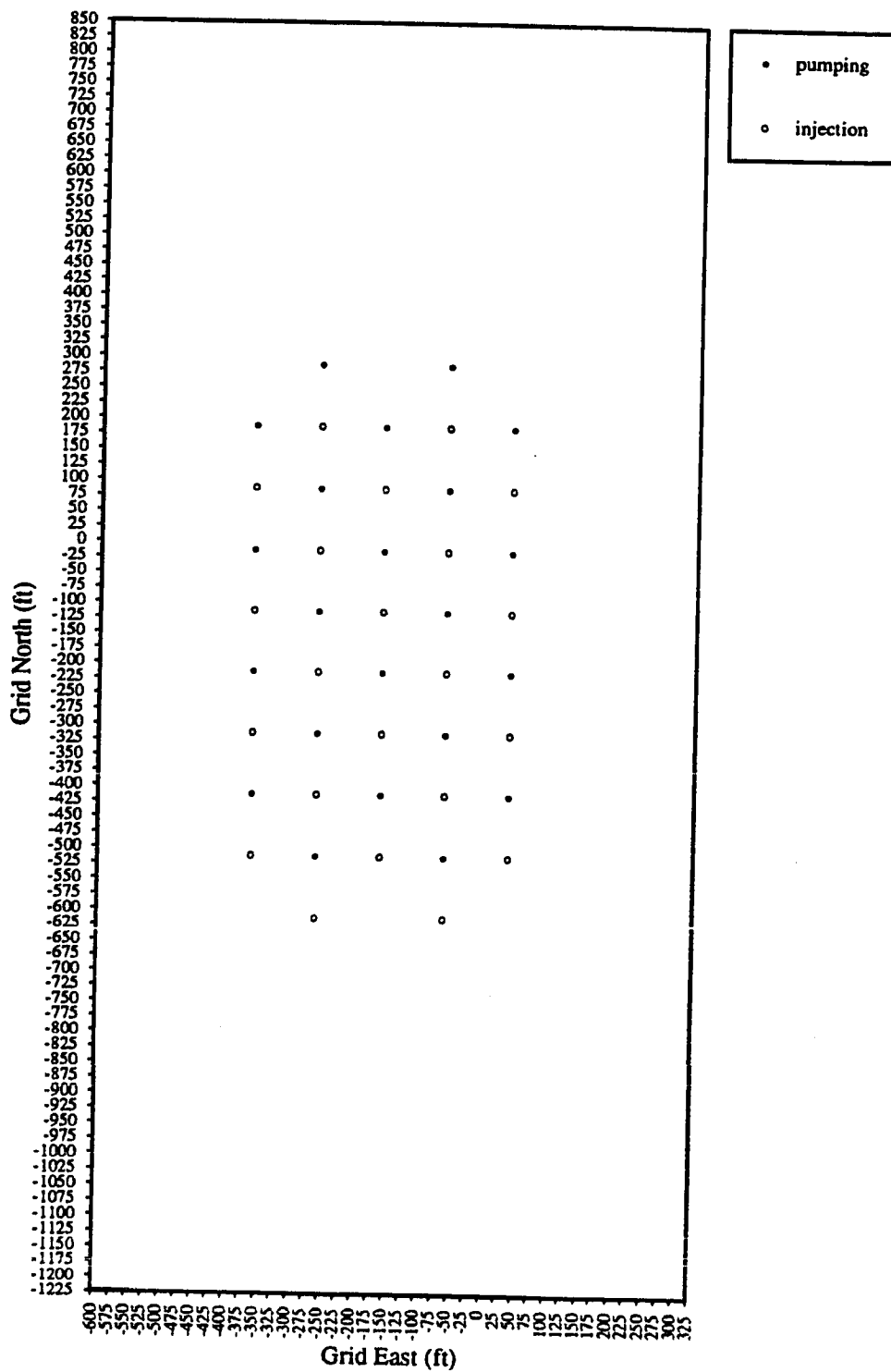


Figure 4.2 Recovery and injection system well locations

Well ID	Site North (ft)	Site East (ft)	Grid North (ft)	Grid East (ft)	Row	Col.
I1	129.56	-349.68	87.50	-362.50	31	10
I2	-69.05	-373.22	-112.50	-362.50	39	10
I3	-267.66	-396.76	-312.50	-362.50	47	10
I4	-466.27	-420.31	-512.50	-362.50	55	10
I5	217.10	-238.60	187.50	-262.50	27	14
I6	18.49	-262.15	-12.50	-262.50	35	14
I7	-180.12	-285.69	-212.50	-262.50	43	14
I8	-378.73	-309.23	-412.50	-262.50	51	14
I9	-577.34	-332.77	-612.50	-262.50	59	14
I10	106.02	-151.07	87.50	-162.50	31	18
I11	-92.59	-174.61	-112.50	-162.50	39	18
I12	-291.20	-198.15	-312.50	-162.50	47	18
I13	-489.81	-221.70	-512.50	-162.50	55	18
I14	193.55	-39.99	187.50	-62.50	27	22
I15	-5.06	-63.54	-12.50	-62.50	35	22
I16	-203.67	-87.08	-212.50	-62.50	43	22
I17	-402.28	-110.62	-412.50	-62.50	51	22
I18	-600.88	-134.16	-612.50	-62.50	59	22
I19	82.48	47.54	87.50	37.50	31	26
I20	-116.13	24.00	-112.50	37.50	39	26
I21	-314.74	0.45	-312.50	37.50	47	26
I22	-513.35	-23.09	-512.50	37.50	55	26
Site	Coordinate system established at the site (Weston, 1985)					
Grid	Coordinate system aligned with the general direction of ground water flow					

Table 4.6 Injection well locations

modeling of a single pumping well using constant representations of hydraulic conductivity and bottom elevation derived the estimated pumping rate of 0.2 gpm. The 20% drawdown criteria is a general design goal for corrective action plans.

4.3.5 Contaminant Loading

When injecting water in a transport simulation, a value representing concentration may be associated with the water being injected.

Concentration values are assigned to injected water in both the natural gradient flow and recovery and injection system modeling.

The chloride loading used in the natural gradient modeling is based on estimates of chloride loading from the ponds to the shallow unconfined aquifer made by Borden (1986a). The chloride loading from the ponds to the aquifer is represented by a concentration associated with the hydraulic loading at each of the 86 injection wells representing the waste ponds. During period 1, chloride loading from the ponds into the shallow unconfined aquifer is estimated as 160 mg/l. During period 2, chloride loading from the ponds into the shallow unconfined aquifer is estimated as 10 mg/l. During period 3, chloride loading from the ponds into the shallow unconfined aquifer is estimated as 10 mg/l. The chloride loading for natural gradient modeling is summarized in Table 4.7.

	Cl Period 1 (mg/l)	Cl Period 2 (mg/l)	Cl Period 3 (mg/l)
Small Pond	160	10	10
Large Pond	160	10	10
Cl Chloride concentration			

Table 4.7 Chloride loading for natural gradient transport (NG-CT) modeling (Borden, 1986a)

For the recovery and injection system modeling, the water injected into the 22 injection wells is assigned a concentration of zero $\mu\text{g/l}$. Clean

water injected into the aquifer displaces the contaminated water produced by the recovery wells.

4.3.6 Boundary Conditions

The boundary conditions for the modeling domain are determined independently from model simulation results. An independent estimation of boundary conditions is used because information regarding which representation of aquifer properties most closely resembles the observed *GWSEs* is desired.

The independent estimation of the two constant head boundary conditions is performed by extrapolating values of *GWSE* at rows 1 and 83 based on the least-squares first-order polynomial approximation of a plane to the observed *GWSE* data. The determined *GWSE* of the northern boundary of the modeling domain, row 1, is 215.74 ft MSL. The *GWSE* of the southern boundary of the modeling domain, row 83, is 205.60 ft MSL.

4.3.7 Initial Conditions

Initial conditions of *GWSE* are not applicable to the flow aspects of the natural gradient or recovery and injection system modeling because steady-state hydraulics are assumed in each of these cases. Initial conditions

of contaminant concentration are required for the transport aspects of the natural gradient and recovery and injection system modeling.

The initial chloride concentration condition for the natural gradient transport (NG-CT) modeling is a chloride concentration equal to zero mg/l in every cell of the modeling domain. A chloride concentration equal to zero mg/l corresponds to the assumption that no chloride concentration above background levels were present prior to time period 1, the facility's initial operation in 1946.

The initial naphthalene concentration condition for the recovery and injection system transport (RI-CT) modeling is generated from a natural gradient transport simulation. Naphthalene loading for the natural gradient transport simulation is derived from those estimated and presented by Borden (1986a). The naphthalene loading used in the natural gradient transport simulation is presented in Table 4.8.

	Naph Period 1 ($\mu\text{g/l}$)	Naph Period 2 ($\mu\text{g/l}$)	Naph Period 3 ($\mu\text{g/l}$)
Small Pond	200	100	10
Large Pond	2000	1000	100
Naph	Naphthalene concentration		

Table 4.8 Naphthalene loading for generation of initial naphthalene concentrations for recovery and injection system transport (RI-CT) modeling (Borden, 1986a)

Constant representations of hydraulic conductivity and bottom elevation are used in the simulation of naphthalene migration in order to minimize the areal extent of the naphthalene plume. The areal extent is minimized to facilitate more pronounced effects in the recovery and injection system transport (RI-CT) modeling. A smaller areal extent of contamination provides a better basis for comparison of the effects of different representations of aquifer properties on recovery and injection system transport (RI-CT) modeling. A plot of the initial naphthalene concentration distribution for the recovery and injection system transport (RI-CT) modeling is presented as Figure 4.3.

4.4 Model Calibration

The purpose of calibration is to establish that the model can reproduce field measured *GWSEs*. Calibration is traditionally done by trial and error adjustment of parameters or by using an automated parameter estimation code to minimize the difference between the observed and simulated *GWSEs*. The *RMSE* of simulated *GWSEs* to observations is a good measure of model calibration. In the research presented here, the traditional trial and error adjustment of parameters is not performed. Instead, different representations of aquifer properties are tried in order to study the effect of each representation on model calibration, as measured by the *RMSE* of *GWSEs*. Rather than compare different values of an aquifer property, the research

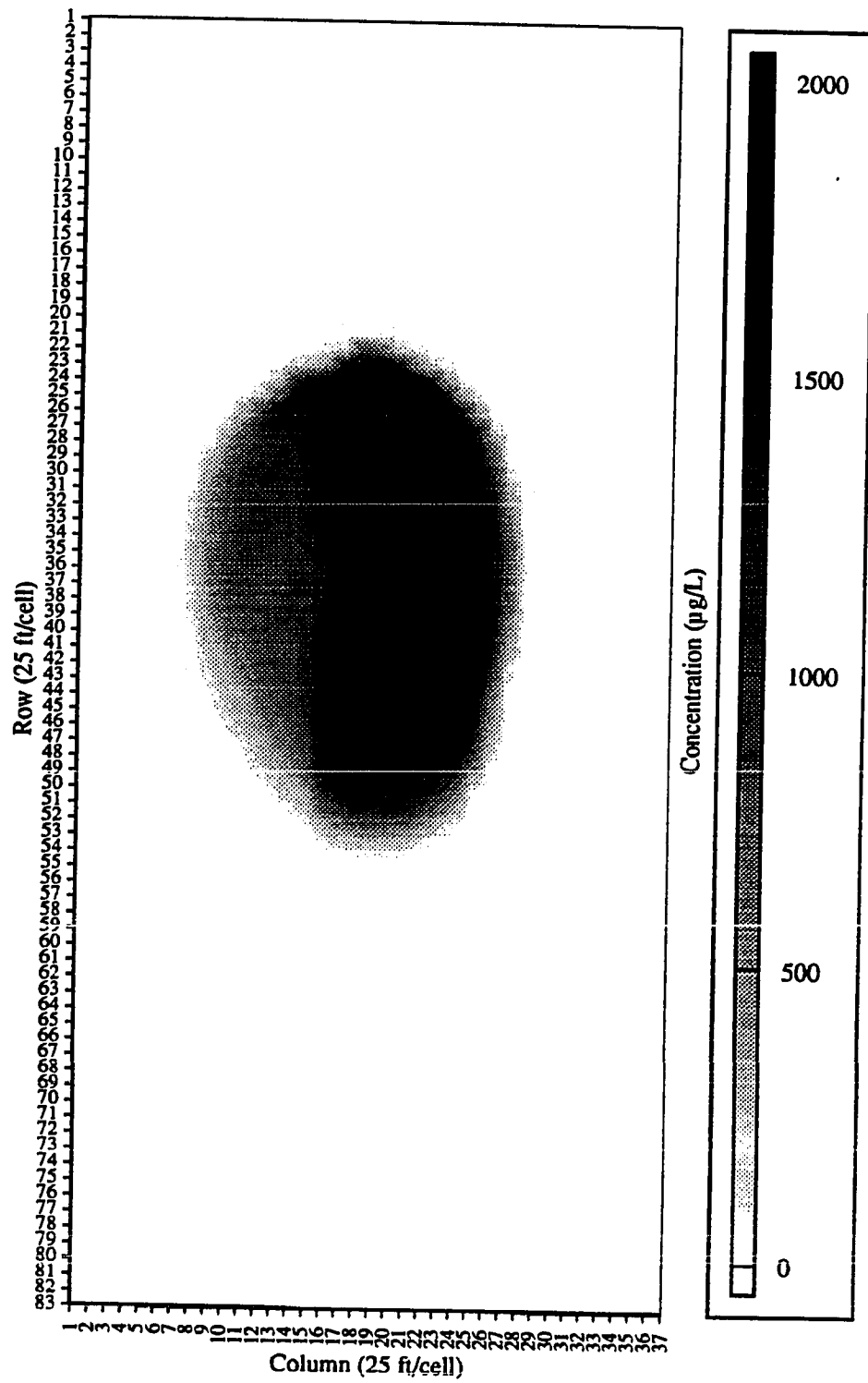


Figure 4.3 Initial naphthalene concentrations for recovery and injection system modeling

presented here compares different independently derived representations of aquifer properties. The natural gradient flow (NG-GF) modeling is used for the calibration procedure.

Another test of the effects of using representations of aquifer properties on model calibration is made by comparing the difference between the observed and simulated chloride concentrations. The *RMSE* of simulated natural log chloride concentrations to observations is another good measure of model calibration. Different representations of aquifer properties are tried in order to study the effect of each representation on model calibration, as measured by the *RMSE* of natural log chloride concentrations. The natural gradient transport (NG-CT) modeling is used for the second calibration procedure.

4.5 Model Prediction

Prediction quantifies the response of the system to future events. The model is run with calibrated values for parameters and loadings, except for those loadings that are expected to change in the future. Estimates of the future loadings are needed to perform the simulation. Uncertainty in a predictive simulation arises from uncertainty in the calibrated model and the inability to estimate accurate values for the magnitude and timing of future loadings.

The effect of representing the spatial variability of aquifer properties on model predictions are studied. Results of predictive model simulations are compared to each other to observe the relative differences in model results. The relative differences in model results serve as an indication of the significance of representing the spatial variability of aquifer properties. The recovery and injection system flow (RI-GF) and transport (RI-CT) modeling are used to study model prediction.

DISCUSSION

Results of the natural gradient modeling include simulated *GWSEs* and chloride concentrations at cells corresponding to cells where observation are made. These results are presented and compared in the following discussion. Natural gradient flow (NG-GF) modeling results are presented as *GWSE* contours and are shown in appendix A. Natural gradient transport (NG-CT) modeling results are presented as chloride concentration distributions and are shown in appendix B.

Results of the recovery and injection system simulations include drawdown at recovery wells and recovery efficiency information. These results are presented and compared in the following discussion. Recovery and injection system flow (RI-GF) modeling results are presented as *GWSE* contours and are shown in appendix C. Recovery and injection system transport (RI-CT) modeling results are presented as naphthalene concentration distributions and are shown in appendix D.

5.1 Natural Gradient

A comparison of the results of simulations is made to determine how the representation of aquifer properties affects natural gradient flow (NG-GF) and transport (NG-CT) modeling at the UCC site. For the natural gradient modeling, comparisons are made of simulation results to actual observa-

tions, providing both a measure of how well each simulation matches the observed data and how natural gradient modeling is affected by the representation of aquifer properties.

5.1.1 Ground Water Flow

The criteria for analyzing the results of simulations of natural gradient flow (NG-GF) are comparing the mean estimation error, the estimation error variance, and the *RMSE* of the observed and simulated *GWSEs*. The observed and simulated *GWSEs* at each monitoring well location, estimation error at each well, mean estimation error, estimation error variance, and *RMSE* for each of the seven NG-GF simulations are presented in Tables 5.1.a, 5.1.b, and 5.1.c.

Representing aquifer properties affects model calibration to observed *GWSEs*. An indication of the overestimation or underestimation of the simulated *GWSEs* compared to the observations is made by comparing the mean estimation error. The simulations in which representation of aquifer properties improve the mean estimation error over sim. KB-C are sim. B-P and B-K. The other simulations worsened model calibration over sim. KB-C, when measured by the mean estimation error of *GWSEs*.

An indication of the match of the shape of the simulated *GWSEs* compared to the observations is made by comparing the estimation error

Well ID	Obs. <i>GWSE</i> (ft MSL)	KB-C <i>GWSE</i> (ft MSL)	KB-P <i>GWSE</i> (ft MSL)	KB-K <i>GWSE</i> (ft MSL)	KB-C <i>r</i> (ft)	KB-P <i>r</i> (ft)	KB-K <i>r</i> (ft)
SW1	214.77	215.74	215.74	215.74	-0.97	-0.97	-0.97
SW2	210.05	211.33	211.94	211.33	-1.28	-1.89	-1.28
SW3	210.25	211.46	212.37	211.74	-1.21	-2.12	-1.49
SW4	208.61	209.70	209.53	208.26	-1.09	-0.92	0.35
SW5	211.00	212.25	213.55	213.42	-1.25	-2.55	-2.42
SW6	212.32	213.33	214.85	214.58	-1.01	-2.53	-2.26
SW7	208.58	210.25	209.51	208.93	-1.67	-0.93	-0.35
SW8	210.49	210.74	210.62	210.22	-0.25	-0.13	0.27
SW9	211.87	212.76	214.25	214.07	-0.89	-2.38	-2.20
SW10	205.01	206.27	205.76	205.79	-1.26	-0.75	-0.78
RU1	211.15	212.45	213.75	213.79	-1.30	-2.60	-2.64
RU2	212.37	213.42	214.88	214.82	-1.05	-2.51	-2.45
RU3	212.60	213.40	215.03	214.74	-0.80	-2.43	-2.14
RU8	212.39	213.62	215.04	214.95	-1.23	-2.65	-2.56
RU9	212.11	213.30	214.76	214.71	-1.19	-2.65	-2.60
RU26	212.03	212.90	214.34	214.34	-0.87	-2.31	-2.31
RU28	211.11	212.45	213.75	213.79	-1.34	-2.64	-2.68
RU29	211.10	212.33	213.58	213.63	-1.23	-2.48	-2.53
RU30	211.99	213.16	214.66	214.55	-1.17	-2.67	-2.56
DW2	212.56	213.61	215.12	214.94	-1.05	-2.56	-2.38
DW7	207.75	209.12	207.46	207.28	-1.37	0.29	0.47
DW9	211.39	212.56	213.91	213.94	-1.17	-2.52	-2.55
Min.					-1.67	-2.67	-2.68
Max.					-0.25	0.29	0.47
\bar{r}					-1.12	-1.95	-1.73
S_r^2					0.07	0.81	1.11
<i>RMSE</i>					1.15	2.15	2.03
Obs.	Observed						
<i>GWSE</i>	Ground water surface elevation						
<i>r</i>	Estimation error						
\bar{r}	Mean estimation error						
S_r^2	Estimation error variance						
<i>RMSE</i>	Root mean squared error						

Table 5.1.a Comparison of *GWSEs* for natural gradient flow (NG-GF) modeling, sims. KB-C, KB-P, and KB-K

Well ID	Obs. <i>GWSE</i> (ft MSL)	K-P <i>GWSE</i> (ft MSL)	K-K <i>GWSE</i> (ft MSL)	K-P <i>r</i> (ft)	K-K <i>r</i> (ft)
SW1	214.77	215.74	215.74	-0.97	-0.97
SW2	210.05	212.19	212.49	-2.14	-2.44
SW3	210.25	212.39	212.83	-2.14	-2.58
SW4	208.61	209.41	209.74	-0.80	-1.13
SW5	211.00	213.67	214.14	-2.67	-3.14
SW6	212.32	214.97	215.02	-2.65	-2.70
SW7	208.58	210.47	210.42	-1.89	-1.84
SW8	210.49	211.43	211.43	-0.94	-0.94
SW9	211.87	214.37	214.59	-2.50	-2.72
SW10	205.01	205.87	206.13	-0.86	-1.12
RU1	211.15	214.01	214.52	-2.86	-3.37
RU2	212.37	215.01	215.20	-2.64	-2.83
RU3	212.60	215.02	215.08	-2.42	-2.48
RU8	212.39	215.15	215.27	-2.76	-2.88
RU9	212.11	214.92	215.14	-2.81	-3.03
RU26	212.03	214.53	214.92	-2.50	-2.89
RU28	211.11	214.01	214.52	-2.90	-3.41
RU29	211.10	213.86	214.39	-2.76	-3.29
RU30	211.99	214.81	215.02	-2.82	-3.03
DW2	212.56	215.16	215.24	-2.60	-2.68
DW7	207.75	208.62	208.88	-0.87	-1.13
DW9	211.39	214.15	214.64	-2.76	-3.25
Min.				-2.90	-3.41
Max.				-0.80	-0.94
\bar{r}				-2.19	-2.45
S_r^2				0.56	0.69
<i>RMSE</i>				2.32	2.58
Obs.	Observed				
<i>GWSE</i>	Ground water surface elevation				
<i>r</i>	Estimation error				
\bar{r}	Mean estimation error				
S_r^2	Estimation error variance				
<i>RMSE</i>	Root mean squared error				

Table 5.1.b Comparison of *GWSEs* for natural gradient flow (NG-GF) modeling, sims. K-P and K-K

Well ID	Obs. <i>GWSE</i> (ft MSL)	B-P <i>GWSE</i> (ft MSL)	B-K <i>GWSE</i> (ft MSL)	B-P <i>r</i> (ft)	B-K <i>r</i> (ft)
SW1	214.77	215.74	215.74	-0.97	-0.97
SW2	210.05	209.71	209.22	0.34	0.83
SW3	210.25	209.96	209.40	0.29	0.85
SW4	208.61	208.31	207.73	0.30	0.88
SW5	211.00	210.79	210.40	0.21	0.60
SW6	212.32	212.17	212.02	0.15	0.30
SW7	208.58	208.42	208.14	0.16	0.44
SW8	210.49	209.05	208.76	1.44	1.73
SW9	211.87	211.45	211.22	0.42	0.65
SW10	205.01	205.85	205.80	-0.84	-0.79
RU1	211.15	211.07	210.56	0.08	0.59
RU2	212.37	212.32	211.94	0.05	0.43
RU3	212.60	212.73	211.97	-0.13	0.63
RU8	212.39	212.59	212.25	-0.20	0.14
RU9	212.11	212.11	211.81	0.00	0.30
RU26	212.03	211.62	211.14	0.41	0.89
RU28	211.11	211.07	210.56	0.04	0.55
RU29	211.10	210.92	210.43	0.18	0.67
RU30	211.99	211.93	211.71	0.06	0.28
DW2	212.56	212.84	212.24	-0.28	0.32
DW7	207.75	207.31	207.08	0.44	0.67
DW9	211.39	211.21	210.69	0.18	0.70
Min.				-0.97	-0.97
Max.				1.44	1.73
\bar{r}				0.11	0.49
S_r^2				0.21	0.29
<i>RMSE</i>				0.47	0.72
Obs.	Observed				
<i>GWSE</i>	Ground water surface elevation				
<i>r</i>	Estimation error				
\bar{r}	Mean estimation error				
S_r^2	Estimation error variance				
<i>RMSE</i>	Root mean squared error				

Table 5.1.c Comparison of *GWSEs* for natural gradient flow (NG-GF) modeling, sims. B-P and B-K

variance. There are no simulations in which representation of aquifer properties improve the estimation error variance over sim. KB-C, when measured by the mean estimation variance of *GWSEs*.

An combined indication of the match of the magnitudes and shape of the simulated *GWSEs* compared to the observations is made by comparing the *RMSE*. The simulations in which representation of aquifer properties improve the *RMSE* over sim. KB-C are the same as for improving the mean estimation error, sim. B-P and B-K, when measured by the *RMSE* of *GWSEs*.

The simulations using polynomial approximations of each aquifer property possess mean estimation errors closer to zero, smaller estimation error variances, and smaller *RMSEs* than the simulations using kriging approximations of each aquifer property. Both simulations using variable representations of bottom elevation produce mean estimation errors closer to zero, smaller estimation error variances, and smaller *RMSEs* than the simulation using constant representation. Both simulations using variable representations of hydraulic conductivity produce mean estimation errors further from zero, smaller estimation error variances, and smaller *RMSEs* than the simulation using constant representation. The simulations with conjunctive variable representations of aquifer properties have mean estimation errors

further from zero, smaller estimation error variances, and smaller *RMSEs* than the simulation using constant representation simulation. A summary of the mean estimation errors appears in Table 5.2.

Sim. ID	\bar{r} (ft)	S_r^2 (ft ²)	<i>RMSE</i> (ft)
KB-C	-1.12	0.07	1.15
KB-P	-1.95	0.81	2.15
KB-K	-1.73	1.11	2.03
K-P	-2.19	0.56	2.32
K-K	-2.45	0.69	2.58
B-P	0.11	0.21	0.47
B-K	0.49	0.29	0.72
\bar{r}_2	Mean estimation error		
S_r^2	Estimation error variance		
<i>RMSE</i>	Root mean squared error		

Table 5.2 Summary of *GWSE* comparison for natural gradient flow (NG-GF) modeling

Effects of representing aquifer properties that are not identified by the analysis of the statistics of the simulated and observed values of *GWSEs* include flow direction and velocity deviates. Effects of the choice of representations are apparent by observing the *GWSE* contour plots presented in appendix A. For example, in the region just south of the waste ponds, sim. KB-K indicates a *GWSE* gradient approximately 2.5 times greater than the *GWSE* gradient in sim. B-K. The bunching of the *GWSE* contours is an indication of the *GWSE* gradient. The indication of direction of ground water flow is normal to the *GWSE* contours. Sims. KB-K and K-K indicate ground water flow directions that are not strictly from grid north to grid south.

5.1.2 Contaminant Transport

The criteria for analyzing the results of simulations of natural gradient transport (NG-CT) are basically the same as for natural gradient flow (NG-GF). The mean estimation error, the estimation error variance, and the *RMSE* of the observed and simulated natural log chloride concentrations serves as the basis for comparison. The observed and simulated chloride concentrations for each of the seven NG-CT simulations are presented in Table 5.3.

Well ID	Obs. Cl (mg/l)	KB-C Cl (mg/l)	KB-P Cl (mg/l)	KB-K Cl (mg/l)	K-P Cl (mg/l)	K-K Cl (mg/l)	B-P Cl (mg/l)	B-K Cl (mg/l)
SW1	14	15	15	15	15	15	15	15
SW2	74	107	16	15	16	15	127	149
SW3	80	15	15	78	18	32	15	15
SW4	68	15	15	15	15	15	15	15
SW5	154	16	117	169	117	143	23	21
SW6	26	15	19	19	15	16	15	15
RU1	75	163	174	169	173	170	160	159
RU2	58	159	154	152	159	159	155	151
RU3	8	15	15	15	15	15	15	15
RU5A	58	159	154	151	159	159	155	151
RU5B	52	159	154	151	159	159	155	151
RU5J	28	159	154	151	159	159	155	151
RU7	12	15	15	15	15	15	15	15
RU8	46	159	154	154	159	160	158	153
RU9	13	159	157	154	160	160	155	154
RU26	36	159	155	152	159	159	155	152
RU28	55	163	174	169	173	170	160	159
RU29	74	169	174	174	172	172	166	166
RU30	15	171	174	175	172	173	174	175
Obs. Cl	Observed chloride concentration Chloride concentration							

Table 5.3 Comparison of chloride concentrations for natural gradient transport (NG-CT) modeling

The observed and simulated natural log chloride concentrations at each monitoring well location, estimation error at each well, mean estimation error, estimation error variance, and *RMSE* for each of the seven NG-CT simulations are presented in Tables 5.4.a, 5.4.b, and 5.4.c.

The choice of representations of aquifer properties has a less significant effects on model calibration to observed chloride concentration. The simulations in which representation of aquifer properties improve the mean estimation error over sim. KB-C are sim. B-P and B-K, but because the amount of improvement is so slight, there is practically no improvement. The other simulations worsened model calibration over sim. KB-C, when measured by the mean estimation error of natural log chloride concentrations.

In every simulation, the representation of the spatial variability of aquifer properties improve the estimation error variance over sim. KB-C, with sim KB-N offering the greatest improvement, when measured by the mean estimation variance of natural log chloride concentrations.

Just as for the estimation error variance, every simulation with a spatially variable representation of aquifer properties improve the *RMSE* of natural log chloride concentrations over sim. KB-C. The simulations using polynomial approximations of each aquifer property possessed very similar

Well ID	Obs. ln(Cl) ln(mg/l)	KB-C ln(Cl) ln(mg/l)	KB-P ln(Cl) ln(mg/l)	KB-K ln(Cl) ln(mg/l)	KB-C r ln(mg/l)	KB-P r ln(mg/l)	KB-K r ln(mg/l)
SW1	2.6	2.7	2.7	2.7	-0.1	-0.1	-0.1
SW2	4.3	4.7	2.8	2.7	-0.4	1.5	1.6
SW3	4.4	2.7	2.7	4.4	1.7	1.7	0.0
SW4	4.2	2.7	2.7	2.7	1.5	1.5	1.5
SW5	5.0	2.8	4.8	5.1	2.2	0.2	-0.1
SW6	3.3	2.7	2.9	2.9	0.6	0.4	0.4
RU1	4.3	5.1	5.2	5.1	-0.8	-0.9	-0.8
RU2	4.1	5.1	5.0	5.0	-1.0	-0.9	-0.9
RU3	2.1	2.7	2.7	2.7	-0.6	-0.6	-0.6
RU5A	4.1	5.1	5.0	5.0	-1.0	-0.9	-0.9
RU5B	4.0	5.1	5.0	5.0	-1.1	-1.0	-1.0
RU5J	3.3	5.1	5.0	5.0	-1.8	-1.7	-1.7
RU7	2.5	2.7	2.7	2.7	-0.2	-0.2	-0.2
RU8	3.8	5.1	5.0	5.0	-1.3	-1.2	-1.2
RU9	2.6	5.1	5.1	5.0	-2.5	-2.5	-2.4
RU26	3.6	5.1	5.0	5.0	-1.5	-1.4	-1.4
RU28	4.0	5.1	5.2	5.1	-1.1	-1.2	-1.1
RU29	4.3	5.1	5.2	5.2	-0.8	-0.9	-0.9
RU30	2.7	5.1	5.2	5.2	-2.4	-2.5	-2.5
Min.					-2.5	-2.5	-2.5
Max.					2.2	1.7	1.6
\bar{r}					-0.56	-0.56	-0.65
S_r^2					1.57	1.39	1.11
RMSE					1.37	1.31	1.23
Obs.	Observed						
ln(Cl)	Natural log chloride concentration						
r	Estimation error						
\bar{r}	Mean estimation error						
S_r^2	Estimation error variance						
RMSE	Root mean squared error						

Table 5.4.a Comparison of natural log chloride concentrations for natural gradient transport (NG-CT) modeling, sims. KB-C, KB-P, and KB-K

mean estimation errors, estimation error variances, and *RMSEs* to the simulations using kriging approximations of each aquifer property. The simulations with conjunctive variable representations of aquifer properties have

Well ID	Obs. ln(Cl) ln(mg/l)	K-P ln(Cl) ln(mg/l)	K-K ln(Cl) ln(mg/l)	K-P r ln(mg/l)	K-K r ln(mg/l)
SW1	2.6	2.7	2.7	-0.1	-0.1
SW2	4.3	2.8	2.7	1.5	1.6
SW3	4.4	2.9	3.5	1.5	0.9
SW4	4.2	2.7	2.7	1.5	1.5
SW5	5.0	4.8	5.0	0.2	0.0
SW6	3.3	2.7	2.8	0.6	0.5
RU1	4.3	5.2	5.1	-0.9	-0.8
RU2	4.1	5.1	5.1	-1.0	-1.0
RU3	2.1	2.7	2.7	-0.6	-0.6
RU5A	4.1	5.1	5.1	-1.0	-1.0
RU5B	4.0	5.1	5.1	-1.1	-1.1
RU5J	3.3	5.1	5.1	-1.8	-1.8
RU7	2.5	2.7	2.7	-0.2	-0.2
RU8	3.8	5.1	5.1	-1.3	-1.3
RU9	2.6	5.1	5.1	-2.5	-2.5
RU26	3.6	5.1	5.1	-1.5	-1.5
RU28	4.0	5.2	5.1	-1.2	-1.1
RU29	4.3	5.1	5.1	-0.8	-0.8
RU30	2.7	5.1	5.2	-2.4	-2.5
Min.				-2.5	-2.5
Max.				1.5	1.6
\bar{r}_2				-0.58	-0.62
S_r^2				1.39	1.28
RMSE				1.31	1.29
Obs.	Observed				
ln(Cl)	Natural log chloride concentration				
r	Estimation error				
\bar{r}_2	Mean estimation error				
S_r^2	Estimation error variance				
RMSE	Root mean squared error				

Table 5.4.b Comparison of natural log chloride concentrations for natural gradient transport (NG-CT) modeling, sims. K-P and K-K

mean estimation errors closer to zero, smaller estimation error variances, and smaller *RMSEs* than the simulation using constant representation simulation.

A summary of the mean estimation errors appears in Table 5.5.

Well ID	Obs. ln(Cl) ln(mg/l)	B-P ln(Cl) ln(mg/l)	B-K ln(Cl) ln(mg/l)	B-P r ln(mg/l)	B-K r ln(mg/l)
SW1	2.6	2.7	2.7	-0.1	-0.1
SW2	4.3	4.8	5.0	-0.5	-0.7
SW3	4.4	2.7	2.7	1.7	1.7
SW4	4.2	2.7	2.7	1.5	1.5
SW5	5.0	3.1	3.0	1.9	2.0
SW6	3.3	2.7	2.7	0.6	0.6
RU1	4.3	5.1	5.1	-0.8	-0.8
RU2	4.1	5.0	5.0	-0.9	-0.9
RU3	2.1	2.7	2.7	-0.6	-0.6
RU5A	4.1	5.0	5.0	-0.9	-0.9
RU5B	4.0	5.0	5.0	-1.0	-1.0
RU5J	3.3	5.0	5.0	-1.7	-1.7
RU7	2.5	2.7	2.7	-0.2	-0.2
RU8	3.8	5.1	5.0	-1.3	-1.2
RU9	2.6	5.0	5.0	-2.4	-2.4
RU26	3.6	5.0	5.0	-1.4	-1.4
RU28	4.0	5.1	5.1	-1.1	-1.1
RU29	4.3	5.1	5.1	-0.8	-0.8
RU30	2.7	5.2	5.2	-2.5	-2.5
Min.				-2.5	-2.5
Max.				1.9	2.0
\bar{r}_2				-0.55	-0.55
S_r^2				1.45	1.47
RMSE				1.33	1.33
Obs.	Observed				
ln(Cl)	Natural log chloride concentration				
r	Estimation error				
\bar{r}_2	Mean estimation error				
S_r^2	Estimation error variance				
RMSE	Root mean squared error				

Table 5.4.c Comparison of natural log chloride concentrations for natural gradient transport (NG-CT) modeling, sims. B-P and B-K

Effects of representing aquifer properties that are not identified by the analysis of the statistics of the simulated and observed values of natural log chloride concentrations include downgradient reach and spatial shape of the

Sim. ID	\bar{r} ln(mg/l)	S_r^2 ln(mg/l) ²	RMSE ln(mg/l)
KB-C	-0.56	1.57	1.37
KB-P	-0.56	1.39	1.31
KB-K	-0.65	1.11	1.23
K-P	-0.58	1.39	1.31
K-K	-0.62	1.28	1.29
B-P	-0.55	1.45	1.33
B-K	-0.55	1.47	1.33
\bar{r}_2	Mean estimation error		
S_r^2	Estimation error variance		
RMSE	Root mean squared error		

Table 5.5 Summary of chloride concentration comparison for natural gradient transport (NG-CT) modeling

chloride plume. Effects of the choice of representations are apparent by observing the chloride concentration distributions presented in appendix B. For example, sim. B-P has a down-gradient reach extending to row 58 while sim. KB-P only extends to row 49, a difference of 9 rows or approximately 225 ft. The chloride plume of simulations using kriging hydraulic conductivity representations have quite different spatial shapes than the other simulations. The “bowl” pattern of the hydraulic conductivity distributions is reflected by the contaminant migration around the region of lower hydraulic conductivity.

5.2 Recovery and Injection

A comparison of the results of the simulations is made to determine how the representation of aquifer properties affects recovery and injection

system flow (RI-GF) and transport (RI-CT) modeling at the UCC site. For the recovery and injection system modeling, simulation results are compared to the each other, providing a measure of how recovery and injection system modeling is affected by the representation of aquifer properties.

5.2.1 Ground Water Flow

The criteria for analyzing the results of simulations of recovery and injection system flow (RI-GF) are comparing the maximum relative drawdown and number of recovery wells that went dry under the hydraulic loading. The simulated relative drawdown at each of the recovery wells for each of the simulations are presented in Table 5.6. The maximum relative drawdown and number of recovery wells that went dry under the hydraulic loading for each of the seven RI-GF simulations are presented in Table 5.7.

Sim. KB-P, K-K, and B-K had recovery wells that went dry under the hydraulic loading. The simulations using polynomial approximations of each aquifer property possess maximum relative drawdowns larger than the simulations using constant representation. The simulations using kriging approximations of each aquifer property have one or more wells that go dry.

The representation of aquifer properties affects model prediction by indicating regions in which simulated recovery wells went dry. This is

Well ID	KB-C RD (dim.)	KB-P RD (dim.)	KB-K RD (dim.)	K-P RD (dim.)	K-K RD (dim.)	B-P RD (dim.)	B-K RD (dim.)
R1	0.14	0.04	0.06	0.05	0.03	0.31	0.09
R2	0.11	0.02	0.09	0.05	0.02	0.19	0.06
R3	0.07	-0.01	0.14	0.04	0.01	0.11	-0.01
R4	0.02	-0.05	0.09	0.01	-0.01	0.03	-0.05
R5	0.16	0.10	0.10	0.08	0.05	0.54	0.19
R6	0.13	0.06	0.10	0.09	0.04	0.30	0.08
R7	0.09	0.02	0.16	0.09	0.04	0.16	0.02
R8	0.04	-0.02	0.34	0.06	1.00	0.06	-0.05
R9	-0.03	-0.08	0.03	-0.02	-0.08	-0.02	-0.08
R10	0.15	0.14	0.14	0.13	0.06	0.50	1.00
R11	0.11	0.05	0.14	0.13	0.06	0.26	0.03
R12	0.07	0.00	0.21	0.12	0.09	0.13	-0.03
R13	0.01	-0.04	0.20	0.06	0.05	0.02	-0.06
R14	0.16	0.15	0.16	0.13	0.07	0.51	1.00
R15	0.13	0.08	0.17	0.15	0.07	0.37	0.07
R16	0.09	-0.03	0.14	0.17	0.07	0.22	-0.01
R17	0.04	-0.04	0.22	0.14	0.09	0.08	-0.05
R18	-0.03	-0.09	0.06	0.01	-0.06	-0.02	-0.09
R19	0.15	0.11	0.20	0.14	0.09	0.37	0.16
R20	0.11	1.00	0.18	0.17	0.09	0.31	0.03
R21	0.07	1.00	0.20	0.19	0.09	0.19	-0.02
R22	0.02	-0.04	0.21	0.12	0.02	0.05	-0.05
Max. # Dry	0.16 0	1.00 2	0.34 0	0.19 0	1.00 1	0.54 0	1.00 2
RD	Relative drawdown						
Max.	Maximum drawdown						
# Dry	Number of wells pumped dry						

Table 5.6 Comparison of relative drawdown for recovery and injection system flow (RI-GF) modeling

important from a design standpoint. Effects of representing aquifer properties on flow direction and velocity are minimal because these are primarily a function of the hydraulic loading. The *GWSE* contour plots of simulation results presented in appendix C show the extreme variations in *GWSEs*

Sim. ID	Max. (dim.)	# Dry (dim.)
KB-C	0.16	0
KB-P	1.00	2
KB-K	0.34	0
K-P	0.19	0
K-K	1.00	1
B-P	0.54	0
B-K	1.00	2
Max. # Dry	Maximum drawdown Number of wells pumped dry	

Table 5.7 Summary of relative drawdown comparison for recovery and injection system flow (RI-GF) modeling

between recovery and injection wells in the zones of lower hydraulic conductivity around monitoring well SW7.

5.2.2 Contaminant Transport

The criteria for analyzing the results of simulations of recovery and injection system transport (RI-CT) are comparing the recovery efficiency and relative change in recovery efficiency compared to the simulation using constant representations of aquifer properties. The recovery efficiencies for each of the seven RI-CT simulations are presented in Table 5.8.

Both simulations using variable representations of bottom elevation produce recovery efficiencies greater than the simulation using a constant representation. Both simulations using variable representations of hydraulic

Sim. ID	M_i (ft ³ •mg/l) (×10 ⁸)	M_f (ft ³ •mg/l) (×10 ⁸)	R (dim.)	ΔR (dim.)
KB-C	15.5	5.5	0.64	
KB-P	12.8	3.4	0.73	0.14
KB-K	13.4	3.7	0.73	0.13
K-P	15.5	5.6	0.64	0.00
K-K	15.5	5.1	0.67	0.04
B-P	12.8	3.2	0.75	0.17
B-K	13.4	3.9	0.71	0.10
M_i	Mass initially in system			
M_f	Mass finally in system			
R	Recovery efficiency			
ΔR	Relative change in R compared to sim. KB-C			

Table 5.8 Comparison of recovery efficiency for recovery and injection system transport (RI-CT) modeling

conductivity produce recovery efficiencies approximately equal to the simulation using a constant representation.

Representing aquifer properties affects recovery and injection system transport (RI-CT) modeling. The representation of aquifer properties model prediction by as much as 17%, when measured by recovery efficiency. Effects of representing aquifer properties on downgradient reach and spatial shape of the naphthalene plume are minimal because these are primarily a function of the hydraulic loading and initial naphthalene concentration distribution. The minimal effects are apparent by observing the naphthalene concentration distributions of simulation results presented in appendix D. For example, only slight differences in the southwest region of the naphthalene plume can be detected.

CONCLUSIONS

Numerical ground water modeling is inherently subject to errors. One recourse to help minimize the errors in modeling involves making the best use of observed aquifer properties. The careful interpretation of observed aquifer data may lead to improved modeling results. The process of generating representations of aquifer properties is an important aspect of the interpretation of field site data. The careful analysis of representations of aquifer properties can serve an important role in the attempt to improve the accuracy of modeling results.

6.1 Representations of Aquifer Properties

The analysis of the spatial distribution of an aquifer property may identify the need for field verification of existing data or gathering of additional data. Data which do not conform to the estimated value at the same location may be identified. This process is known as the cross-validation of field data. Trends in the representation of aquifer properties may be detected by visual inspection of contour plots of the representation and may reveal trends in the aquifer property distribution.

Considering the hydraulic conductivity data used in the research presented here, the observed value of hydraulic conductivity at monitoring well SW2 is identified as an extreme observation because it does not fit into an

obvious trend. Both the polynomial and kriging cross-validations at monitoring well SW2 yield relatively large estimation errors. The observed values of bottom elevation at monitoring wells SW10 and RU1 are identified as potential erroneous observations because they are not consistent with other nearby observations and there is no evidence of a physical explanation for the discrepancies observed over such a short distance. The polynomial and kriging cross-validations at monitoring wells SW10 and RU1 yield large estimation errors.

Analysis of representations of aquifer properties may also identify the need for gathering of additional data. If a region exhibits a trend that is fairly well cross-validated, but a physical explanation for the trend is not known, then a comprehensive site investigation is needed to determine the reasons for the trend. An example is the lower bottom elevation in the southern region of the modeling domain. More data are needed to determine the detailed stratigraphy between monitoring wells DW4, DW7, and DW10.

Considering the representations of hydraulic conductivity generated by either polynomial or kriging methods, the observed values of hydraulic conductivity in the region of monitoring wells SW2, SW7, and SW8 are notably different than the observed values of hydraulic conductivity in the regions to the north or the south of the described region. While the apparent local zone of reduced hydraulic conductivity may be explained geologically

by a number of reasons such as local variation in the alluvial deposits or fouling of the aquifer media by wastes from the UCC facility operation, no reasons were identified by Weston (1985) in the initial site investigation. A physical basis for the local zone of reduced hydraulic conductivity should be determined and verified before making design decisions with the data.

6.2 Modeling

Representing the spatial variability of aquifer properties can serve an important role in the attempt to improve the accuracy of the interpretation of modeling results. The effect of representing the spatial variability is a function of the modeling purpose.

Natural gradient flow modeling is significantly affected by including information about the spatial structure of an aquifer property. The representation of the bottom elevation improved model calibration while the representation of hydraulic conductivity worsened model calibration, when measured by the mean estimation error and *RMSE* of *GWSEs*. The estimate error variance is minimized in the simulation using constant representations of bottom elevation and hydraulic conductivity. Other effects of representing aquifer properties include the variation of flow direction and velocity.

Natural gradient transport modeling is less affected by the representation of the spatial variability of aquifer properties. The use of representa-

tions of aquifer properties generally did not improve or worsen model calibration, when measured by the mean estimation error, estimation error variance, and *RMSE* of natural log chloride concentrations. Other effects of representing aquifer properties include the downgradient reach and spatial shape of the chloride plume.

Recovery and injection system flow modeling is affected by the use of detailed representations of aquifer properties. The representation of aquifer properties affects model prediction by indicating regions in which the simulated recovery wells were shown to go dry. This is important from a design standpoint. Effects of representing aquifer properties on flow direction and velocity are minimal because these are primarily a function of the hydraulic loading.

Recovery and injection system transport modeling is less affected by the representation of the spatial variability of aquifer properties. The representation of aquifer properties vary model prediction by as much as 17%, when measured by recovery efficiency. Effects of representing aquifer properties on downgradient reach and spatial shape of the naphthalene plume are minimal because these are primarily a function of the initial naphthalene concentration distribution.

Model users must realize that model results often appear to be more certain, more precise, and more authoritative than they really are. To successfully interpret the results of a model, the model user must be fully aware of the limitations and accuracy of the model. Often, the most important use of a model is the study of the model's sensitivity of predictions to parameters. Not only are the magnitudes of the values of parameters important in studying a model's sensitivity, but the choice of representations of aquifer properties are just as important.

Crucial to the successful modeling of a system is the model user's consideration of confidence in the data. It is the responsibility of the model user to properly design a model and then intelligently interpret the simulation results. The research presented here will hopefully help improve the accuracy of model use by indicating the significance of the effects of representing the spatial variability of aquifer properties on modeling.

REFERENCES

- Ahmed, S. and G. de Marsily, 1987, Comparison of geostatistical methods for estimating transmissivity using data on transmissivity and specific capacity, *Water Resources Research*, 23(9), pp. 1717-1737.
- Anderson, M.P., 1987, Treatment of heterogeneities in ground water flow modeling, *In: Proceedings of the Solving Groundwater Problems with Models Conference*, National Water Well Association and the International Ground Water Modeling Center, Denver, CO, pp. 444-463.
- Anderson, M.P. and W.W. Woessner, 1992, *Applied Groundwater Modeling*, Academic Press, San Diego, CA, 381 p.
- Bear, J., 1987, Transport Modeling, *In: Proceedings of the NATO Advances Research Workshop on Advances in Analytical and Numerical Groundwater Flow and Quality Modeling* (Custodio, E., A. Gurgui and J.P.L. Ferreira, eds.), D. Reidel Publishing Company, Lisbon, Portugal, pp. 805-813.
- Bedient, P.B., A.C. Rodgers, T.C. Bouvette, M.B. Tomson and T.H. Wang, 1984, Ground water quality at a creosote waste site, *Ground Water* 22(3), pp. 318-329.
- Bedient, P.B., R.C. Borden and D.I. Leib, 1985, Basic concepts for ground water transport modeling, *In: Ground Water Quality* (Ward, C.H., W. Giger and P.L. McCarty, eds.), John Wiley and Sons, New York, NY, pp. 512-531.
- Borden, R.C., 1986a, *Influence of Adsorption and Oxygen Limited Biodegradation on the Transport and Fate of a Creosote Plume: Field Methods and Simulation Techniques*, Ph.D. thesis, Rice University, Houston, TX.
- Borden, R.C. and P.B. Bedient, 1986b, Transport of dissolved hydrocarbons influenced by oxygen-limited biodegradation, 1. Theoretical development, *Water Resources Research* 22(13), pp. 1973-1982.
- Borden, R.C. and P.B. Bedient, 1987, In situ measurement of adsorption and biotransformation at a hazardous waste site, *Water Resources Bulletin* 23(4), pp. 629-636.

- Committee on Ground Water Modeling Assessment, Water Science and Technology Board, Commission on Physical Sciences, Mathematics, and Resources, National Research Council, 1990, *Ground Water Models: Scientific and Regulatory Applications*, National Academy Press, Washington, DC, 303 p.
- Custodio, E., A. Gurgui and J.P.L. Ferreira, Ed., 1988, *Groundwater Flow and Quality Modeling*, D. Reidel, Dordrecht, Holland.
- Davis, A.D., 1987, Determination of mean transmissivity values in the modeling of ground water flow, *In: Proceedings of the Solving Groundwater Problems with Models Conference*, National Water Well Association and the International Ground Water Modeling Center, Denver, CO, pp. 1162-1174.
- Davis, J.C., 1986, *Statistics and Data Analysis in Geology*, John Wiley & Sons, New York, NY, 646 p.
- de Marsily, G., 1986, *Quantitative Hydrogeology*, Academic Press, San Diego, CA, 440 p.
- Domenico, P.A. and F.W. Schwartz, 1990, *Physical and Chemical Hydrogeology*, John Wiley & Sons, New York, NY, 824 p.
- Englund, E. and A. Sparks, 1991, *Geo-EAS 1.2.1, Geostatistical Environmental Assessment Software User's Guide*, U.S. Environmental Protection Agency, Environmental Monitoring Systems Laboratory, Las Vegas, NV.
- Freeze, R.A. and J.A. Cherry, 1979, *Groundwater*, Prentice-Hall, Englewood Cliffs, NJ, 604 p.
- Haselow, J.S. and R.A. Greenkorn, 1991, An experimental investigation of the effect of idealized heterogeneity on the dispersion of miscible fluids, *Water Resources Research*, 27(9), pp. 2473-2482.
- Hughes, J.P. and D.P. Lettenmaier, 1981, Data requirements for kriging: Estimation and network design, *Water Resources Research*, 17(6), pp. 1641-1650.
- Isaaks, E.H. and R.M. Srivastava, 1989, *Applied Geostatistics*, Oxford University Press, New York, NY, 561 p.

- Journel, A.G., 1989, *Fundamentals of Geostatistics in Five Lessons*, American Geophysical Union, Washington, DC, 40 p.
- Journel, A.G. and C.J. Huijbregts, 1978, *Mining Geostatistics*, Academic Press, San Diego, CA, 600 p.
- Keely, J.F., 1989, Introduction, *In: Transport and Fate of Contaminants in the Subsurface*, U. S. Environmental Protection Agency, Center for Environmental Research Information, Cincinnati, OH, pp. 1-4.
- Kitanidis, P.K. and E.G. Vomvoris, 1983, A geostatistical approach to the inverse problem in groundwater modeling (steady state) and one-dimensional simulations, *Water Resources Research*, 19(3), pp. 677-690.
- Konikow, L.F. and J.D. Bredehoeft, 1978, Computer model of two-dimensional solute transport and dispersion in ground water, *In: Techniques of Water Resources Investigations of the U.S. Geological Survey, Book 7*, U.S. Geological Survey, Washington, DC, pp. 1-79.
- Lee, M.D. and C.H. Ward, 1984a, Microbial ecology of a hazardous waste disposal site: Enhancement of biodegradation, *Paper Presented at the Second International Conference on Ground Water Quality Research*, Oklahoma State University, Tulsa, OK.
- Lee, M.D., J.T. Wilson and C.H. Ward, 1984b, Microbial degradation of selected aromatics at a hazardous waste site, *Developments in Industrial Microbiology*, 25, pp. 557-566.
- McDonald, M.G. and A.W. Harbaugh, 1988, A modular three-dimensional finite-difference ground-water flow model, *In: Techniques of Water-Resources Investigations of the U.S. Geological Survey, Book 6, Chapter A1*, U.S. Geological Survey, Washington, DC, 576 p.
- Mercer, J.W. and C.R. Faust, 1986, *Ground Water Modeling*, National Water Well Association, Columbus, OH, 60 p.
- Mercer, J.W., D.C. Skipp and D. Giffin, 1990, *Basics of pump-and-treat ground water remediation technology*, U. S. Environmental Protection Agency, Robert S. Kerr Environmental Research Laboratory, Ada, OK, 31 p.

- Peck, A., S. Gorelick, G. de-Marsily, S. Foster and V. Kovalevsky, 1988, *Consequences of Spatial Variability in Aquifer Properties and Data Limitations*, International Association of Hydrological Sciences, Oxfordshire, UK, 272 p.
- Rifai, H.S., P.B. Bedient, R.C. Borden and J.F. Haasbeek, 1987, *BIOPLUME II; Computer Model of Two-Dimensional Contaminant Transport Under the Influence of Oxygen Limited Biodegradation in Ground Water, User's Manual, Version 1.0*, National Center for Ground Water Research, Rice University, Houston, TX.
- Ripley, B.D., 1981, *Spatial Statistics*, John Wiley & Sons, New York, NY, 252 p.
- RockWare, Inc., 1990, *TrendSurface, Version 1.01*, Wheat Ridge, CO.
- Satkin, R.L. and A.P. Georgakakos, 1991, Geostatistical mapping for hazardous waste sites, *In: Proceedings of the 1991 Georgia Water Resources Conference* (Hatcher, K.J., ed.), The University of Georgia, Athens, GA.
- van der Heijde, P.K.M., A.I. El-Kadi and S.A. Williams, 1988, *Groundwater Modeling: An Overview and Status Report*, U. S. Environmental Protection Agency, Robert S. Kerr Environmental Research Laboratory, Ada, OK, 242 p.
- Wagenet, R.J., R.E. Knighton and E. Bresler, 1984, Soil chemical and physical effects on spatial variability of hydraulic conductivity, *Soil Science*, 137(4), pp. 252-262.
- Weston, Inc., 1985, *Final Site Investigation Report, United Creosoting Company Site, Conroe, Texas*, Houston, TX.
- Wilson, J.T., J.F. McNabb, J.W. Cochran, T.H. Wang, M.B. Tomson and P.B. Bedient, 1985, Influence of microbial adaptation on the fate of organic pollutants in ground water, *Environmental Toxicology and Chemistry*, 4, pp. 721-726.

**APPENDIX A Figures of *GWSE* for natural gradient flow (NG-GF)
modeling**

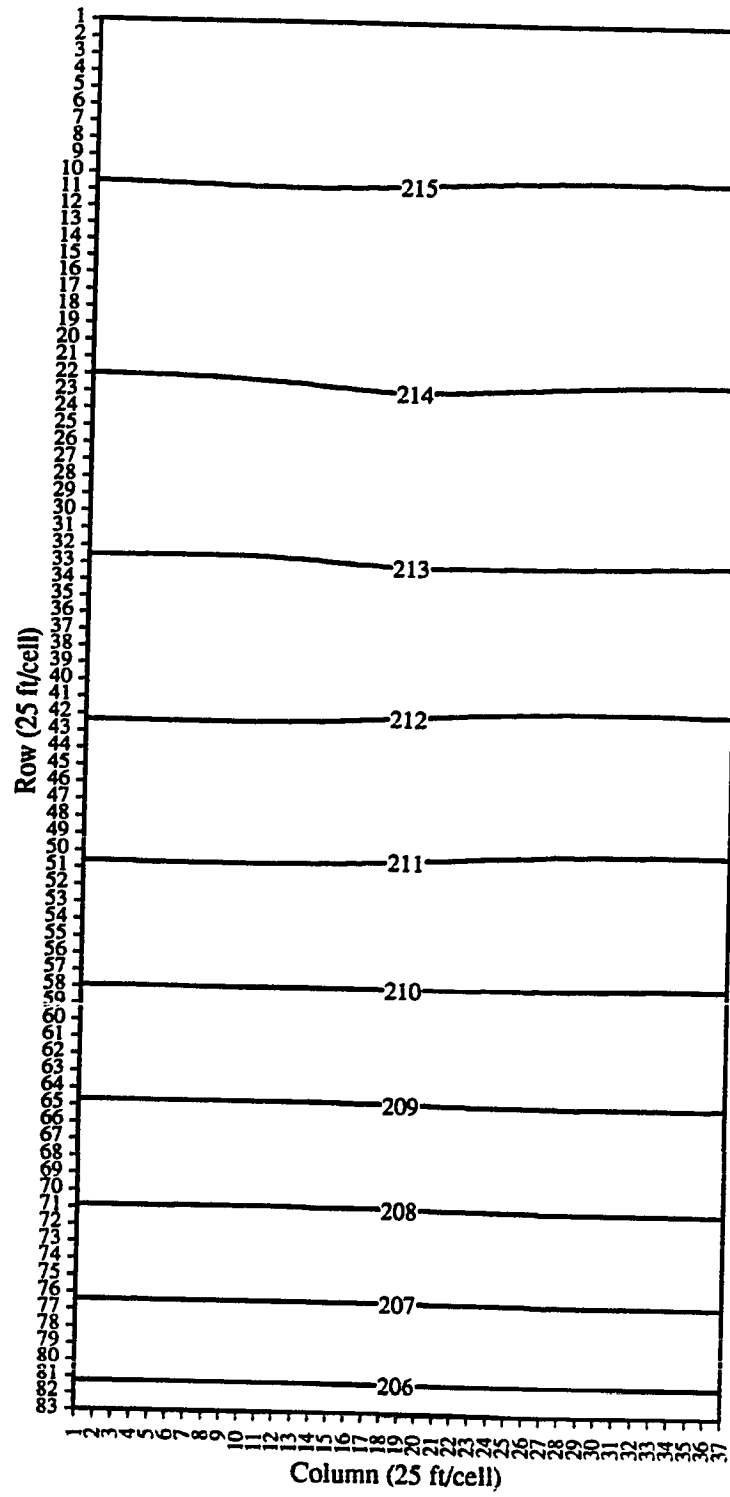


Figure A.1

GWSEs for sim. NG-GF-KB-C

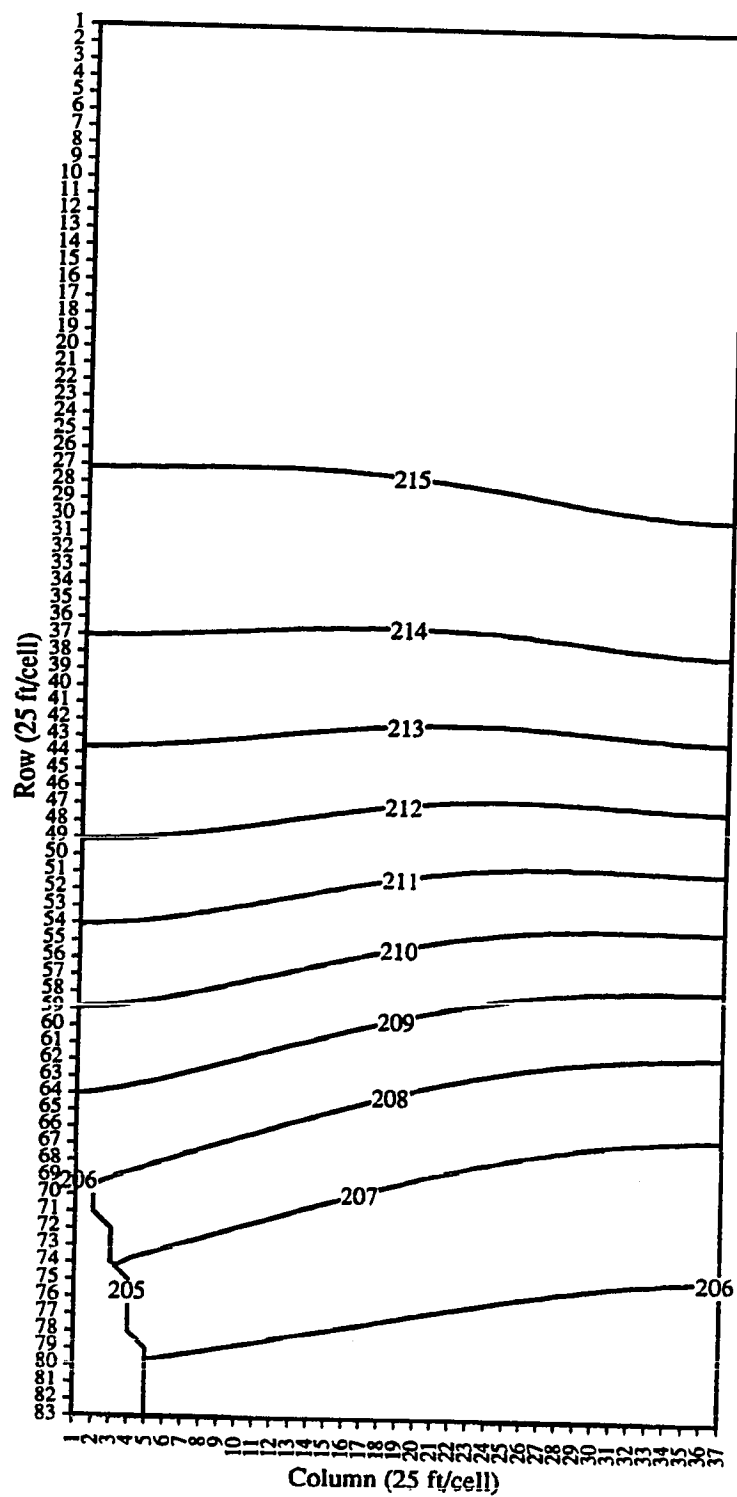


Figure A.2

GWSEs for sim. NG-GF-KB-P

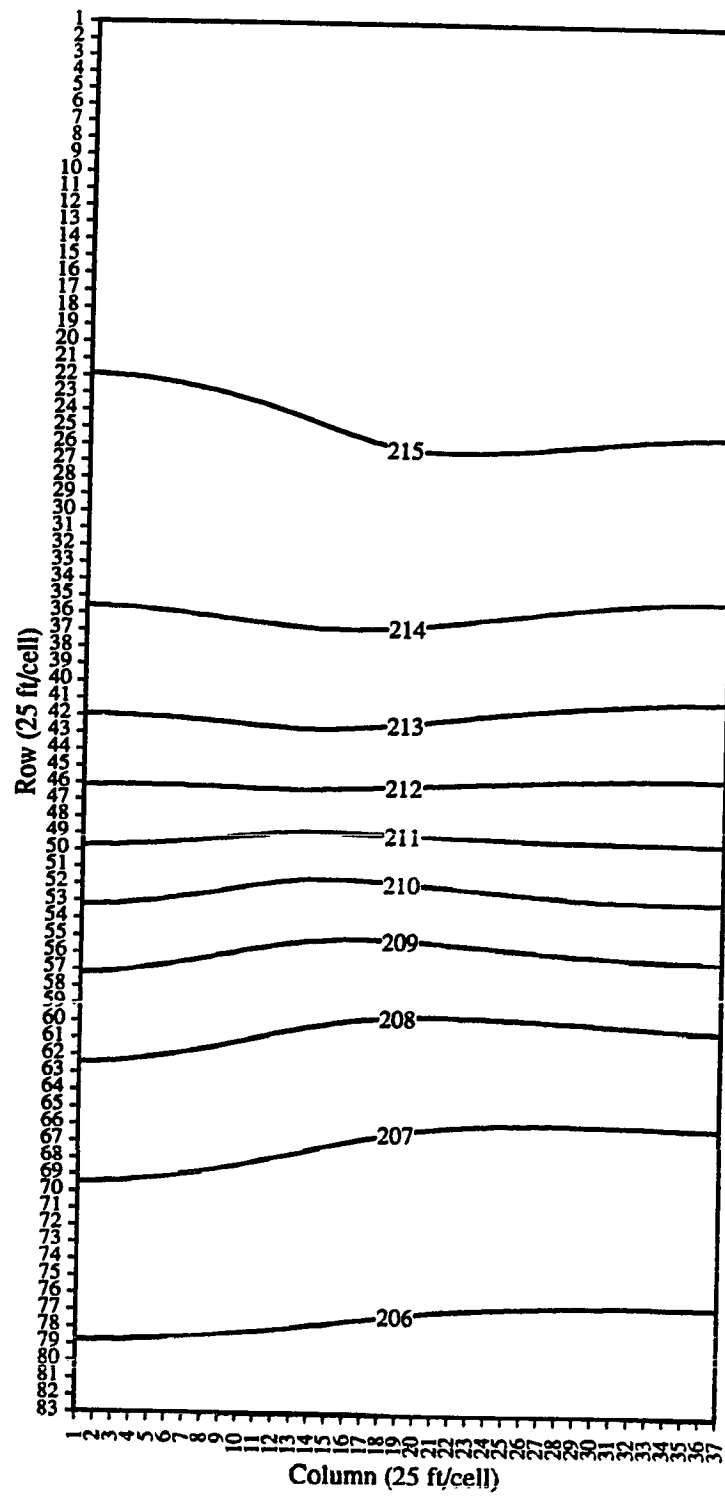


Figure A.3

GWSEs for sim. NG-GF-KB-K

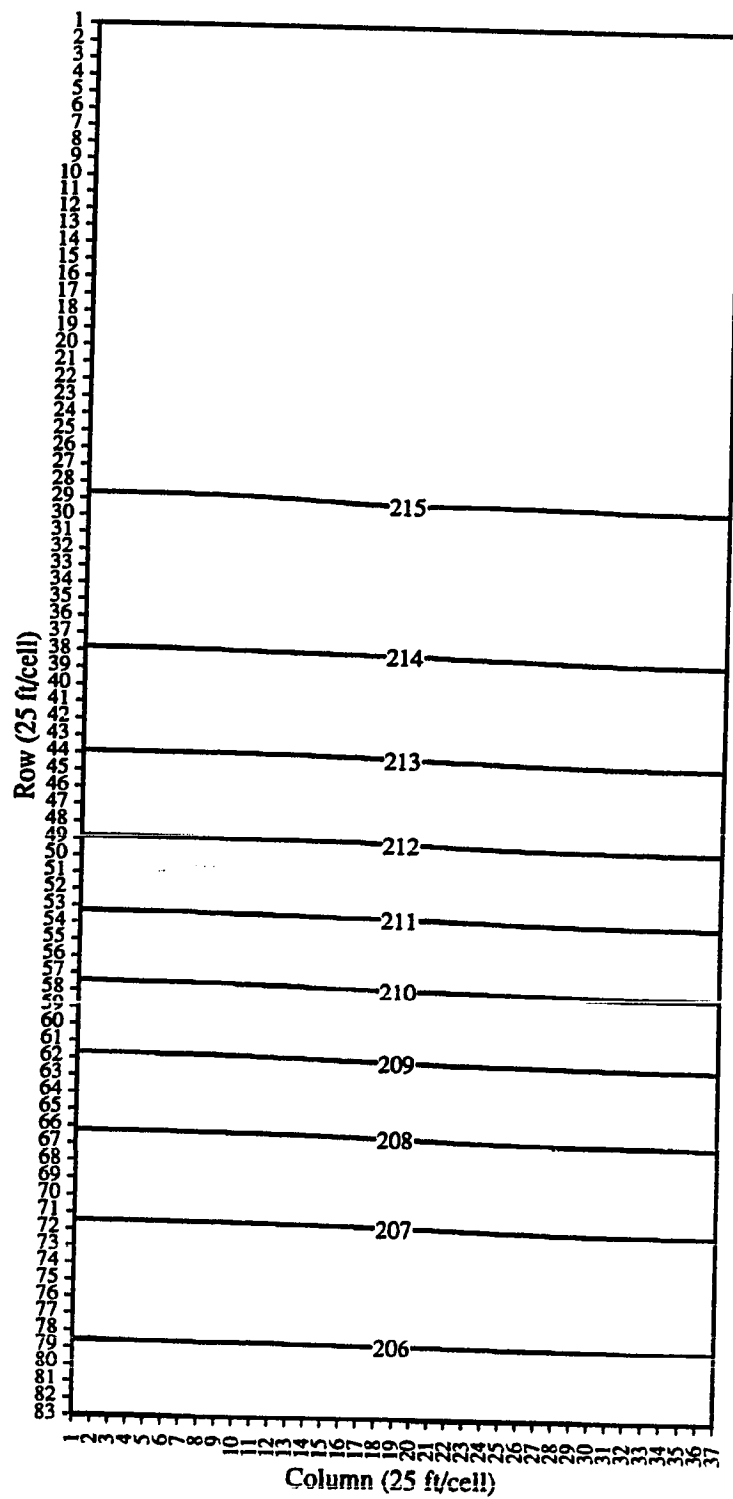


Figure A.4 GWSEs for sim. NG-GF-K-P

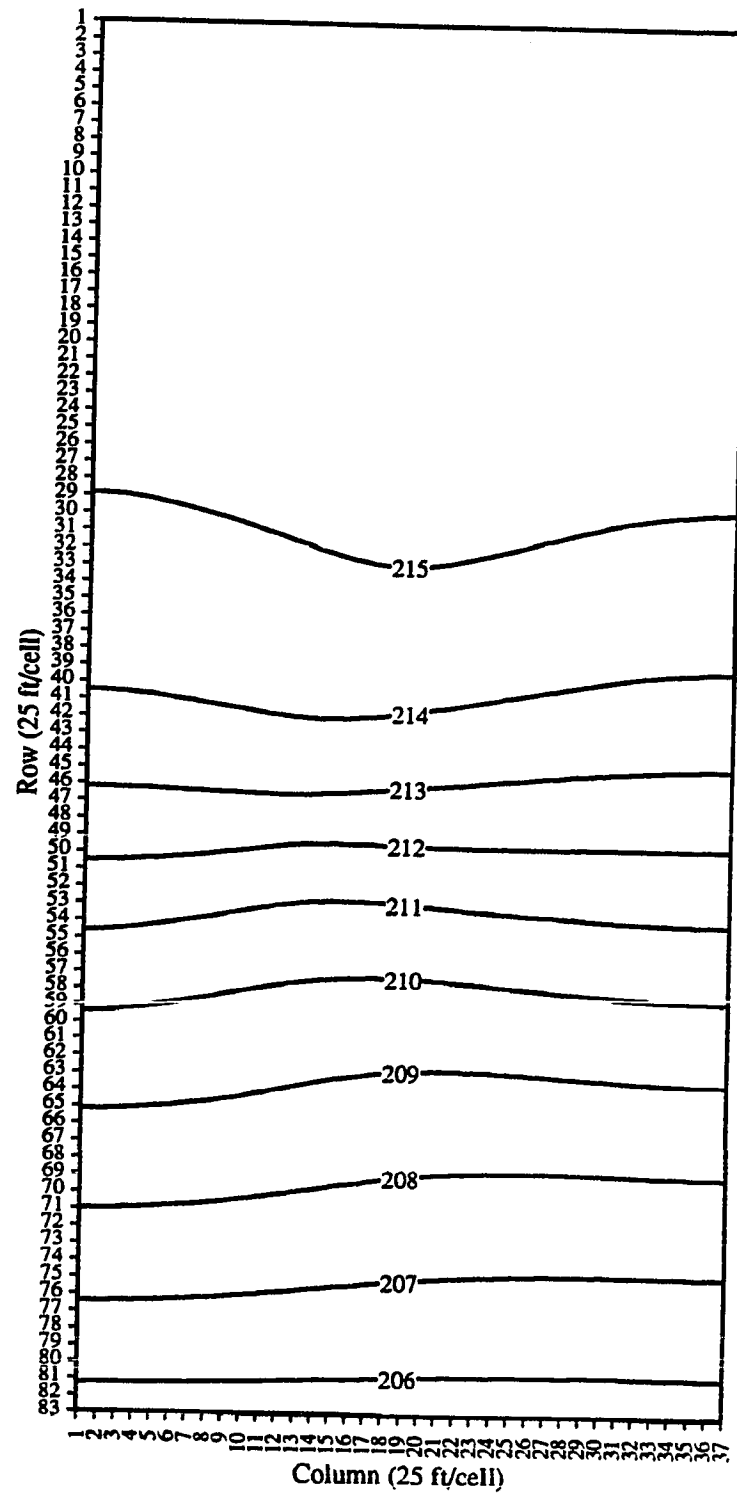


Figure A.5 GWSEs for sim. NG-GF-K-K

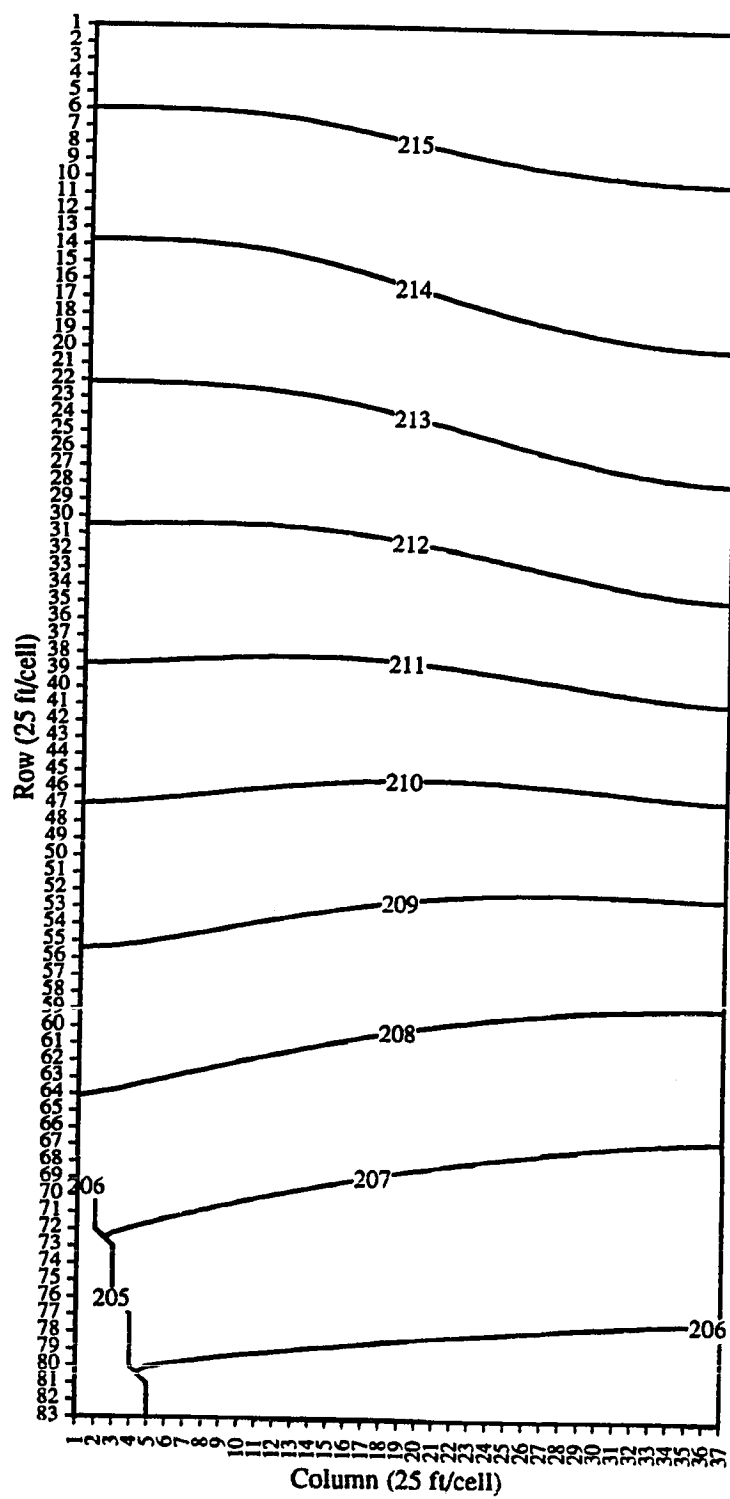


Figure A.6 GWSEs for sim. NG-GF-B-P

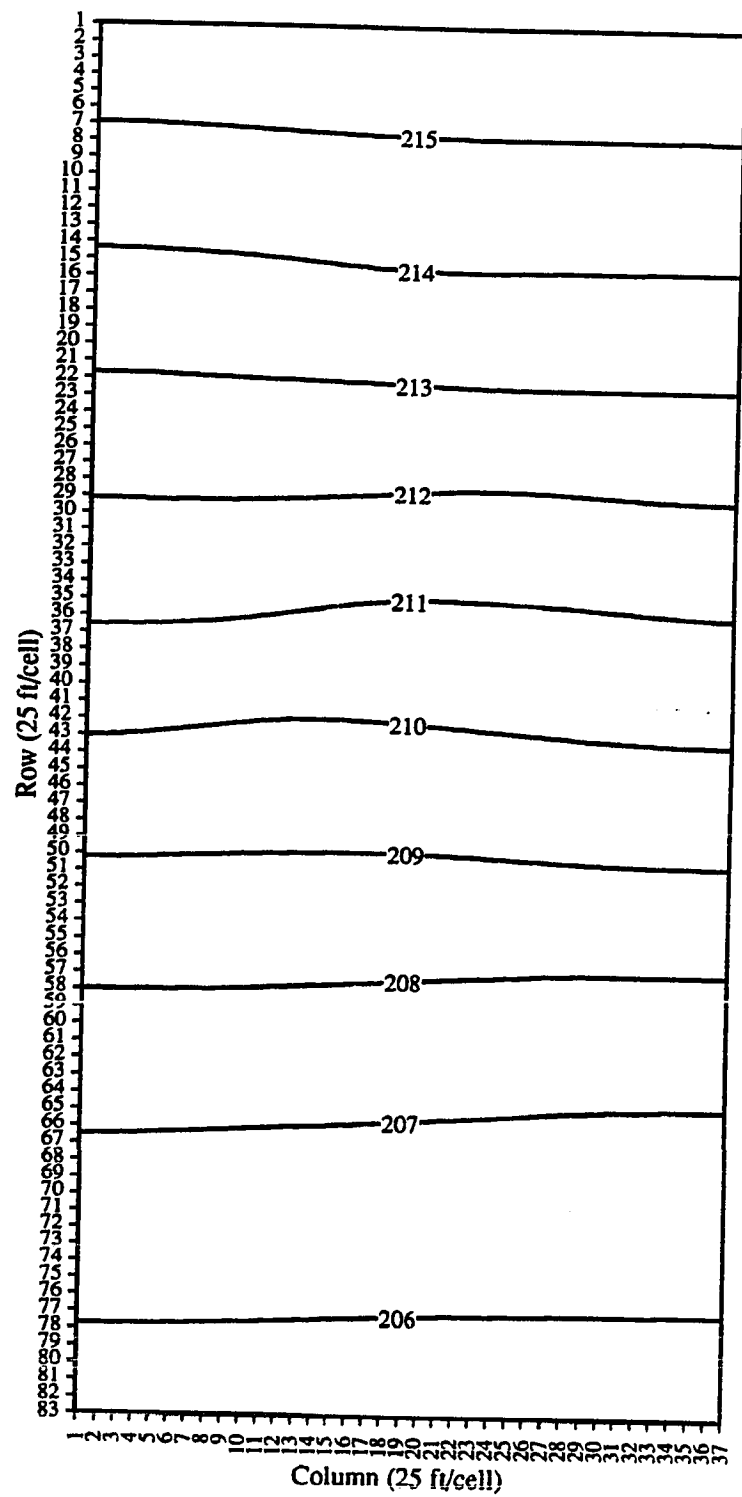


Figure A.7 GWSEs for sim. NG-GF-B-K

APPENDIX B **Figures of chloride concentration distribution for natural
gradient transport (NG-CT) modeling**

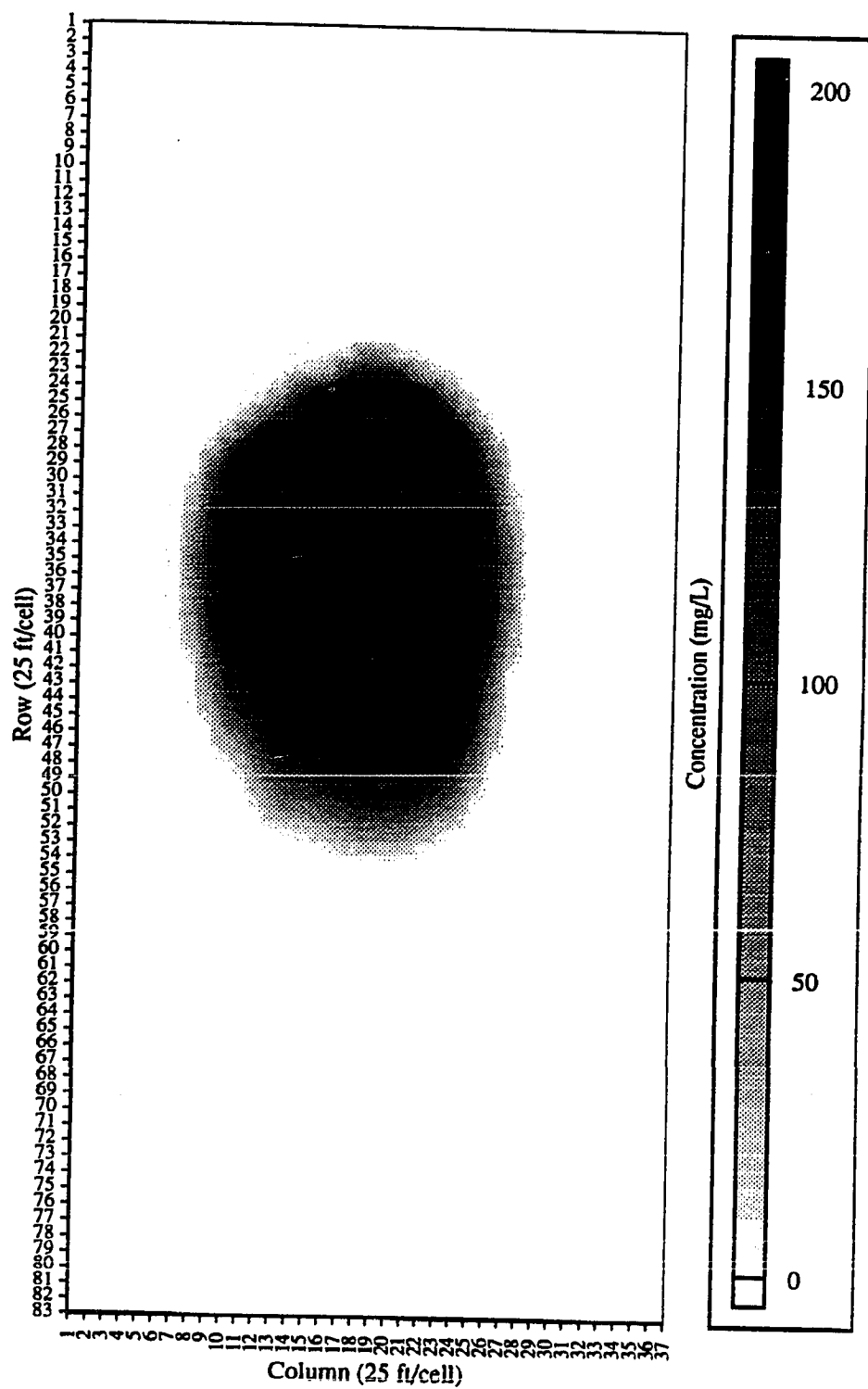


Figure B.1 Chloride conc. distribution for sim. NG-CT-KB-C

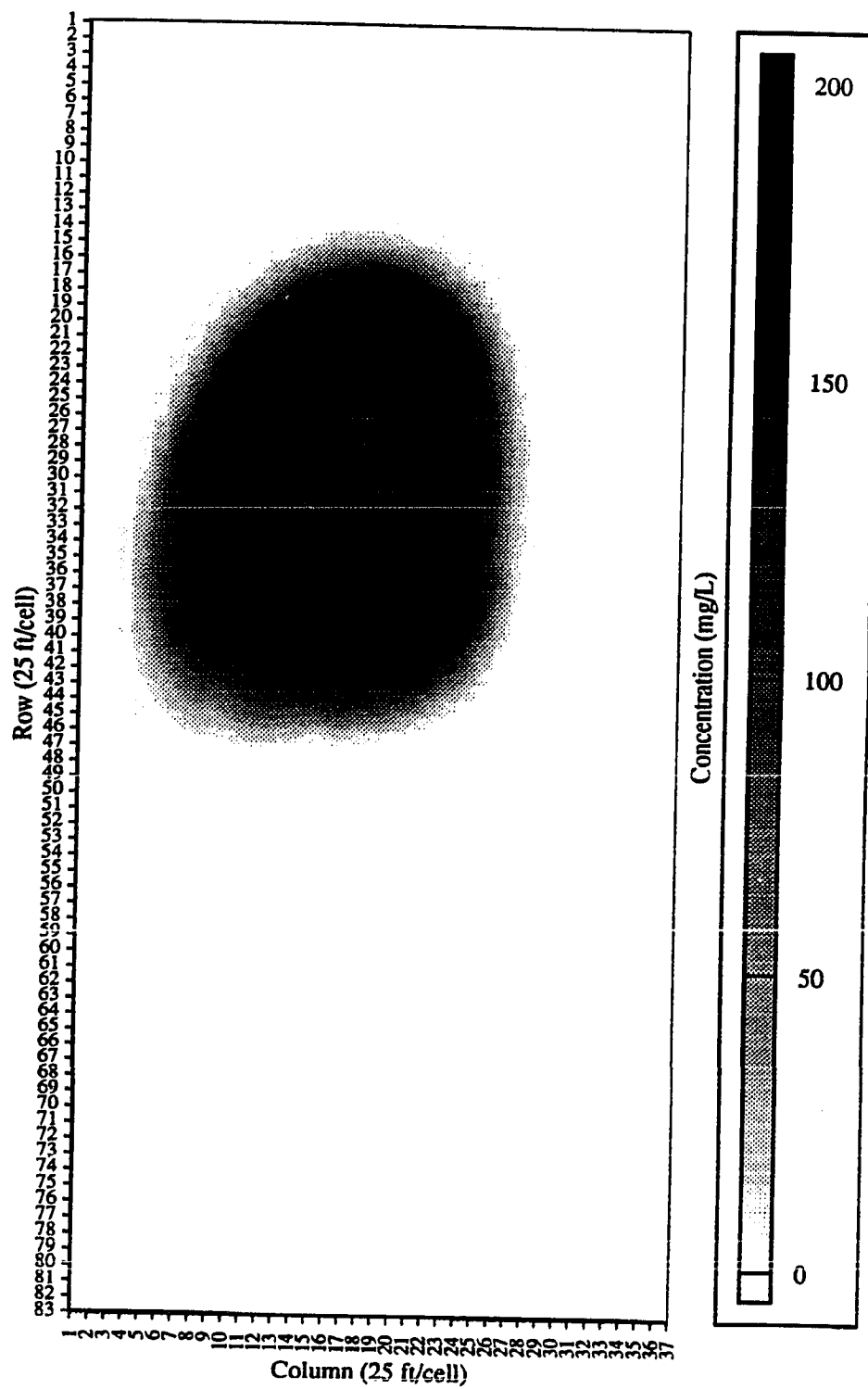


Figure B.2 Chloride conc. distribution for sim. NG-CT-KB-P

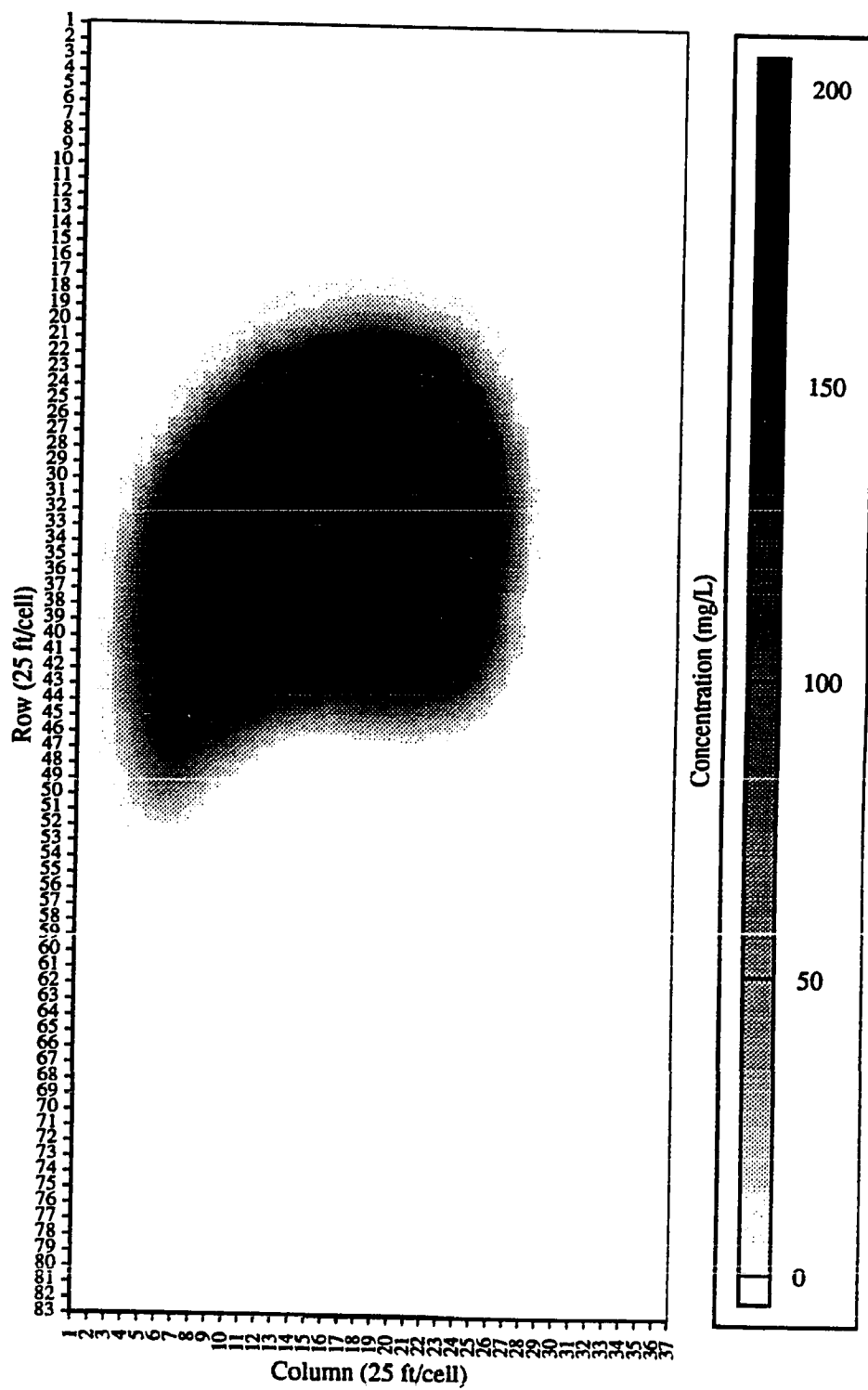


Figure B.3 Chloride conc. distribution for sim. NG-CT-KB-K

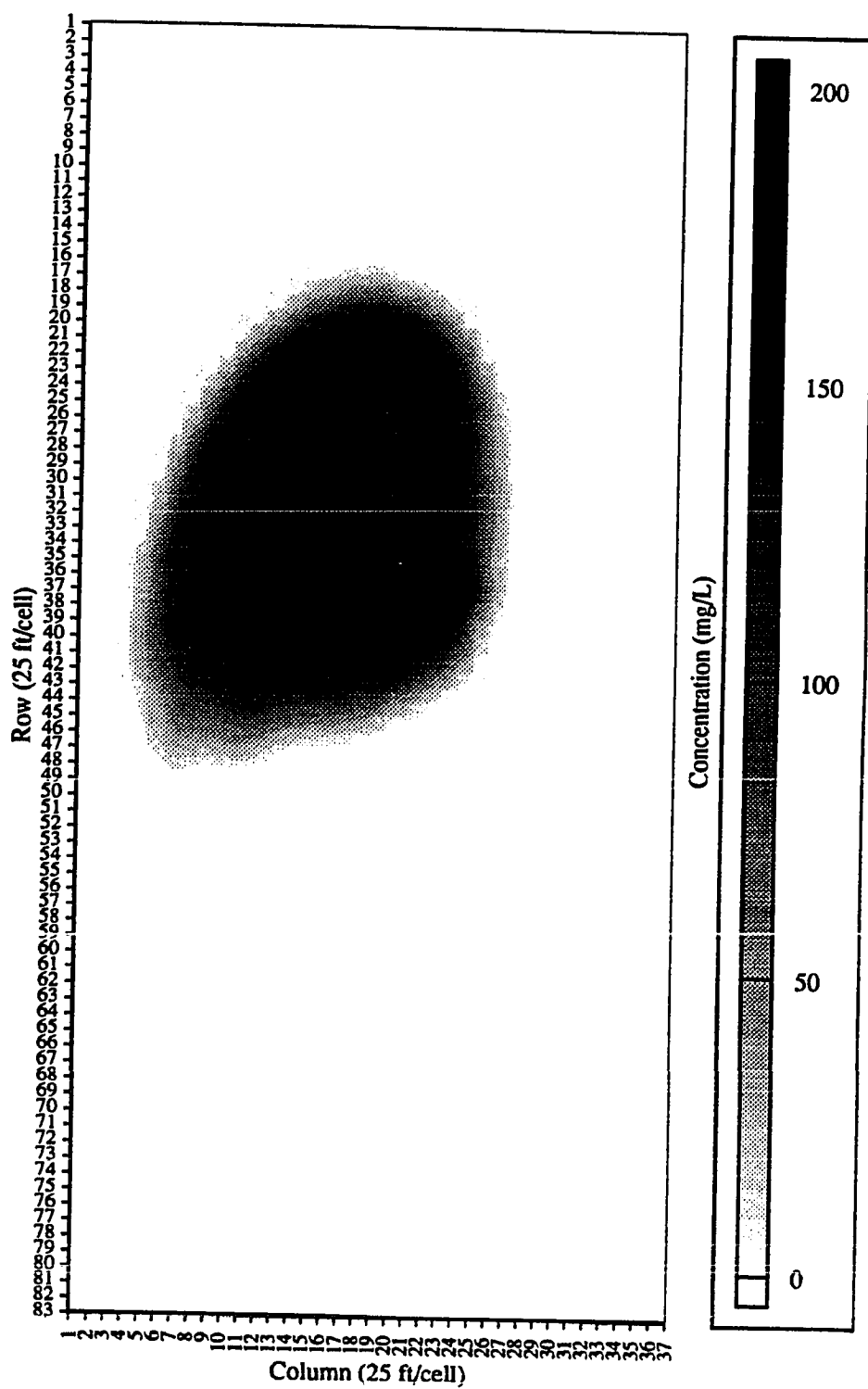


Figure B.4 Chloride conc. distribution for sim. NG-CT-K-P

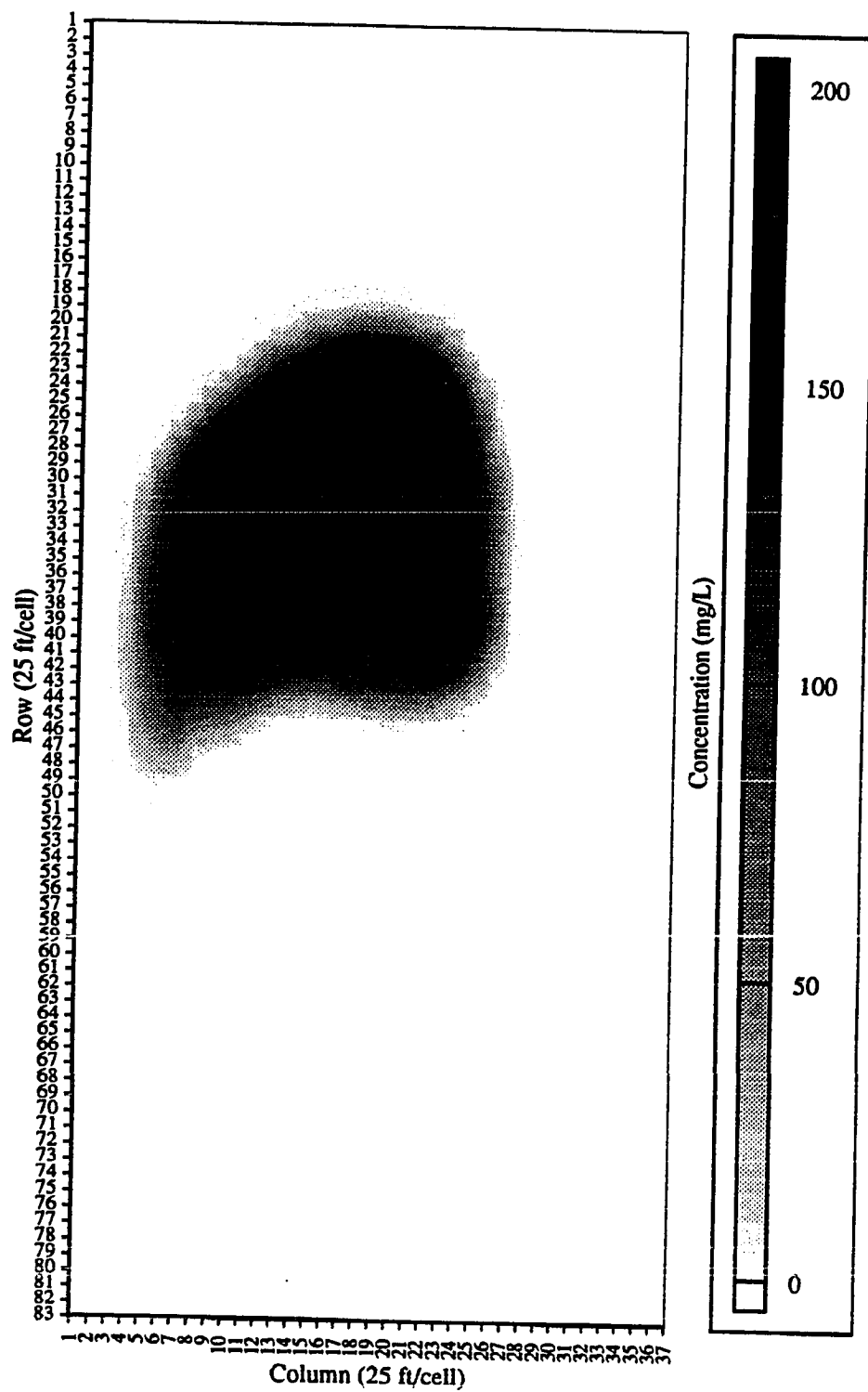


Figure B.5 Chloride conc. distribution for sim. NG-CT-K-K

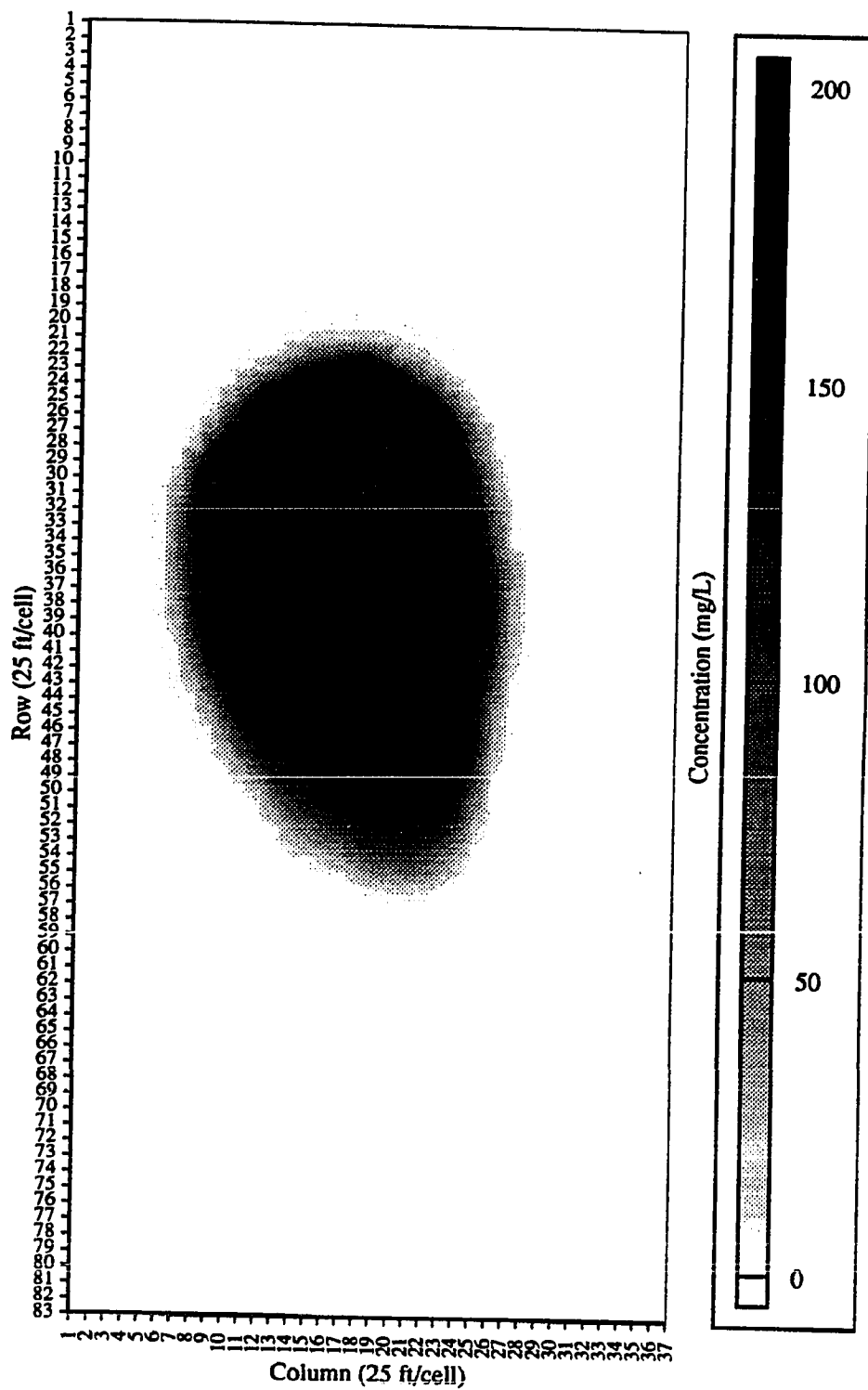


Figure B.6 Chloride conc. distribution for sim. NG-CT-B-P

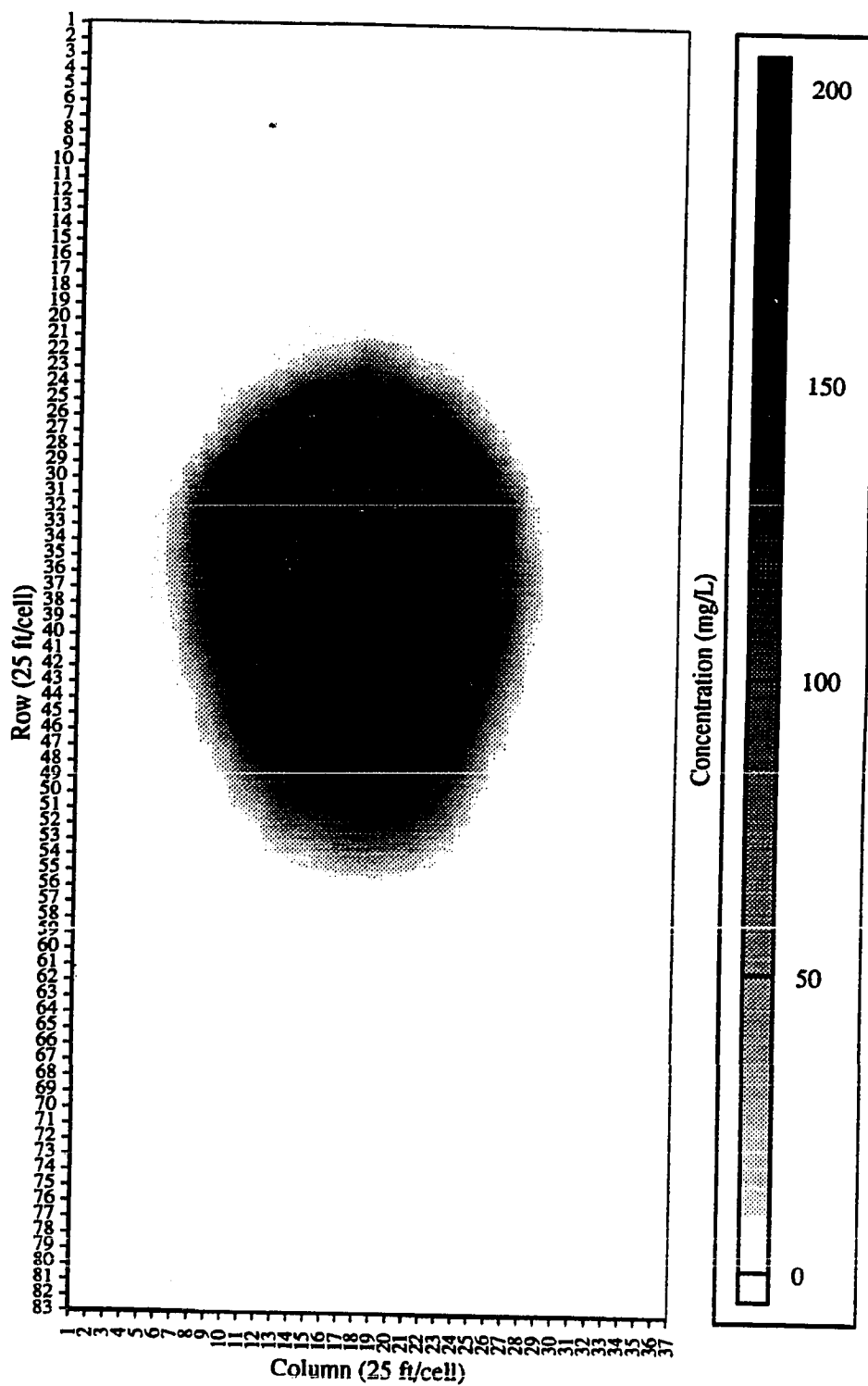


Figure B.7 Chloride conc. distribution for sim. NG-CT-B-K

APPENDIX C **Figures of *GWSE* for recovery and injection system flow
(RI-GF) modeling**

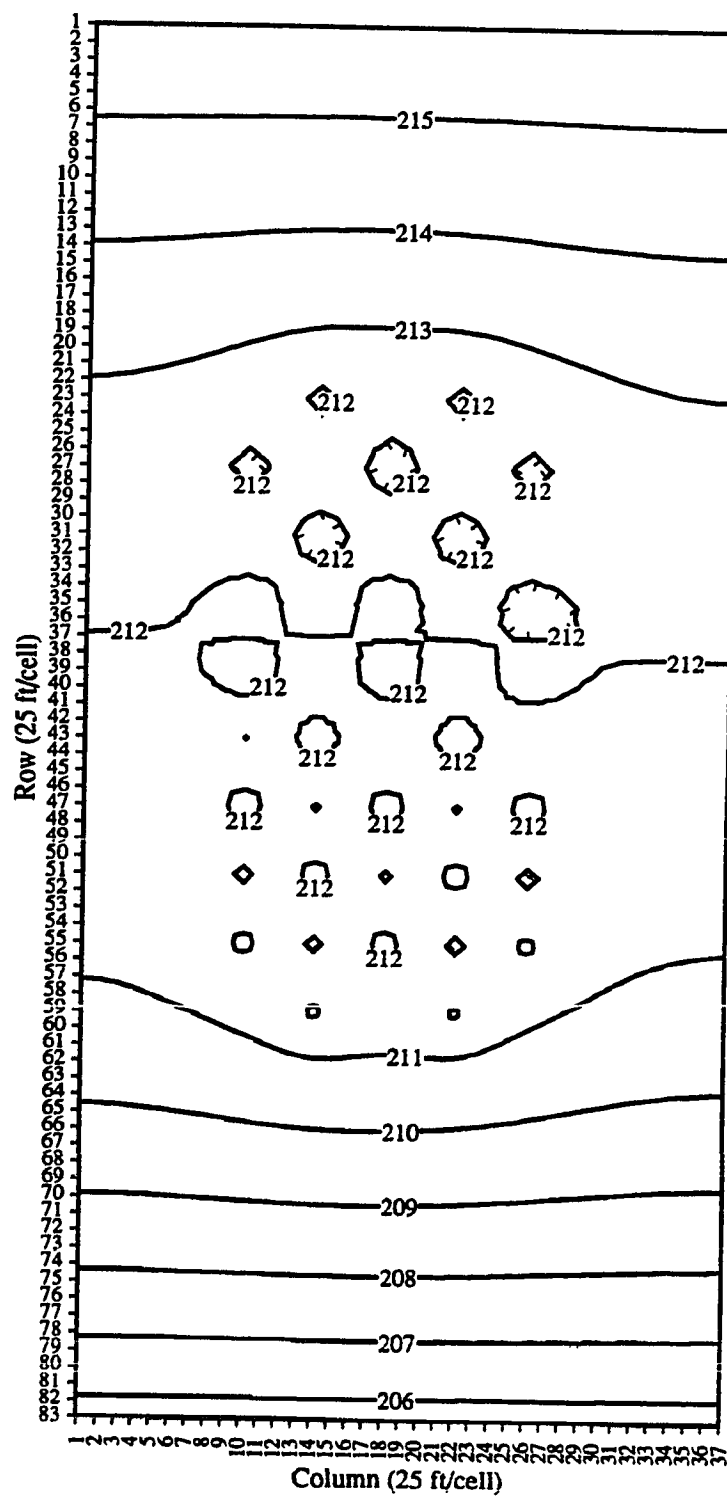


Figure C.1 GWSEs for sim. RI-GF-KB-C

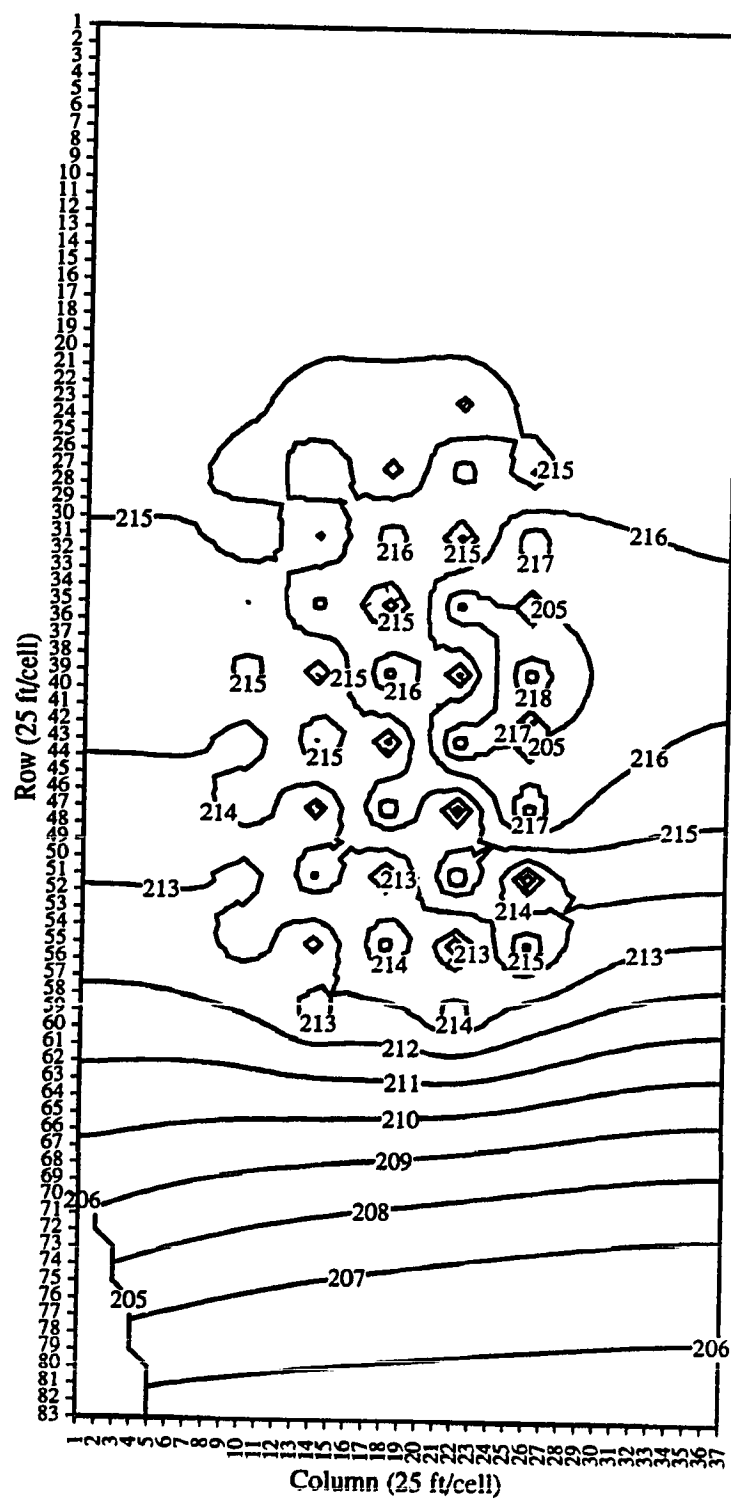


Figure C.2 GWSEs for sim. RI-GF-KB-P

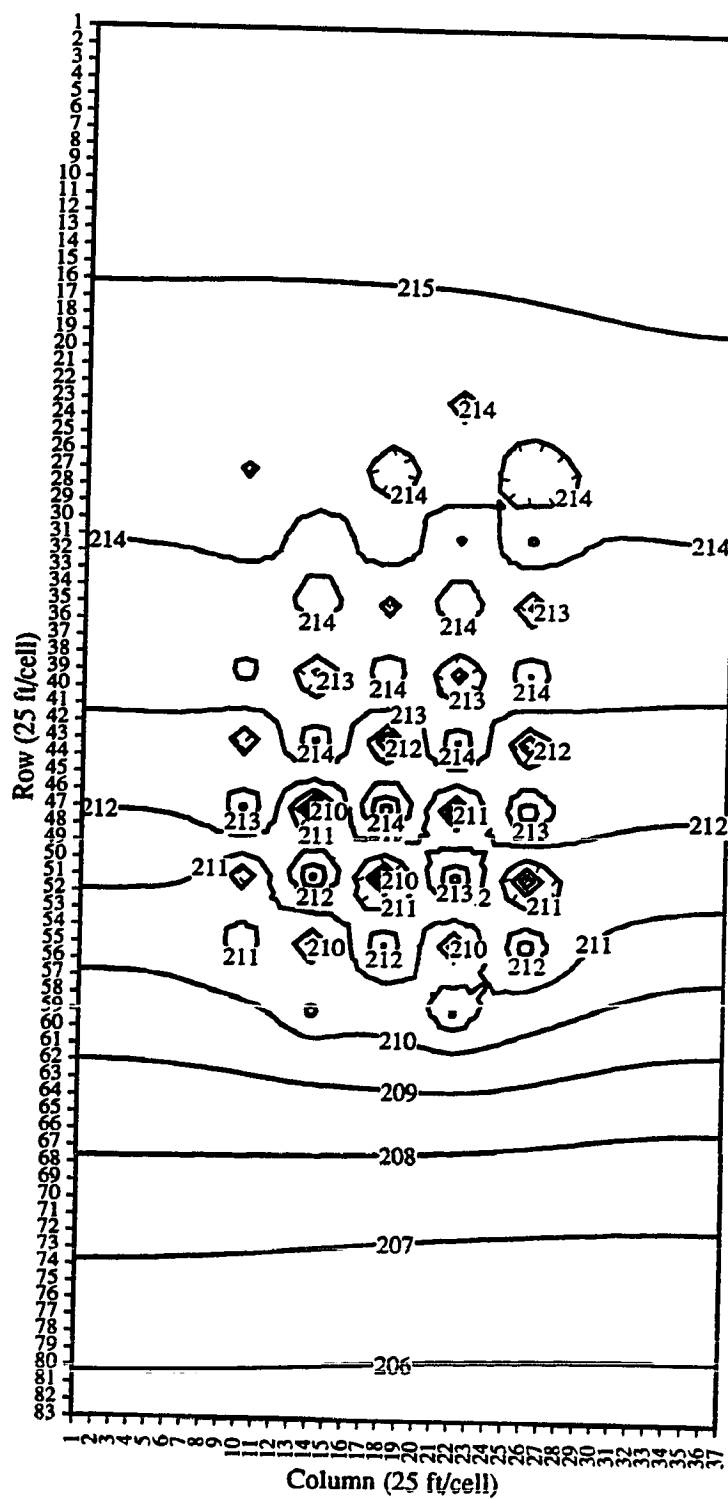


Figure C.3

GWSEs for sim. RI-GF-KB-K

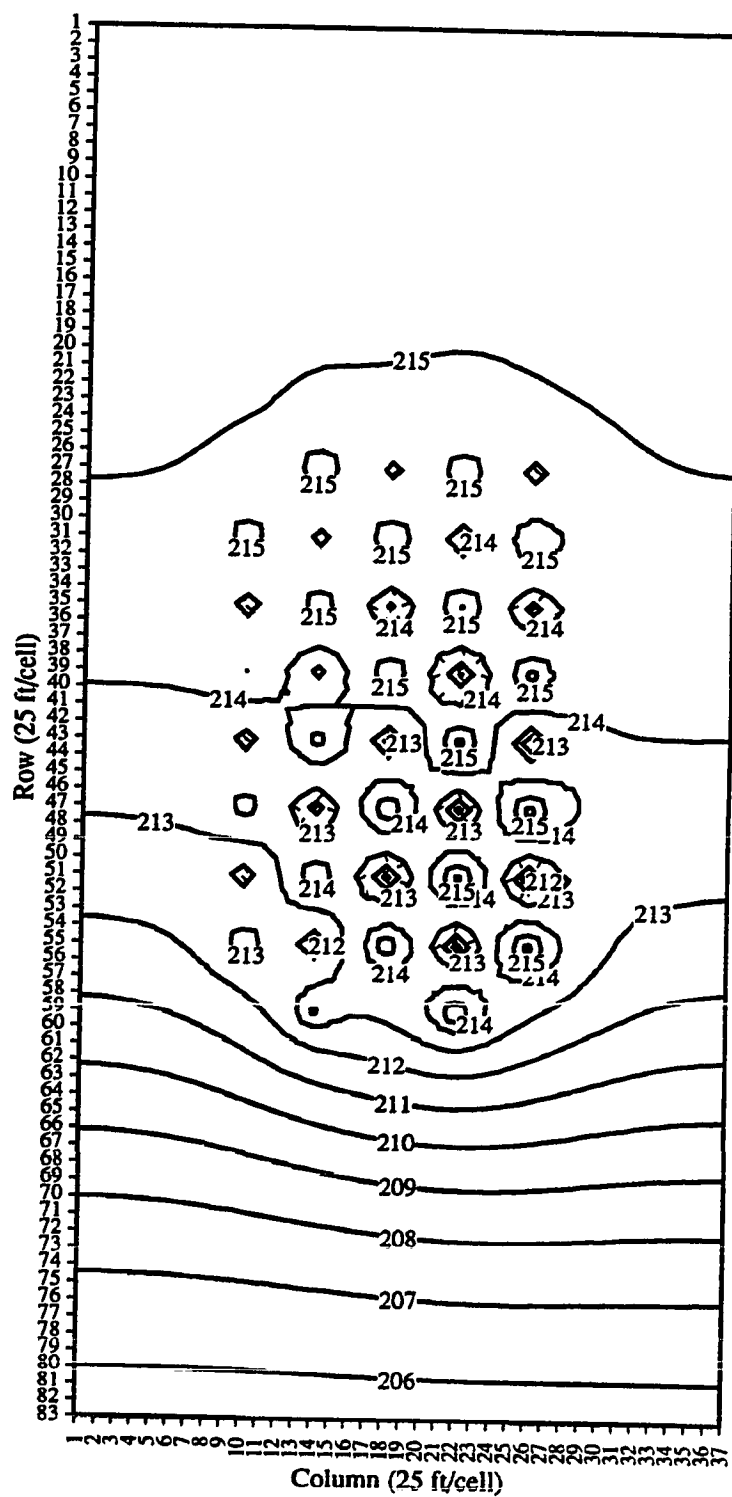


Figure C.4 GWSEs for sim. RI-GF-K-P

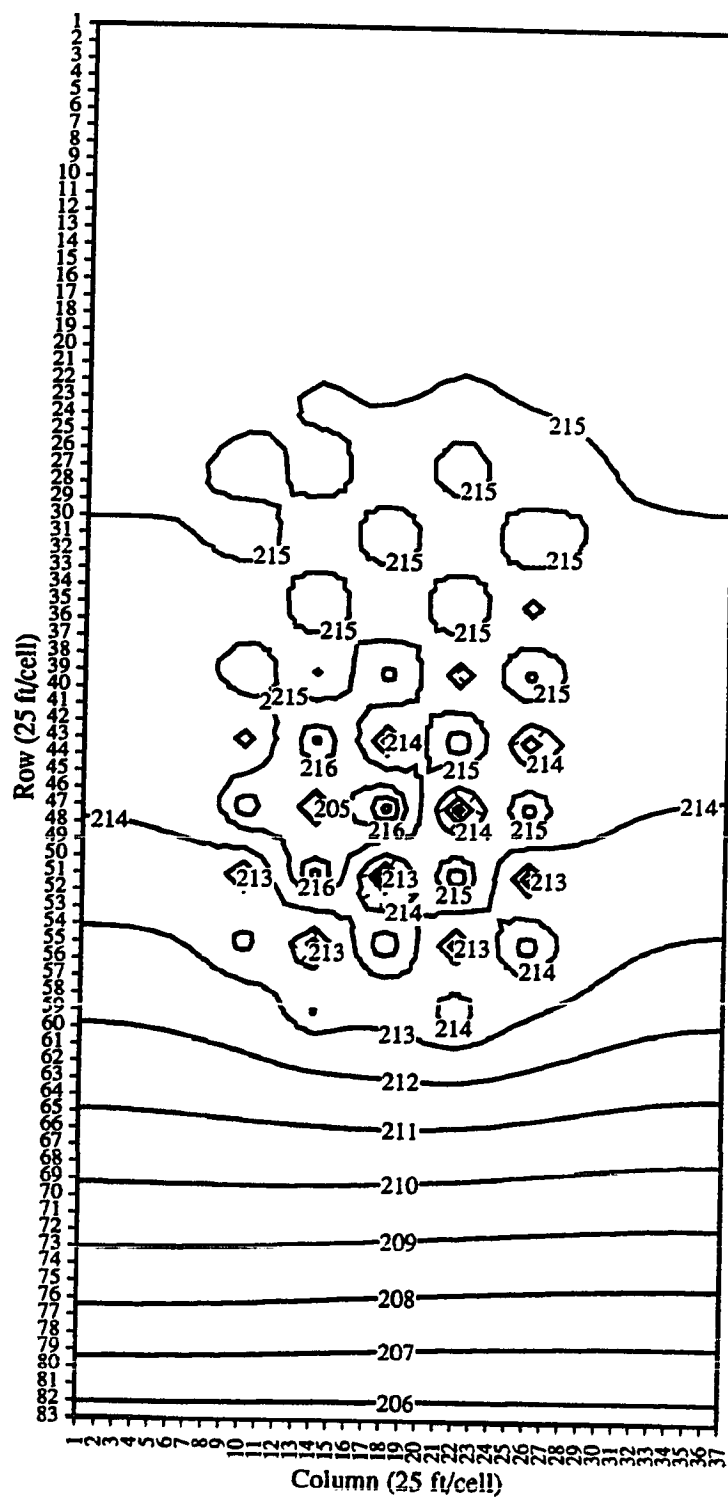


Figure C.5 GWSEs for sim. RI-GF-K-K

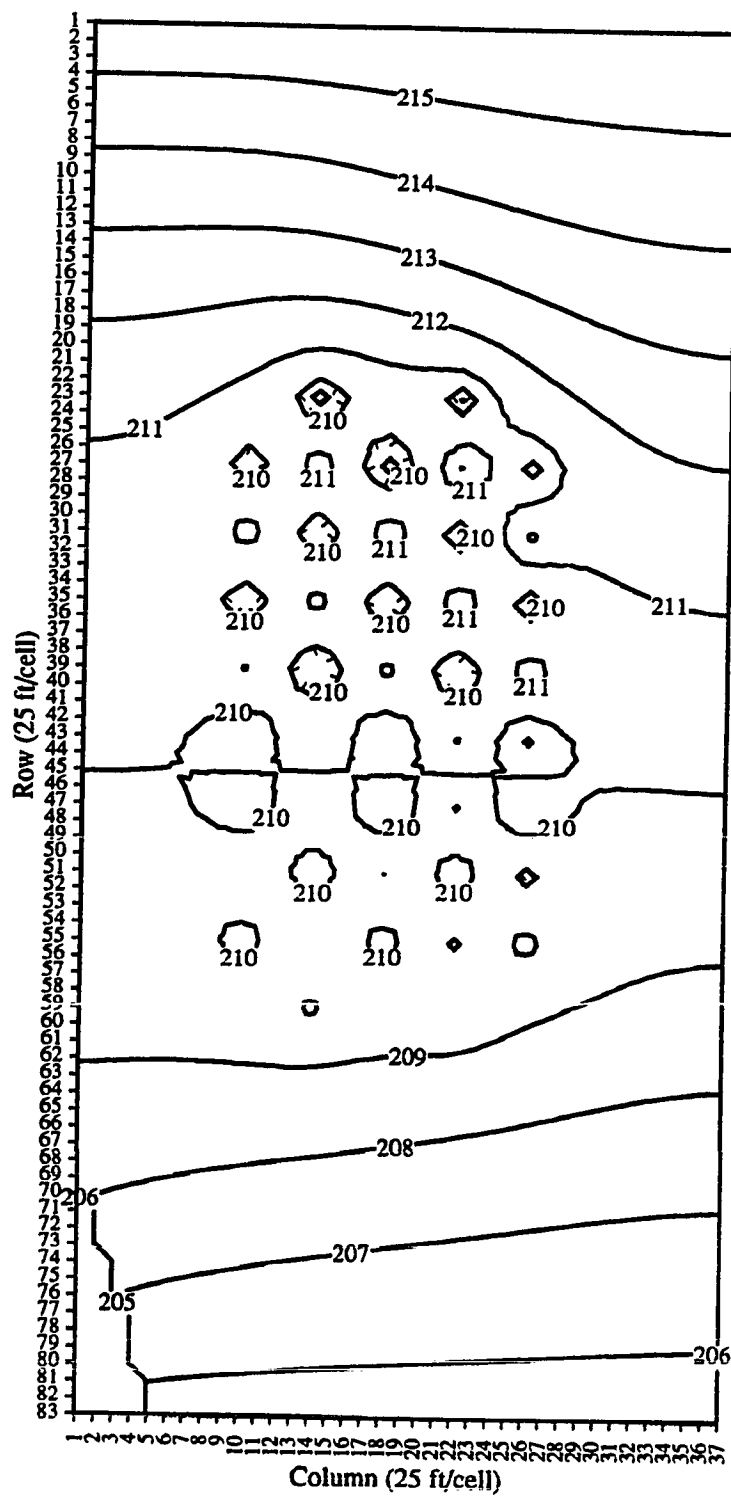


Figure C.6 GWSEs for sim. RI-GF-B-P

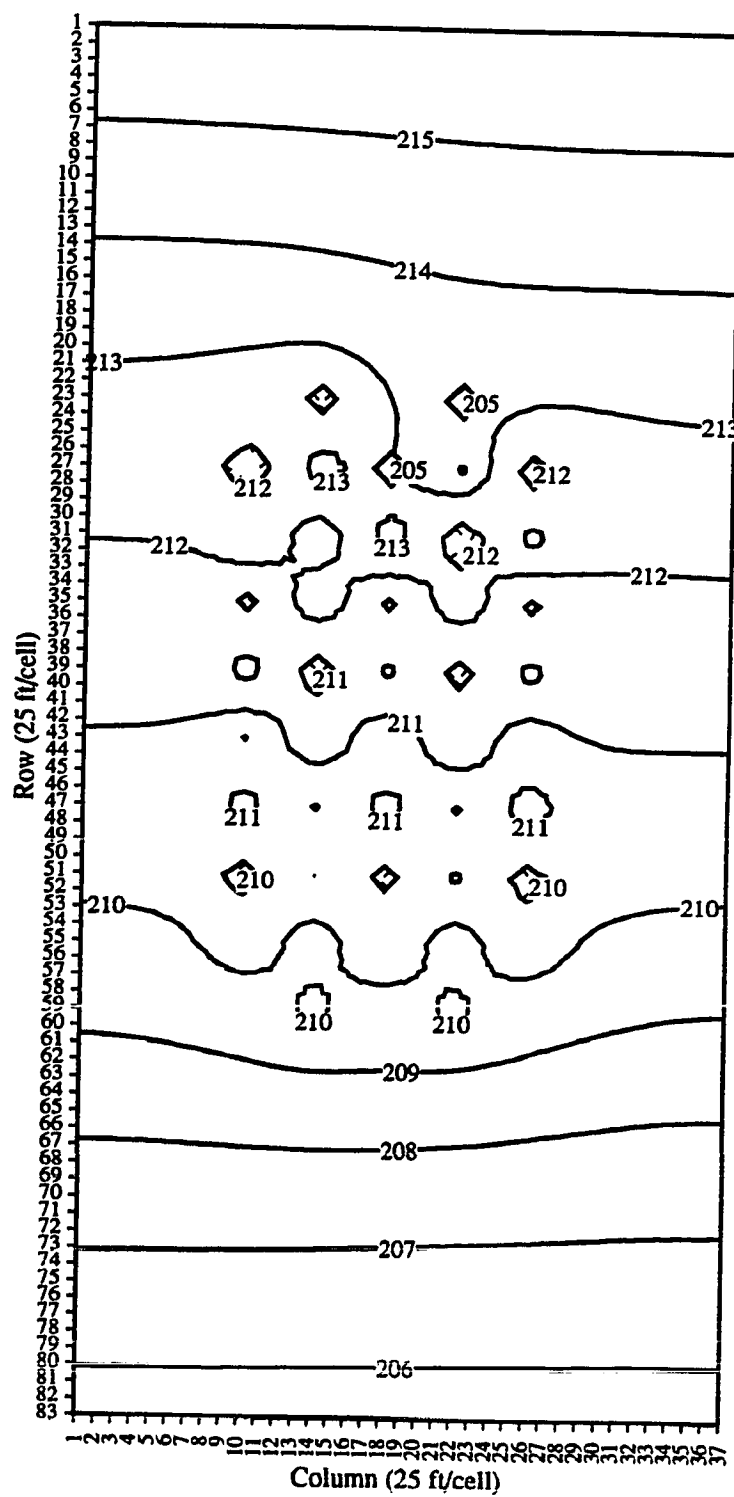


Figure C.7 GWSEs for sim. RI-GF-B-K

APPENDIX D Figures of chloride concentration distribution for recovery and injection system transport (RI-CT) modeling

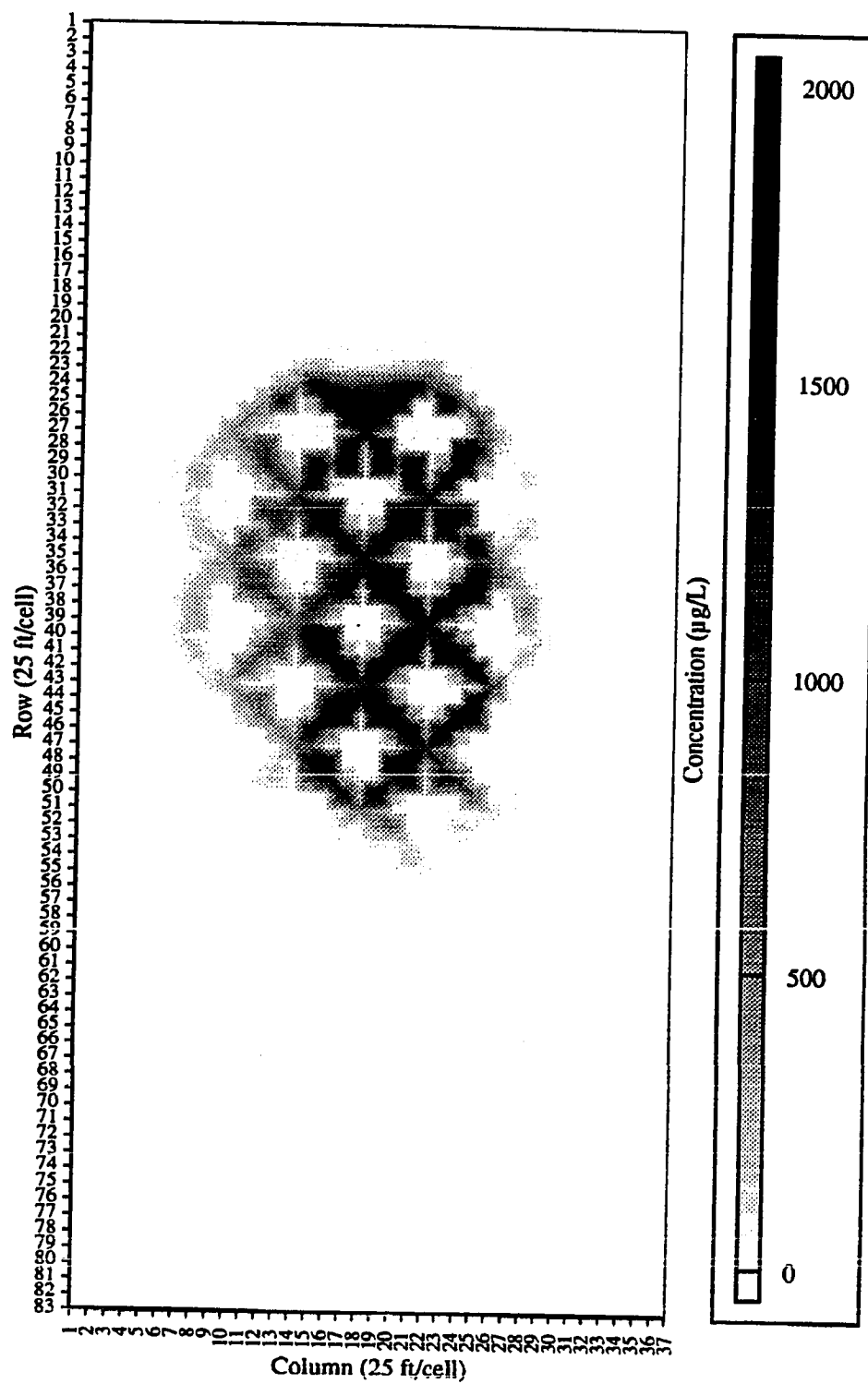


Figure D.1 Naphthalene conc. distribution for sim. RI-CT-KB-C

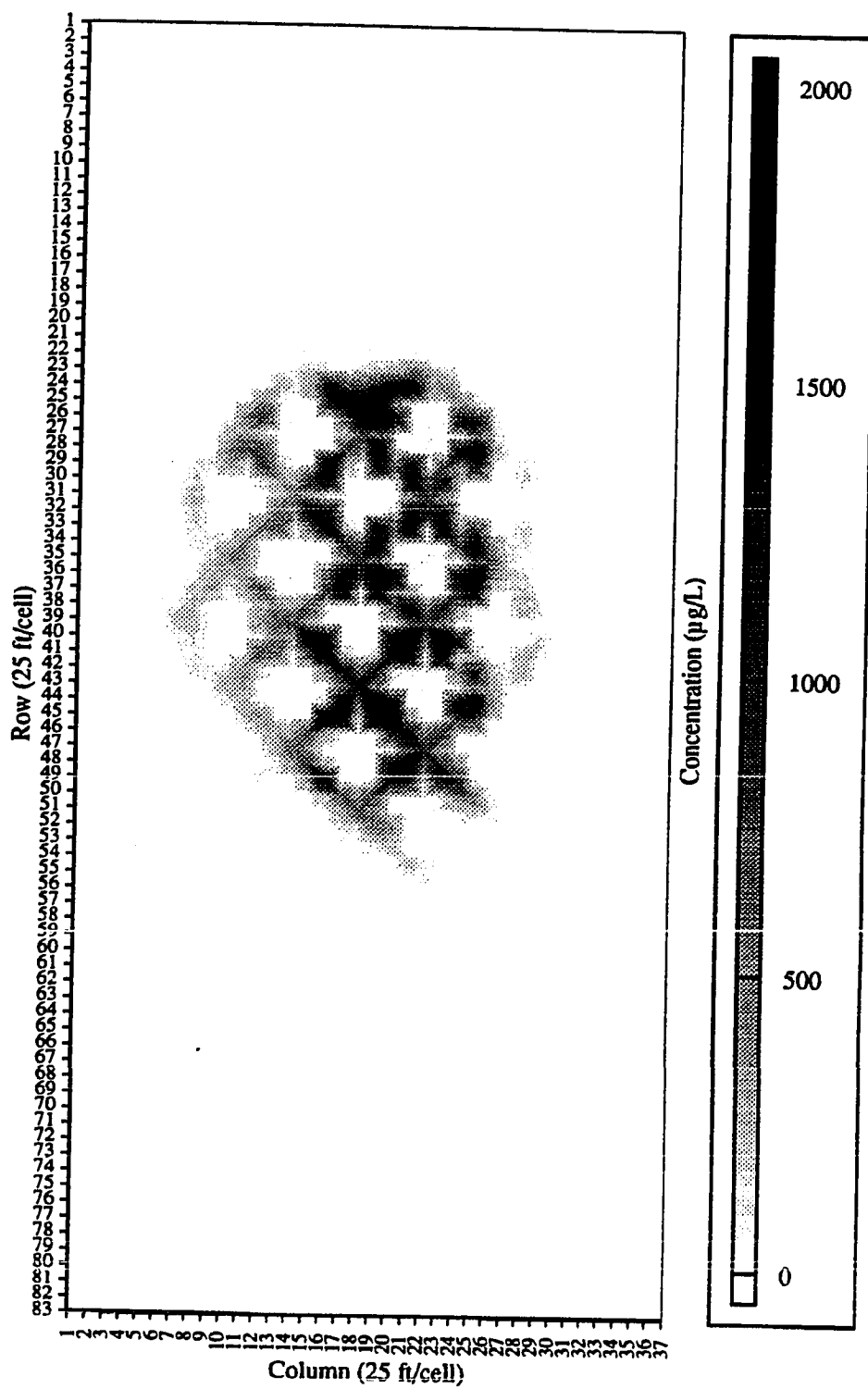


Figure D.2 Naphthalene conc. distribution for sim. RI-CT-KB-P

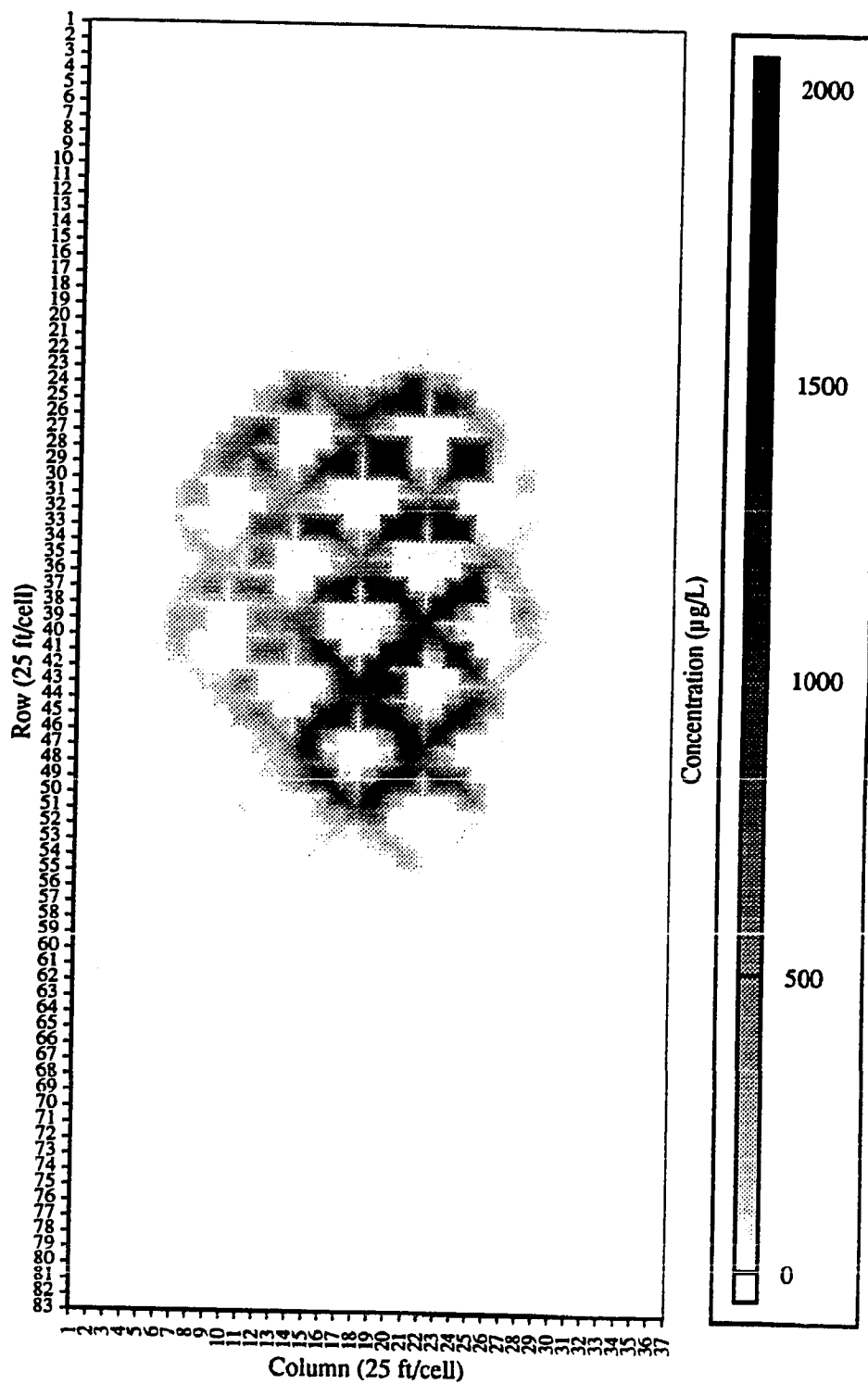


Figure D.3 Naphthalene conc. distribution for sim. RI-CT-KB-K

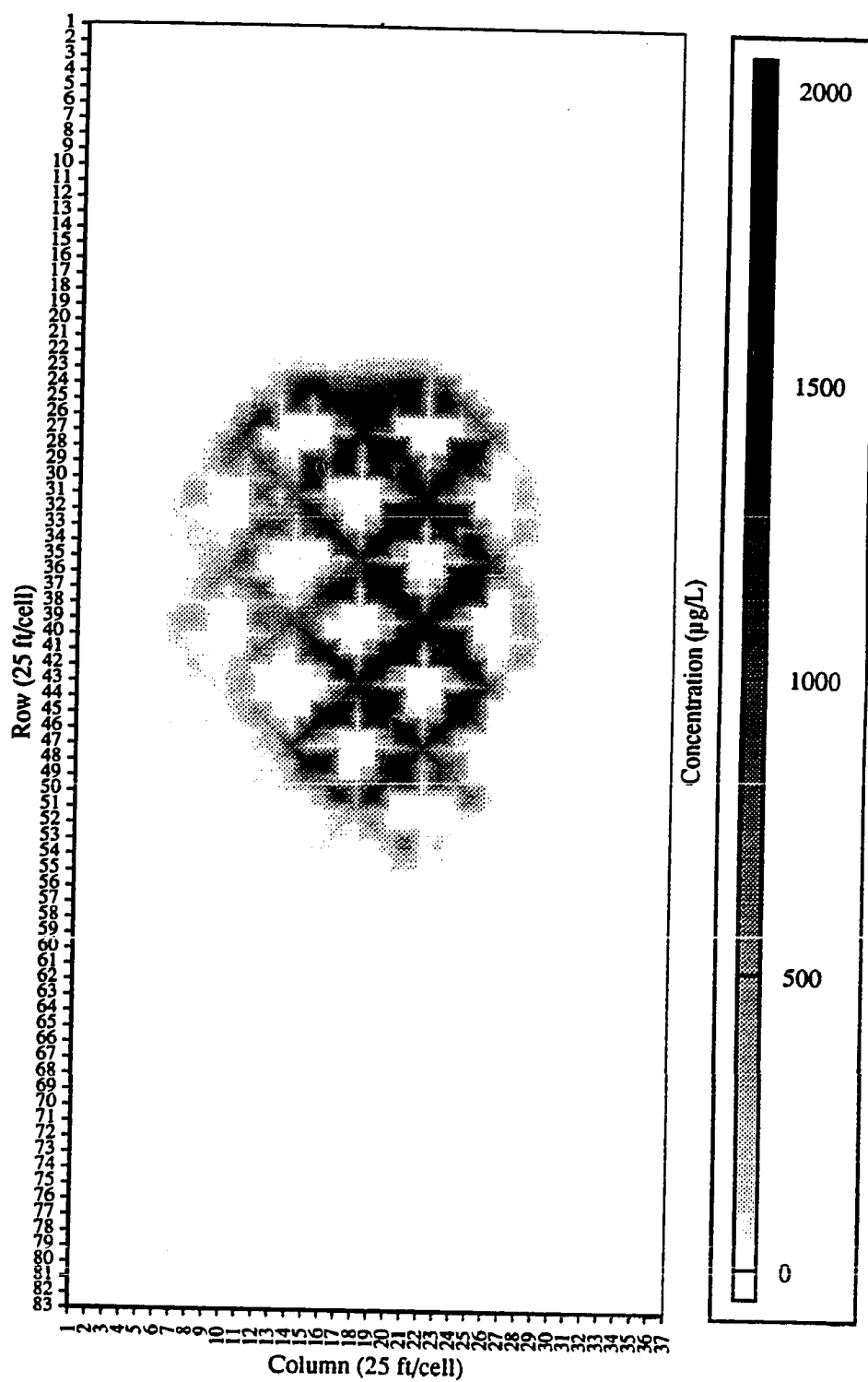


Figure D.4 Naphthalene conc. distribution for sim. RI-CT-K-P

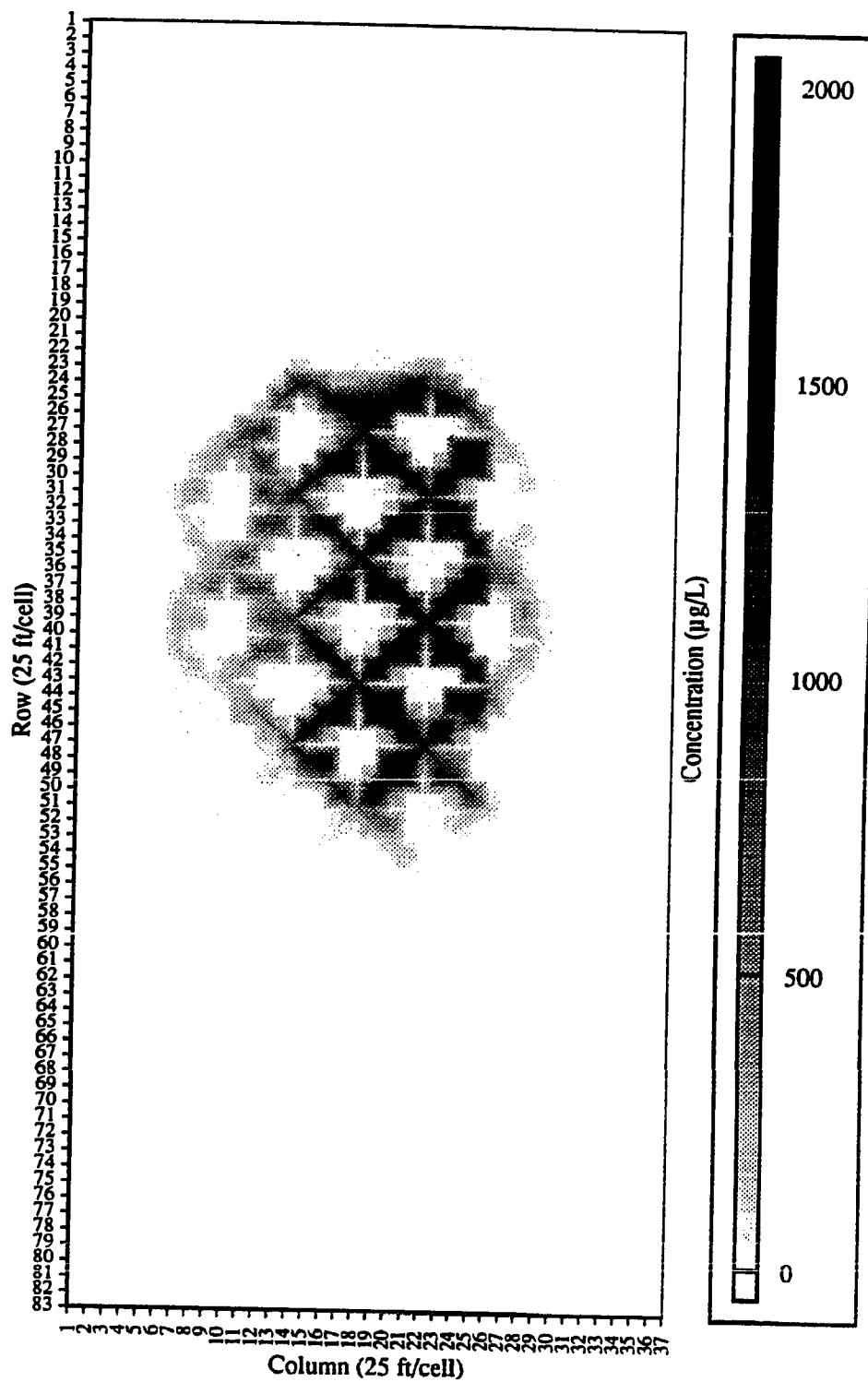


Figure D.5 Naphthalene conc. distribution for sim. RI-CT-K-K

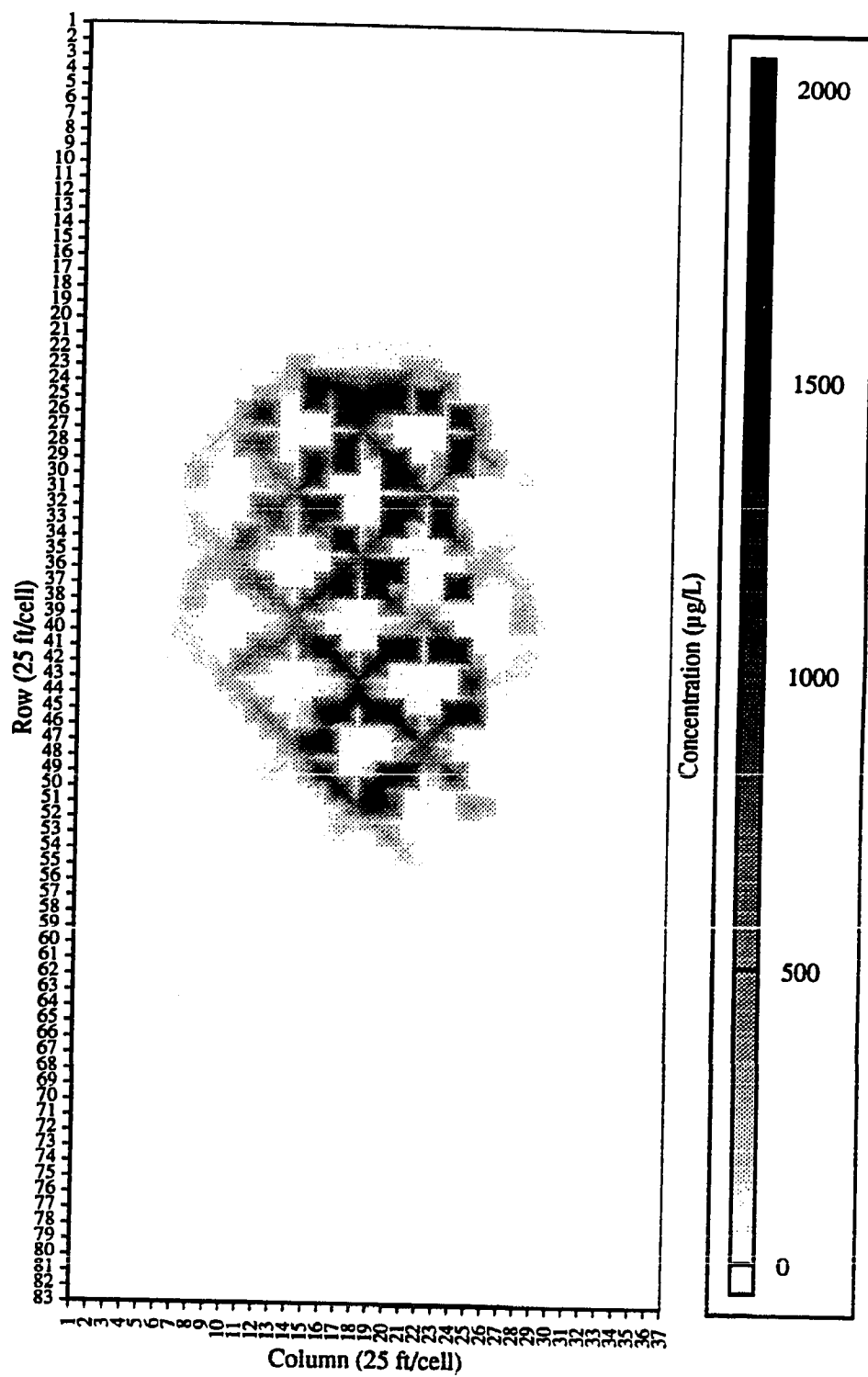


Figure D.6 Naphthalene conc. distribution for sim. RI-CT-B-P

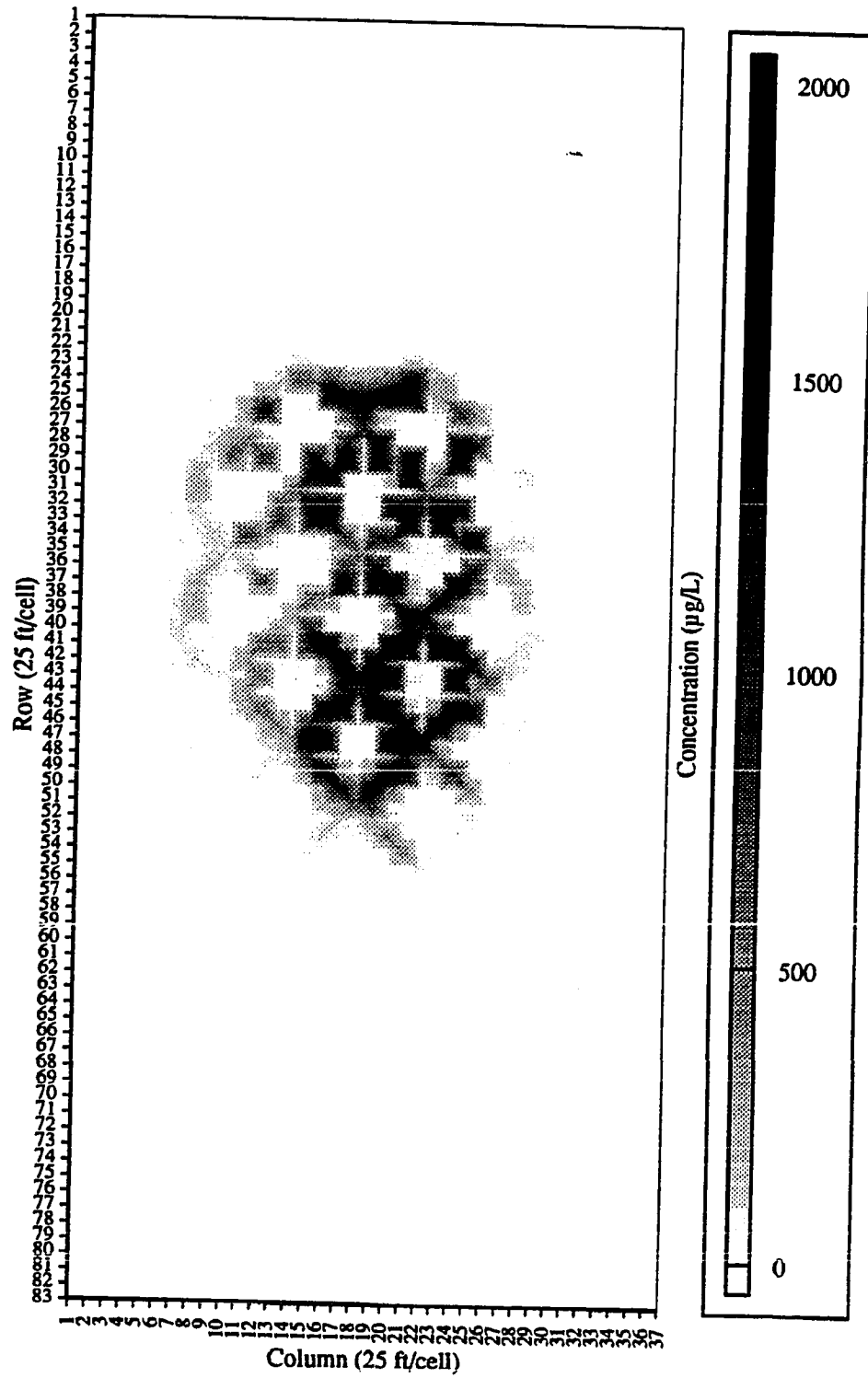


Figure D.7 Naphthalene conc. distribution for sim. RI-CT-B-K